POLITECNICO DI MILANO
Scuola di Ingegneria Industriale e dell'Informazione
Corso di Laurea Magistrale in Ingegneria Elettrica

FOREIGN OBJECT DETECTION IN WIRELESS-POWER-TRANSFER CHARGING SYSTEMS FOR ELECTRIC VEHICLES

Relatore: Prof. Giordano Spadacini

Tesi di Laurea Magistrale di:
Lorenzo Diomede,
Matricola: 898485

Anno accademico 2019/2020

ACKNOWLEDGMENTS

My master's degree path is coming to an end. This thesis leads to a long and hard path, but I can certainly say that it was an adventure that made me a better person from all points of view.

I would like to thank the Politecnico di Milano for forming me professionally with great joys and efforts. But above all, having placed me in an international context, first in Milan and then through a double degree program with the Xi'an Jiaotong University. The year spent in China has been special and I thank all the professors, friends and colleagues I met on my way.

China will always remain an important chapter in my life. I express my gratitude to my supervisor Professor Liu JinJun who supervised my thesis work with extreme availability and answering my doubts always transmitting me tranquility and security. In addition, I also thank him for helping me find an internship by listening to my needs. Without him, it would not have been possible.

A special thanks to Professor Chris Mi for hosting me in his laboratory at the San Diego State University as a research scholar giving me the opportunity to learn a lot in the field of electric vehicles and wireless power transfer. Prof. Mi has always made himself available to all my problems and has been of fundamental help during my entire period of research.

Thanks to Dr. Jianghua Lu, my colleague, in the realization of the work done. Together we have developed ideas, considerations and implementations present in this project.

A further thanks to Professor Spadacini who made himself very helpful for the final draft of this document.

Last but certainly not least, I thank infinitely the support of my family during these years. I have always been able to count on unconditional help from them, at all times, even the hardest.

ABSTRACT (EN)

Over the past years, electric vehicles (EVs) have become an increasingly attractive mobility solution. Consequently, the research for an adequate, efficient and safe recharging system is constantly in progress. Alternative charging systems have been proposed by the world of engineering and wireless charging presents a good solution to some requirements such as the need for frequent, high-performance and safe charging for users. However, among the various research topics of this type of recharge there is the concept of Foreign Object Detection (FOD) for metal object (Screws, tools, coin etc.) and living objects (animals or people). The Field-Based method is a good compromise between results accuracy and cost containment. Different methods are often necessary for detecting metal and living objects separately. In this thesis a new Field-Based method is proposed with the advantage of being able to detect metal and living objects with the same device. The Detection coil and a sensing circuit are the characterizing and fundamental elements of the method; these components are designed through a simulation path with Electromagnetic and circuital simulation software. Furthermore, a laboratory experimental validation was carried out to confirm the results obtained.

The project is organized through five chapters. In the first chapter the background of the thesis topic is reported, from the motivation of alternative charging systems for electric vehicles, to wireless charging and the concept of foreign objects detection. Finally, an overview of the current FOD methods is presented. In Chapter 2 the Field-Based method, both for the detection of Metal Objects (MOD) and for the detection of Living Objects (LOD) was chosen as a research topic and a state of the art is reported through a summary of the most current works in literature. In Chapter 3 the model of the proposed Field-based method is developed focusing on the design of the detection coil, which consist of a sensing pattern suitable for the detection of foreign objects. The design consists of a path of Electrostatic and Eddy Current simulations with the ANSYS software of the various parameters of the detection coil, and laboratory measurements to confirm the results obtained. In Chapter 4 a second simulation part of this thesis is carried out with the aim of designing the sensing circuit of the proposed method. The simulations were carried out through the LTspice software. Finally, in Chapter 5, conclusions and possible future works are reported based on the results obtained in the previous chapters.

The proposed method satisfies the objective set for a single method for the detection of both metal objects (MOs) and living objects (LOs), presenting sensitivity results comparable with the current state of the art of FOD methods. The detection of the position of the object (DoP) is another important result obtained. The flexibility in the design of some parameters for the method makes it adaptable to different applications in wireless power transfer.

ABSTRACT (IT)

Nel corso degli anni, il graduale inserimento di veicoli elettrici (EVs) nel settore della mobilità risulta essere una soluzione sempre più convincente. Come diretta conseguenza, è in continuo sviluppo la ricerca di un sistema di ricarica adeguato, efficiente e sicuro. Fra le varie tipologie studiate, la ricarica wireless rappresenta una tecnologia ottimale per soddisfare la necessità di una ricarica frequente, ad alte prestazioni e sicura per gli utenti. Tuttavia, tra i molteplici problemi di ricerca affrontati in questo campo è di particolare interesse lo studio della rilevazione di oggetti estranei (FOD) nello spazio di ricarica; nello specifico si considerano oggetti metallici (viti, chiavi, monete ecc.) ed oggetti "viventi", ovvero animali o persone. Il metodo di rilevamento Field-Based è un efficace compromesso tra accuratezza dei risultati e contenimento dei costi. In genere, questo metodo presenta proprietà intrinseche dei componenti differenti per rilevare oggetti metallici e/o viventi. In questa tesi, viene proposto un nuovo metodo Field-Based con il vantaggio di poter rilevare oggetti metallici e viventi con un unico dispositivo. Gli elementi caratterizzanti e fondamentali del metodo sono una bobina di rilevamento (Detection Coil) ed un circuito sensitivo (Sensing Circuit). Questi componenti sono ideati tramite un percorso di simulazioni elettromagnetiche, un'analisi circuitale ed una validazione sperimentale.

Il lavoro è organizzato in cinque capitoli. Nel primo capitolo viene riportato il background dell'argomento di tesi; In primo luogo si motivano sistemi di ricarica alternativi per i veicoli elettrici e si evidenzia la convenienza della ricarica wireless. Successivamente, viene esposta la problematica e la casistica degli oggetti estranei in questo contesto. Per concludere, viene presentata una panoramica degli attuali metodi di rilevamento (FOD). Nel capitolo 2 è stato scelto il metodo Field-Based come argomento di ricerca e viene riportato un attuale stato dell'arte della tecnologia sia per il rilevamento di oggetti metallici (MOD) che per il rilevamento di oggetti viventi (LOD). Nel capitolo 3 viene sviluppato il modello del metodo Field-Based proposto, incentrato sulla progettazione della bobina di rilevamento, la quale consiste in un percorso sensitivo adatto al rilevamento di corpi estranei. Il design prevede diverse simulazioni Elettrostatiche ed Elettromagnetiche realizzate con il software ANSYS per l'ottimizzazione dei parametri della bobina. In seguito, i risultati ottenuti vengono validati tramite delle misurazioni sperimentali su un prototipo reale. Nel capitolo 4 viene condotta una seconda parte di simulazioni con l'obiettivo di teorizzare un circuito sensitivo per il metodo proposto. In questa sezione, il circuito viene simulato tramite il software LTspice. Infine, nel capitolo 5, sono riportate le conclusioni e possibili lavori futuri basati sui risultati ottenuti nei capitoli precedenti.

Il metodo proposto soddisfa lo scopo fissato di un unico metodo Field-Based per il rilevamento sia di oggetti metallici (MO) che di oggetti viventi (LO), presentando risultati, in termini di sensibilità, comparabili con gli attuali metodi presenti in letteratura. Il rilevamento della posizione dell'oggetto (DoP) è un ulteriore importante risultato ottenuto. Inoltre, la flessibilità nella scelta di alcuni parametri di progetto, rende il lavoro adattabile a diverse applicazioni nell'ambito del trasferimento di energia wireless.

CONTENTS

LIST OF FIGURES

LIST OF TABLES

NOMENCLATURE

ICE	Internal Combustion Engines
HEV	Hybrid Electric Vehicles
EV	Electric Vehicles
FCV	Hydrogen Fuel Cells Vehicles
WPT	Wireless Power Transfer
IPT	Inductive Power Transfer
TX	Transmitting coil
RX	Receiving coil
FO	Foreign Object
MO	Metal Object
LO	Living Object
FOD	Foreign Object Detection
MOD	Metal Object Detection
LOD	Living Object Detection
DoP	Detection of Position

CHAPTER 1. INTRODUCTION

In this chapter the expansion of electric vehicles is taken into account, highlighting the benefits but also how some limitations are still present. After justifying how the research for an alternative charging system can solve some of the problems of EVs, the wireless charging system is introduced in its forms. Then, the problematic, properties and the detection of foreign objects is explained.

1.1 Background: The Electric Vehicles

For well-known environmental reasons, a reduction in fossil fuel demand is necessary. As the transport sector is the largest consumer of fossil fuel, the so-called "Electrification" of this sector it could be a good solution to reduce the demand for fossil fuel. By electrification is meant the total or partial replacement of internal combustion engines (ICE) with hybrid electric vehicles (HEV) or electric vehicles (EV). There are also other clean energies applicable to the transport sector such as for example the hydrogen fuel cells vehicles (FCV). This transformation is in continuous development and a continuous research of the engineering world is trying to develop this expansion. In the railway system or in buses, electrification has already been an important part of the sector for some years as the fixed path makes electric recharging structures easy to implement. By focusing on EVs, they have the best advantages in terms of environmental impact and CO_2 emission ss the engine is purely electric. However, EVs are not so attractive to consumers for their still high selling cost and their limitations. The world of research is therefore constantly looking for new technological solutions to increase their development by reducing costs and the still present problems. The trend of the last years shows how the number of EVs is continually increasing making them possible to compare with the ICE in terms of costs, performance and drive reliability. For the complete extension of EV (or HEV) it is necessary to frame the limitations, how it is possible to improve them and how.

The main limitations of EVs can be summarized in these main points:

- Cost and performance of the battery: up to 30% of cost of the vehicle;
- Limited driving range: related to the lifetime of the batteries;
- Safety and reliability.

These concerns are all related to the design of the batteries. In fact, a battery that meets certain specifications solves or improves all three of the above points. However, the design of a battery it is not so easy as many requirements must be achieved at the same time. Some of them are high energy and power density, long cycle lifetime, good safety and reliability always trying to keep their cost affordable. Lithium-ion batteries seem to be the most adequate to achieve these specifications, however costs and performances need to be improved in comparison with the ICE. An adequate charging system is the key to reducing the limits of the batteries, so in this way the driving range and performances can be improved and the overall cost can be decreased. Safety for the users is also strictly related to the charging system.

1.1.1 Charging System of the EVs

We can say the main problem of EVs is the limited drive distance of the vehicle (much less than traditional vehicles) due to the recharging of the batteries, so the HEVs are still favoured, as they can extend this limit, until the battery technology will be able to make the costs and autonomy of EVs acceptable. A pure electric car indeed, requires a battery system capable of storing enough energy for acceptable driving distances. The batteries, as chemical accumulators, require particular materials for their construction, which often have a decisive influence on the cost of EVs, often making it about twice as much as ICE vehicles. The EV charging technology is therefore the key to the expansion of electric cars as faster and more efficient charging times contribute to reducing the cost of batteries, which as mentioned is the main component of high costs. In fact, faster recharges imply the possibility of more frequent recharges and in this way the energy storage of the batteries on board can be decreased.

There are substantially two type of charging for vehicles: Conductive Charging, and the Wireless Charging. There is also the possibility of replacing the batteries (battery swapping) but this solution has too high costs and questionable eco-sustainability.

The conductive charging (Fig. 1-1 (a)) is the most common, since it is the simplest and is more efficient. In this type of charging the user must insert a cable into a car socket that includes a connector that connects the vehicle to the charging structure. The recharge can happen with isolated columns or grouped in charging stations. However, there are several disadvantages. Leakage from cracked old cable, can bring additional hazardous conditions to the owner. Also, people may have to brave the wind, rain, ice, or snow with the risk of an electric shock. In addition, the charging station needs frequent maintenance. These factors report the reliability and safety of conductive charging questionable.

As a result, over the years, alternative charging technologies have been investigated and inductive charging, or more generally wireless charging (Fig. 1-2 (b)), has been

developed as it does not present the problems just mentioned of conductive charging. This technology is intended to make charging stations more accessible to the user. In this type of system, the cable is replaced by a wireless coupling between a circuit under the road surface and a circuit inside the vehicle chassis, thus avoiding contact between the user and electric parts. The system, not presenting interactions between humans and the infrastructure would therefore be automated. In addition, the charging stations can be inserted in places where vehicles normally stop as traffic lights, bus stops or taxis and parking lots; in this way, the charging could be more often and the charging time can be reduced.

Figure 1-1: Charging System for EVs. Conductive Charging (a), Wireless Charging (b).

Thus, we can say that the wireless power transfer (WPT) technology applied to the EV's charging, which can eliminate/reduce all the conductive charging troublesome, is desirable by the EV owners. By wirelessly transferring energy to the EV, the charging becomes an easier task. For a stationary WPT system, the drivers just need to park their car and wait for the recharge to complete by itself. Furthermore, for a dynamic WPT system (charging while driving), the EV is possible to run forever without any stop. As a direct consequence the battery capacity of EVs with wireless charging could be reduced if compared to EVs with conductive charging.

A general classification of the methods (or system) to charge the electric vehicles is shown in the Fig. 1-2.

The WPT is classified on the basis of the energy carrier which can be mechanical or electromagnetic, the latter and much more widespread are divided are divided into three types: electromagnetic radiation or by induction which can be capacitive or inductive. The Inductive Power Transfer (IPT), is the most popular wireless technology as present long transfer distance, large transfer power capability, and high efficiency. It also has the advantages of good safety and moderate costs compared to the other wireless methods. For these reasons, WPT and IPT are often considered the

same technology. The frequency of the power transfer and the electromagnetic structures differentiate these two types.

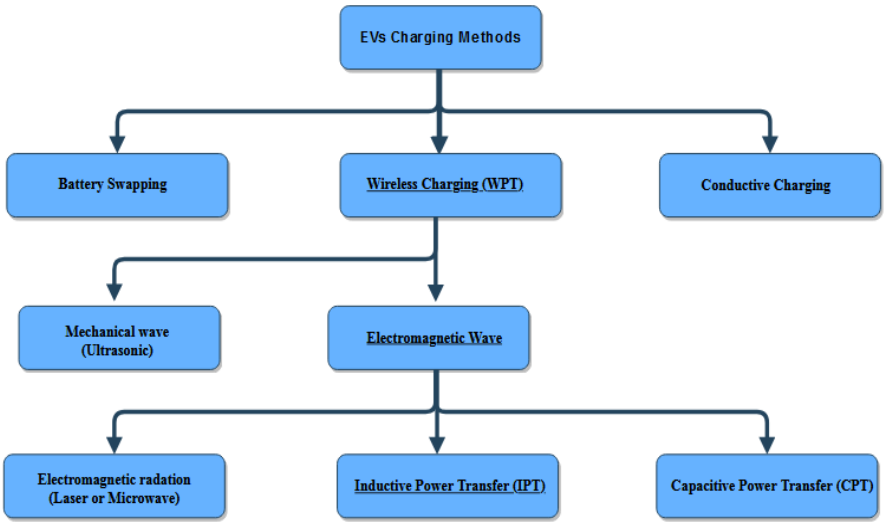

Figure 1-2: Charging Methods for EVs.

The central branch of the chart shows the path taken in this thesis; in fact, we focus on wireless charging and specifically the IPT.

1.1.2 The Inductive Power Charging in EVs

This section evaluates the IPT used in electric vehicles. The components of the system are analysed, highlighting their function and the current state of the art. A typical topology for wireless EV charging is depicted in Fig. 1-3.

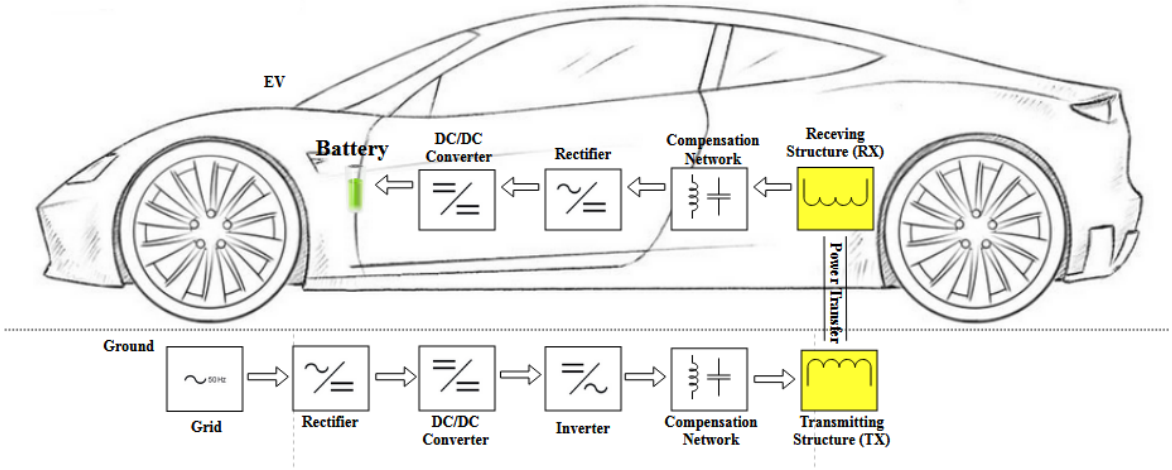

Figure 1-3: Typical WPT topology for EVs.

Starting from the ground side, there are several stages to charge an EV wirelessly. First, the utility ac power (grid) is converted to a dc power source by an AC to DC rectifier usually with a power factor correction. Then, the dc power is converted to a high-frequency ac inverter to drive the transmitting coil through a compensation network. In this part the converters work at the resonant frequency of the compensation network. Thus, in the ground side we have an AC/DC/AC power conversion.

The high-frequency AC current flows through the transmitting coil (TX), generating magnetic flux, part of which is linked to the receiving coil (RX) making possible the wireless power transfer through the air. An air gap is therefore present between the ground and the car chassis. The TX and the RX are also called charging pads. In both the TX and RX structures, in addition to the power pads is present an aluminum plate and a ferrite plate; The first has the function of a shield to do not disperse the magnetic flux, while the second serves to confine the magnetic flux in the air gap. In this way the magnetic field outside the charging pads can be greatly mitigated. In fact, it is important to achieve a high coupling coefficient k and quality factor $Q = \frac{\omega L}{R}$. In general, by increasing the geometrical dimensions of the pads, the system response with higher efficiency, but this is not an optimal approach for costs. To increase the value of Q, high frequencies are often used as proportional to it. In the recent state of art. frequency between 20 and 150 kHz are used [1]. These high frequencies involve the use of Litz wire to contain the ac losses of the copper coils. For what concern the coupling coefficient k different geometry, configuration and material of the coupling coils are designed and studied to obtain high values of k. First, it is possible to divide the types of pads into double-sided and single-sided types, according to the magnetic flux distribution area [1]. For the double sided a flattened solenoid inductor are usually used while for the single sided types a Unipolar pad or a Rectangular (DD)

pad are the two most used geometries [1]. The IPT with dynamic applications, on the other hand, has different structures. In fact, since the vehicle is recharging while it is in movement, the TX and RX structures are not pads anymore, but tracks to cover long distances such as, for example, part of a fixed route of a bus. The most common shapes are the U, W or I type [1].

In addition to the electromagnetic structure, it is present a LC compensation network that works with a resonance frequency both in the vehicle and ground side to improve the efficiency of the power transfer. In fact, the pads are loosely coupled with a large leakage inductance. The network is composed of one or more capacitors which work at a fixed resonance frequency to reduce the reactive power of the circuit. According to the circuit topology both in the primary (ground side) and secondary (vehicle side) side there are different types of networks: SS, SP, PS, PP and combinations of these types. The first letter indicates whether the resonance is series “S” or parallel “P” type for the primary side while the second letter specifies the secondary side. The Series compensation is the most used in the primary side while on the secondary side parallel compensation is often preferred for better load control. [2].

Finally, in the vehicle side the power is converted back to dc with another rectifier and a DC/DC converter powers the car battery making possible its control.

An important concept regarding IPT and WPT in general is the user's exposure to electromagnetic radiation. As mentioned before, IPT avoids the electrocution danger from the traditional conductive recharge. However, during the charging time, a high-frequency magnetic field existing between the TX and the RX. An important goal, to maintain the safety towards the user of wireless charging is therefore to ensure that the magnetic field should meet the safety guidelines when people are outside the vehicle or sitting inside, Thus, it is important to define safe area for the users. During the years, three standards have been issued. Two standards in 1998 and 2010 were published by the International Commission on Non-Ionizing Radiation Protection (ICNIRP) while the third one by the IEEE International Committee on Electromagnetic Safety in 2005. Specifications are shown below in Tables 1 and 2.

Note that for the ICNIRP standards, the limit values of the magnetic field and the type of exposure depend on the IPT frequency of the IPT while the third standard replaces the frequency with the part of the body exposed. The 2010 standard being the most conservative is the most followed for high power applications. The ferrite and the aluminium plates can greatly mitigate the magnetic field outset the charging airgap reaching the above standards.

Table 1-1: ICNIRP 1998/2010 safety guidelines [3].

Type of exposure	**Frequency**	**Limit (Maximum value of magnetic field permitted)**
Occupational exposure	[0.82-65] kHz	30.7 μT (until 1998), 100 μT (from 2010)
	[0.065-1] MHz	$2/f_{(MHz)}$
General public exposure	[0.8-150] kHz	6.25 μT (until 1998), 27 μT (from 2010)

Table 1-2: IEEE 2005 Electromagnetic safety standard [4].

Type of exposure	**Body part exposed**	**Limit (Maximum value of magnetic field permitted)**
Occupational exposure	Head and torso	615 μT
	Limbs	1130 μT
General public exposure	Head and torso	205 μT
	Limbs	1130 μT

1.2 Foreign Object Detection in the IPT

As we have seen in Subsection 1.1.2, a high-frequency AC current flows through the TX, generating a strong magnetic flux, part of which is linked to RX.

If some conducting material, such as metal object like a key, a clip, a coin, a screw, or a staple, falls between the TX and the RX during the charging time, an eddy current will be generated in the metal object. This current first overheats the object and over time could cause a fire in the charging area. Since the airgap between TX and RX is quite high in EVs charging, other dangerous scenarios may be animals such as a cat or a dog present between the pads or toddlers grabbing a ball rolling under the vehicle or a driver who could put his arm under the vehicle to retrieve some fallen objects. In fact, the magnetic field of IPT could be dangerous also for the human or animal skin. As safety is one of the strong points of IPT, it is absolutely necessary to study these problems and avoid possible complications associated with them.

To deal with these problems, the IPT system should be able to detect Foreign Objects (FOs) which may be present in the airgap. From the examples cited above, the FO divides into two categories according to the nature of the object: conductive or Metal Objects (MO) and Living Objects (LO). Cases with both types can be present as for the last example of the human arm (LO) that tries to recover a key or a coin (MOs) under the vehicle. In recent years, the study of these cases has created the term Foreign Object Detection (FOD) divided into Metal Object Detection (MOD) and Living Object Detection (LOD). FOD is the key to solving these issues and making IPT increasingly attractive to the transportation market.

As a first step, the next two subsections MO and LO are analysed separately.

1.2.1 The Metal Object concern

Focusing on metal objects, the influence of their intrusion in the charging zone has the effect of increasing the temperature of the object. The cause, instead, is the so-called Eddy current which is created in the MO exposed to a high frequency magnetic field. The effects of the eddy current are analysed in two aspects, one is the magnetic field, and the other is the impedance characteristic of the TX.

In [5] is the Eddy current effect from the magnetic point of view is explained. Fig. 1-4 shows the schematic diagram of the eddy current.

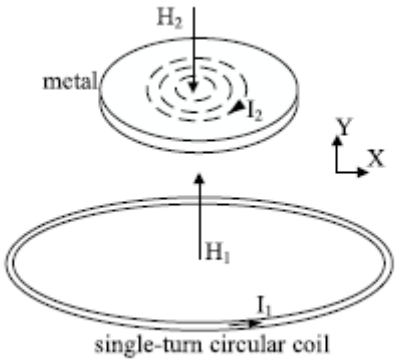

Figure 1-4: Eddy Current effect [5].

The magnetic field H_1 and the primary current I_1 represent the TX. We can see that if there is a MO an induced electromotive force (EMF) will be generated resulting in a current I_2 inside the object. This current is the Eddy Current. Consequently, the magnetic field H_2 will be generated in the metal which is opposed to the magnetic field of the TX that generated it. From this phenomenon we can define the mutual inductance M between the TX and the object and the induced voltage U in the MO.

$$M = \frac{\phi}{I_2} = \frac{\iint B dS}{I_2} \tag{1.1}$$

$$U = \omega M I_1 \tag{1.2}$$

Where, referring again to Fig. 1-4, ϕ is the portion of the magnetic flux linked with the MO with area S, placed parallel to the TX and B is the magnetic field strength at the object area.

From the magnetic analysis it was therefore first explained the origin of the overheating of the object and then from the analysis of the derived quantities it is deduced how the presence of a MO causes the variations of the system parameters. In fact, M and U will affect the TX parameters. A safety problem can therefore also turn into a functional IPT problem.

Dangerous situations are illustrated in Fig. 1-5 from [6]: the temperature of the MO can rise to 300°C within several minutes. Moreover, we note how even a little object such as a gum wrapper can damage the TX.

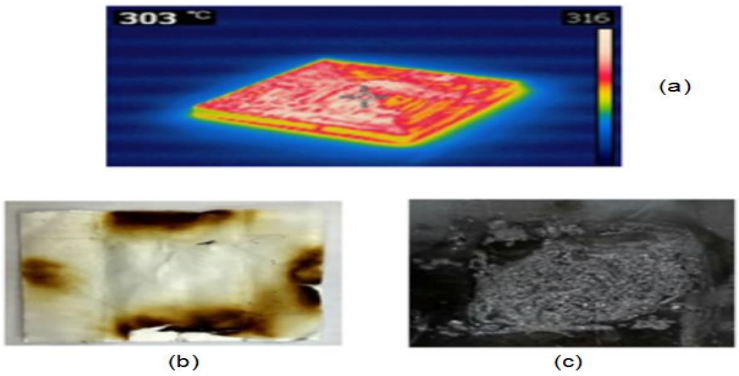

Figure 1-5: Dangerous situations caused by MO in IPT: (a) Temperature of the MO, (b) Example of a burned gum wrapper, and (c) Damage of a TX due to a burned MO [6].

In order to analyse the detection methods, a second circuital approach to the eddy currents effect is considered. In this case the characteristic impedance of the TX is carried out. As explained above, a magnetic coupling is established between the MO and the TX and therefore its impedance undergoes a variation. In [7] this fact is explained by Fig 1-6:

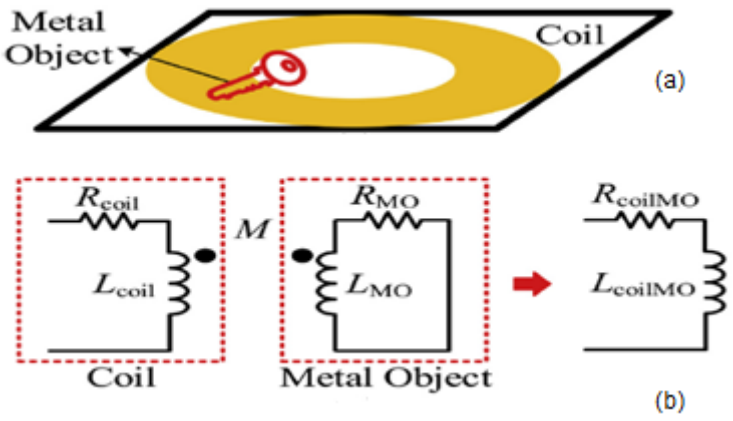

Figure 1-6: Schematic (a) and Equivalent circuit of the TX with the presence of a MO [7].

In Fig. 1-6 (b): L_{coil} and R_{coil} model the TX, L_{MO} and R_{MO} model the metal object, M is the mutual inductance of (1.1) between the TX and the MO and finally L_{coilMO} and R_{coilMO} are the equivalent inductance and resistance of the TX after inserting the MO.

Thus, the new impedance of the TX can be derived:

$$Z_{TX} = R_{coil} + j\omega L_{coil} + \frac{(\omega M)^2}{R_{MO} + j\omega L_{MO}} \tag{1.3}$$
$$= \left(R_{coil} + \frac{(\omega M)^2 R_{MO}}{{R_{MO}}^2 + (\omega L_{MO})^2} \right) + j\omega (L_{coil} - \frac{(\omega M)^2 L_{MO}}{{R_{MO}}^2 + (\omega L_{MO})^2})$$

The very important conclusions are that, with an MO, compared with the reference case without an MO, the TX equivalent inductance decreases and the equivalent resistance increases.

An important challenge for a detention system is to be able to distinguish the difference between the existence of an MO and coil misalignment. In fact, the misalignment between TX and RX could also cause variation in the coil impedance.

For a ferrous MO, such as the ferrite pad of the IPT, the equivalent inductance may increase related to the sign of M.

Even with this second approach, we can conclude that a MO will influence the safety, as well as the system charging performance.

This phenomenon will be exploited both in the Electrical system parameters detection methods and in the Field-Based methods for the MOD. In fact, the analysis above can be referred not only to the TX but also to the RX or to a generic coil (detection coil). In the first case the impedance variation of the transmission coil is directly exploited to detect the MO; In the second case, the circuit above analysed will no longer be the one that models the coupling between the transmitter coil and the MO but it will be the circuit modelling the coupling between the MO and a coil external to the power transfer system.

From the analysis above, it is possible to conclude that the fundamental parameters to be considered in the various MOD methods are

- The Induced Voltage and its inductance variation;
- The Mutual Inductance with his voltage induced.

1.2.2 The Living Object concern

Even in some application such as food industry, airport runway, security inspection or item recovery FOD is present and the detection of MO may be enough as human interference in areas at risk of exposure are reduced to a minimum. However, in IPT for EV's, a protection system also for the so called "Living Objects" is necessary. In fact, in Subsection 1.1.2 we have seen the limits of the magnetic field imposed by the ICNIRP and IEEE standards and, in the area between TX and RX, the magnetic field values may exceed the reference values of the general public exposure standards. The LOD system must be able to detect the LO and promptly stop charging if it is already in progress or do not start it in offline configuration.

In the study of this problem, we can think about practical scenarios: for example a cat that is under the vehicle which may not be seen by the user intending to start the recharge or a child intent on grapping a ball that has rolled under the car. The example of the user (LO) intent on recovering a key (MO) was also mentioned previously. LOs electrical influence differently the IPT system respect to MOs as the magnetic field does not undergo significant variations; therefore, the detection of foreign objects must take into account the distinction and the ability to detect both types of objects.

1.3 Overview of Foreign Object Detection Methods

According to the difference in the detecting objects (MOs or LOs), the detection of foreign object can be divided into MOD and LOD, as shown in Fig. 1-7.

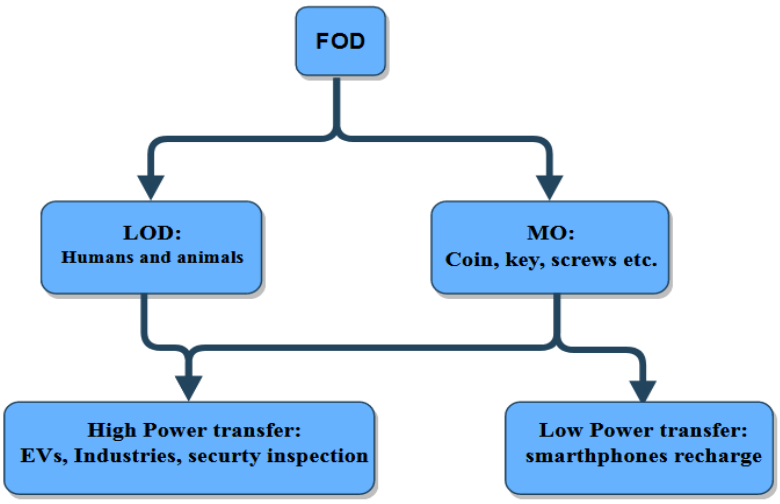

Figure 1-7: Category of FOD according to the detection object.

High power applications require detection of both types of objects as their presence implies both functional problems of the system (high temperatures and loss of efficiency) and safety problems for LOs. The MOD is enough for low power applications such as wireless charging of our smartphone as the exposure to the magnetic field to LOs does not involve safety problems.

There are several detection methods at the current state of the art; it is therefore possible to make a second classification based on the detection technology principle [8].

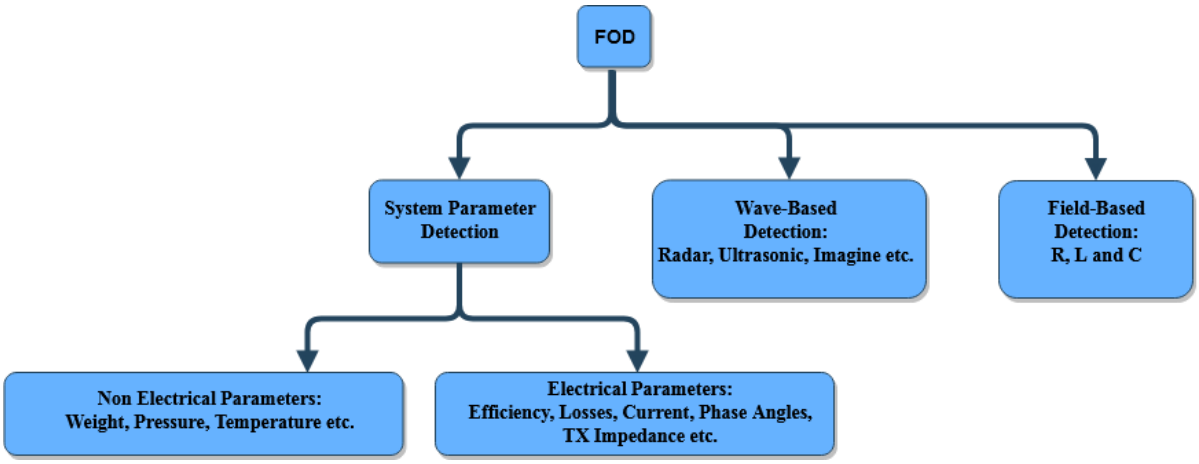

Figure 1-8: Category of FOD according to the detection method.

Starting from the left of Fig. 1-8, in the system parameter detection methods, there are two kinds of system parameters, namely electrical parameters and non-electrical parameters.

The use of electrical parameters such as a current, the efficiency, a phase angles or the TX impedance of the IPT system does not require any additional equipment as it simply measures these parameters making this the simplest and cheapest method. As explained in sub 1.2.1, the presence of a FO, specifically a MO, causes an extra power consumption of the IPT due to the presence of the eddy currents. This therefore causes a different efficiency, currents, impedance etc. A variation of the parameter caused by a FO is related to the same parameter of the system before the presence of the FO; for this reason this method works well for low-power applications while for high-power applications the parameter variation could be relatively too small compared to the absolute value of the system. Furthermore, the detection of living objects is not often practicable.

To extend this method to high power levels and to detect also LO's, it is more convenient to measure physical but not electrical system parameters (a typical

example is the temperature of the charging area) as their variations are not related to the IPT parameters. In this case, a thermal/pressure sensor and/or a transducer is required to measure this quantity increasing the total cost of the FOD. It is to be specified how these sensors do not distinguish if an object is a MO or a LO.

Changing completely the principle, Wave-based methods use sensing devices to detect FO's in the system such as imaging/thermal cameras or ultrasonic and radar sensors; In addition to visibly detecting the object, an imaging camera can also be useful for identifying the type of the latter. Thermal cameras work well for MOs as eddy currents significantly increase the temperature of the object. Ultrasonic and radar sensors instead, measure the distance to the target point that may be obstructed by a FO using the Frequency-modulated continuous-wave (FMCW) principle illustrated in Fig 1-9 studied in [9]. Basically, a radar sensor transmits an input signal $x(t)$ on a target and the receiving signal $y(t)$ will presents a frequency difference $\Delta\omega$ and a time delay Δt which represents the distance measured from the whole signal. A foreign object, obstructing this path, alters the radar parameters and it can be detected. This solution is useful for LOs where other methods may fail.

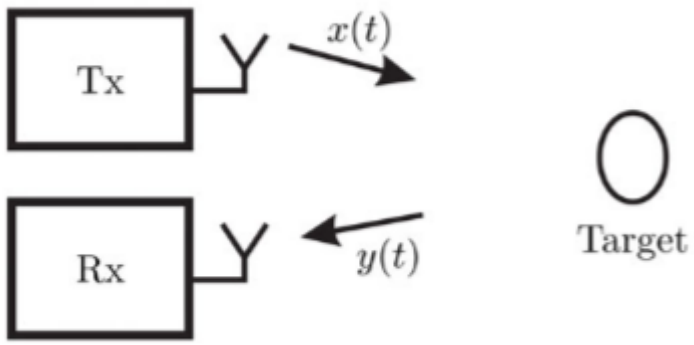

Figure 1-9: Principle of FMCW radar sensors in Wave-Based Detection methods [9].

In this method, it is important to consider the position of the radar. In fact, the radars can be positioned both on the EV side and on the ground side and the signal must cover the entire charging area and must not hinder the power transfer, all while maintaining a not excessive cost. Good results for any level of power (even if typically used for high powers) and type of object can be achieved but the extra equipment makes the cost of the method very high and often unsustainable. In addition, the detection system becomes complex to design.

Finally, there are Field-based methods. These methods are a derivation of the electrical system parameters methods since even in this case, the detection of a FO consists in detecting electrical parameters. The difference lies in the fact that instead of measuring a parameter already existing in the IPT, an extra coil (called detection coil), is designed in order to be used as a detection medium. Thus, the electrical

parameters become the resistance, the inductance or the capacitance of this coil. The cost and complexity of the system increase slightly but, in this way good results are obtained for any power level and it is possible to detect both metal and living objects. In Table 3, a comparison of the detection methods is shown underlining the power level application, the detectable objects, the costs and the accuracy of each method.

Table 1-3: Comparison of Detection Methods

Method	Power level application	FOD	Cost and Accuracy
Electrical System Parameter	Low	MOD	Low
Non-Electrical System Parameter	High and Low	MOD and LOD	Low
Wave-Based	High	MOD and LOD	High
Field-Based	High and Low	MOD and LOD	Medium

CHAPTER 2.
THE FIELD-BASED DETECTION METHOD

In this Chapter, the Field-Based detection methods are analysed with some literature examples belonging to the most recent state of the art (2018-2019). The Field-Based method is used for both MOD and LOD. First, MOD is explained considering each component of the system (Sensing pattern of the detection coil, sensing circuit and other main stages). The problem of blind zones is presented. Then, LOD is shown, considering the similar parts to the MOD and the different features.

2.1 Field-Based Detection for MOs

The field-based method is widely used for the detection of metal objects since the effects explained in subsection 1.2.1 are exploited. A coil is inserted in the system over the TX in order to detect the MOs (Fig 2-1). This component is called Detection Coil. Field-based method for MO is also known as Magnetic-Field change sensing (MFCS).

Figure 2-1: Field-Based schematic for MOD [5].

The inductances and the quality factors, therefore the impedance, of the detection coils change with an adjacent MO, the same as shown in Subsection 1.2.1. The eddy currents that are created in the object, create a distortion of the magnetic field. In electrical system parameters this distortion is measured through the transmission coil while in this method the same principle is used with the detection coil. The advantage is possible to design the coil with the specific purpose of detecting metal objects as it is not an active part of the IPT. The smaller the object, the more the distortion of the magnetic field is relatively small compared to the system. By decreasing the total size of the coil, it is possible to make the effect of small MOs relatively higher. Therefore, we note the advantage of being able to size the detection coil ad hoc to detect pre-

selected metal objects, which is not possible with the system parameter detection methods since the TX size is set by the system's energy needs.

Theoretically, the change in inductance of the coil can also be caused by the misalignment between the TX and the RX but in general the airgap is large enough to make this effect negligible and bring back the change in inductance to foreign objects only.

Thus, the MOD system includes a detection coil mounted on the surface of the TX pad, and sensing circuit. If the magnetic field change exceeds a predefined threshold caused by one or more MO, the system will send a signal to stop, reduce or do not start the power of the IPT.

2.1.1 Design of the MOD Sensing Pattern

Besides affecting the inductance and the equivalent resistance, as we have seen in Subsection 1.2.1, the existence of an MO will also affect the mutual inductance between the transmitting coil and the detection coil and its induced voltage. In the various Field-Based methods present in the current state of the art, the reference, based on the application, is made to one or more of these quantities based keeping in mind that they are connected to each other. The most used quantity as reference is the induced voltage variation; Starting from this quantity, there are two kinds of detection methods.

- **Passive Method:**
  This method uses the magnetic field of the IPT to induce a voltage on the detection coil, i.e., the TX acts as the source coil. No extra source is employed.
  Subsequently the sensing circuit will be introduced which is an active circuit; however, it is still a passive method since we mean by source those active parts of the system with powers similar or equal to the IPT system. The sensing circuit, on the other hand, is mainly a signal conditioning with reduced power.
- **Active Method:**
  In this more complicated method, the detection coil is composed of a transmitter and a receiver in a similar way to IPT.

In this Subsection and in the following ones, the main components of the system are analysed assuming a passive system therefore without auxiliary active detection coils. The active method will be analysed subsequently specifying the differences from the passive method.

The detection coil, the main component of this method, is essentially composed of a sensing pattern or sensing path which is an inductive circuit or loop designed to accentuate the magnetic distortions of metallic objects. The sensing pattern can be designed also for living object detection as we will see in Subsection 2.2.1 and in the developed method present in Chapter 3. This circuit must be able to be sensitive to metal objects of as many shapes and sizes as possible and must not affect the IPT power transfer. In this Subsection are reported the principles for the design of this sensing pattern with some examples present in the current literature.

To detect a magnetic field change (voltage/inductance variation), a first classification divides the sensing paths in two types shown in Fig. 2-2:

- Overlapping type;
- Non-overlapping type.

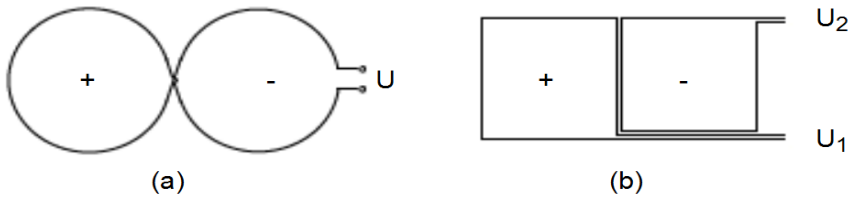

Figure 2-2: Basic shape principle of sensing coils for MOD: (a) overlapping type, and (b) non-overlapping type [6].

The two configurations not only show the first works for this method but are useful for explaining the fundamental principle of operation present in even more complex coils.

The first one was developed by WiTricity [10], and it is called overlapping type because it includes only one wire which creates two identical loops. According to the well-known Faraday's law, the induced voltage U, on the wire is determined as follows:

$$U = \frac{d\phi(t)}{dt} \begin{cases} = 0 \; without \; MO \\ \neq 0 \; with \; MO \end{cases} \tag{2.1}$$

Where ϕ is the magnetic flux flowing through the area of the two loops over time. As shown in Fig. 2-2(a), the loop current flow through the wire in opposite directions; + direction for the left loop, - direction for the right loop. As shown in Eq. 2.1, the resulting induced voltage U in the wire, assuming a uniform magnetic field is zero since the left component cancels the right component. The presence of an MO distorts the magnetic field unevenly making the components of the two loops different. As a result, U has a non-zero value and the object can be detected. At least two detection

coils are connected in reverse directions, forming balanced coils, to cancel out the induced voltage. Fig. 2-3 shows some examples:

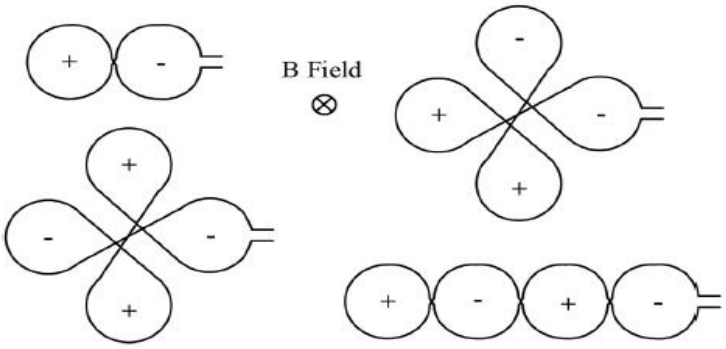

Figure 2-3: Different detection coil overlapping shapes [10].

Measuring the voltage change is obviously a direct consequence of the detection coil inductance change being two directly proportional parameters:

$$U_{loop} = j\omega L_{loop} \tag{2.2}$$

However, a MO could position itself in a location which presents a symmetrical distortion of the magnetic field, without causing the induced voltage to deviate from zero. This is the blind zone problem which will be take into consideration in the next subsection.

On the other hand, the non-overlapping sensing coil developed by KAIST [11], has two wires which form two independent loops. The voltage U is calculated from the difference of the individual voltages of the loops:

$$U = U_1 - U_2 \begin{cases} = 0 \; without \; MO \\ \neq 0 \; with \; MO \end{cases} \tag{2.3}$$

As in the previous case, an MO causes a resulting induced voltage different from zero. The non-overlapping design usually requires only one-layer. However, blind zones could affect this configuration too.

Regardless of the shape and type of coil, during the sensing pattern design phase it is therefore necessary to have a zero voltage as a reference condition. In this way the detection of the object will be simpler since the voltage will be different from the reference point which is zero. Furthermore, having a zero voltage in the detection coil is necessary to avoid affecting the performance of the power transfer (decoupling between the TX and the detection coil).

Different coil geometries both overlapping and non-overlapping as shown in Fig. 2-4 [12]. The types a, c, f, g and h are non-overlapping coils; the models b, d and c are overlapping types. Different sensitivities of the inductance are presented in [12] and other works but as a general result more complex shapes present better results but cause greater complexity and costs of the detection coil.

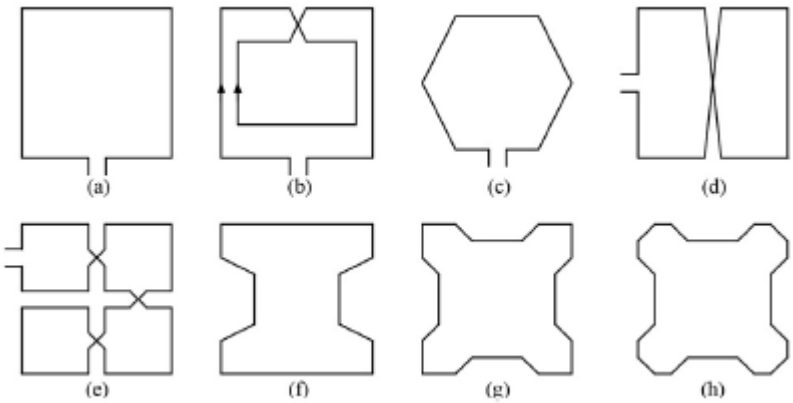

Figure 2-4: Overlapping and Non-Overlapping coil shape examples: (a) Conventional rectangular coil. (b) Rectangular double loop coil. (c) Hexagonal coil. (d) Double-D coil. (e) Quadruple-D coil. (f) Clover leaf-shaped coil 1. (g) Clover leaf-shaped coil 2. (h) Clover leaf-shaped coil 3 [12].

Once the type and shape of the coil have been chosen, the multiple elementary cells of the chosen form/type are distributed along the surface of the power transfer thus forming the layer of the complete detection coil.

Starting from the principle of Fig. 2-2 (b), an example of non-overlapping type coil with zero reference voltage is presented in [11]. The null voltage reference condition is achieved with the symmetrical arrangement of two coils in reverse direction called D coils and Q coils as shown in Fig. 2-5.

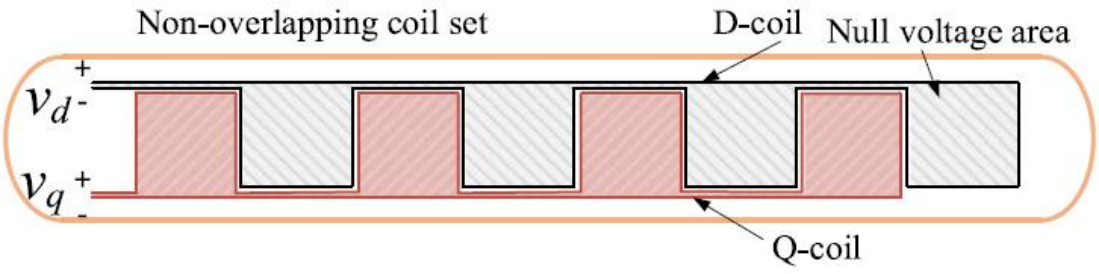

Figure 2-5: Non-Overlapped coil arrangement [11].

For both coil D and Q the magnetic flux is computed with Eq. 2.1 and the total induced voltage is calculated as in Eq. 2.3. Some null voltage area will be different from zero in the presence of a MO. The work in [11] allows us to introduce a further topic often present in the FOD methods: the Detection of Position (DoP) concern. Therefore, in addition to wanting to detect the FO, the aim is to detect the exact position of the object in the charging area.

To be able to detect the position of an MO but also of the vehicle position (DoP), longitudinal and lateral coil sets are combined to fully cover the charging area above the TX.

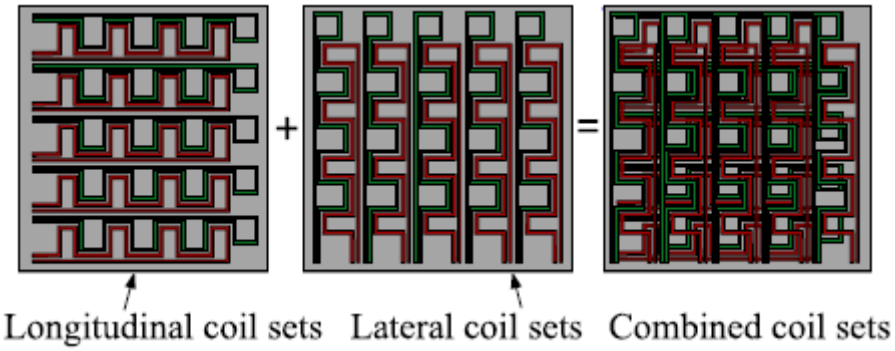

Figure 2-6: Space combination sets for a non-overlapped detection coil [11].

Fig. 2-6 shows that the coil sets are categorized into a longitudinal and a lateral placement to obtain information about the MO. This is an example how a non-overlapping structure becomes an overlapping structure to solve advanced problems as blind-zone or in this case the DoP combined with MOD. For each row and column of the arrangement there is a pair of coils D and Q. The system outputs can be grouped into two matrices: the induced voltages matrix and the induced voltages difference matrix. The first matrix deals with DoP as the voltages subject to the eddy currents of the MO vary with respect to the reference value. The second matrix instead serves for the MOD going to look for the differences of voltages different from the null value.

In [13], the sensing pattern, which consists of multiple rectangular coil sets where each loop has two coils connected in series with the opposite polarity to obtain again the condition of induced null voltage without the presence of a MO. The whole detection coil is shown in Fig. 2-7: the front view shows the opposite polarity of each coil and the blue and red arrows indicate the connections in series.

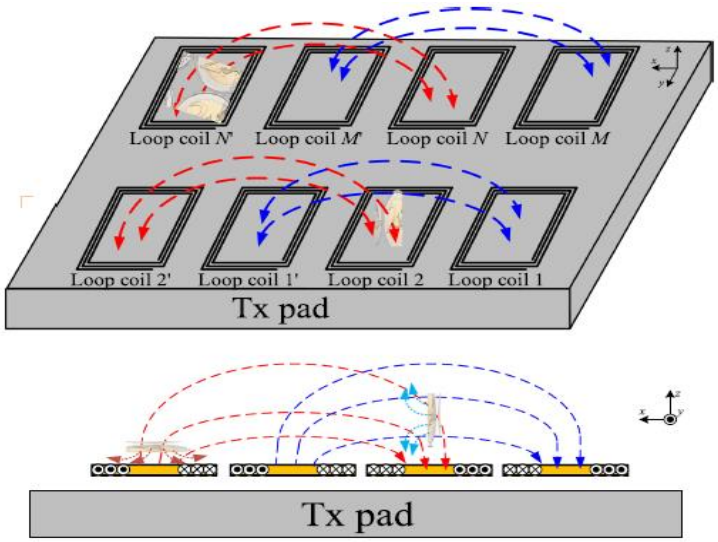

Figure 2-7: Multiple Rectangular coil in series for MOD [13].

In this project the variation in inductance is taken as a reference for the sensitivity of the system. This example shows us the trade-off between the sensitivity of the coil and the number of total sensing patterns. In fact, as the size of the single coil loop increases, its sensitivity decreases since the amount of the magnetic flux generated by the eddy current of the MO is relatively reduced compared to the one generated by the detection coil. Thus, thinking about small-sized coil, it is necessary to consider that a certain amount of sensing patterns are required to cover the entire area of the TX pad. Furthermore, a detection coil composed of multiple sensing patterns requires a signal processing system (Subsection 2.1.3) in order to scan each sensing coil which has dynamic performance inversely proportional to the number of sensing paths. Considering also costs and complexity of the system, a compromise solution is adopted.

Similar, in [6], the sensing pattern set includes many rectangular sensing coils, connected in series symmetrically along the axis parallel to the TX. Fig. 2-8 shows the normalized voltages induced on the coils along the TX pad. It can be seen how symmetrically opposed coils connected in series have the same voltage values induced with reverse polarity. With this design, the blind zone between two adjacent coils is eliminated without using multiple layers (subsection 2.1.2).

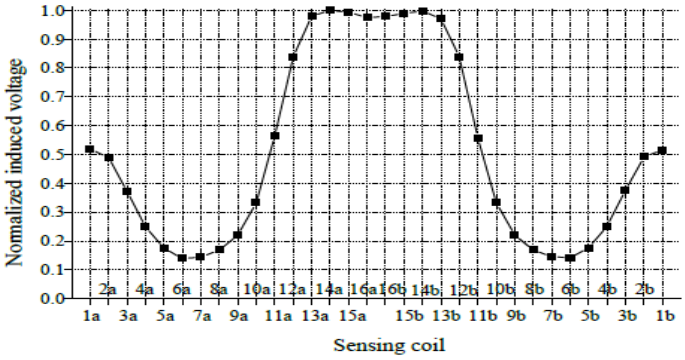

Figure 2-8: Induced voltages for a symmetrical detection coil [6].

We have seen in Subsection 1.2.1 how, another fundamental parameter when verifying the presence of a MO is the mutual inductance of the detection coil with the MO. In [5] this parameter is used. Simple rectangular detection coils are used also in this work.

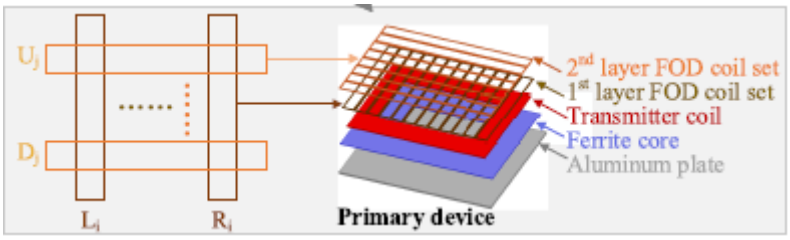

Figure 2-9: Two-layer Rectangular coil set [5].

In Fig. 2-9 we note how there is a layer with rectangular coils arranged vertically and a second layer with coils arranged horizontally making the DoP also possible. By dividing the detection coil surface in half, the first layer can be divided into a “Right” part and a “Left” part, while the second into an “Up” part and a “Down” part. In this way, by arranging an even number of coils, it is possible to couple them in pairs. The mutual inductance difference of the i-th coil set can be expressed as:

$$\begin{cases} |\Delta M_1| = \big||M(L)| - |M(R)|\big| & 1^{st}\ layer \\ |\Delta M_2| = \big||M(U)| - |M(D)|\big| & 2^{st}\ layer \end{cases} \tag{2.4}$$

Where:

- All mutual inductances are referred between the coil taken into consideration and the transmitting coil;

- $M(L)$and $M(R)$ represent the mutual inductance of the "Left" and "Right" detection coils side of the 1st layer.
- $M(U)$and $M(D)$ represent the mutual inductance of the "Up" and "Down" detection coils side of the 2nd layer.

Being a parameter proportional to the induced voltage, as in [6] the reference mutual inductance is the null value (without the object) as shown in Fig. 2-10. In Fig, 2-8 an even symmetry of the graph has been noticed along the TX axis because the induced voltages have equal modules but opposite polarity; In Fig. 2-10 instead, the graph shows an odd symmetry in that the inverse polarity of the induced voltages causes an opposite sign of the mutual inductance.

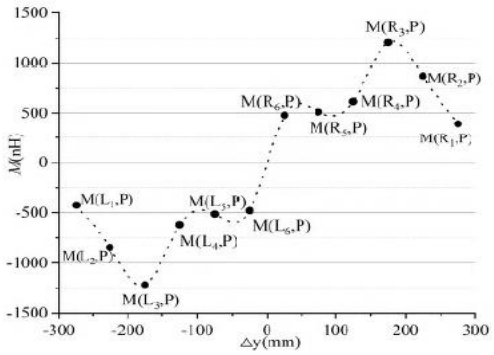

Figure 2-10: Mutual inductance without any object [5].

As in [11] it was done for the induced voltages, in [5] the single mutual inductances peaks with respect to the TX are used for the DoP while the difference of the mutual inductances along the symmetry makes the MOD possible by looking for values other than zero.

2.1.2 Blind zones: Multi-Layer coils

In the previous subsection it was mentioned how in the design of the sensing path of the detection coil we must face the problem of the blind zones both for overlapping and non-overlapping coils. Here, is explained what blind zones are and then some solutions for this problem are reported.

For blind zones is meant that, in specific positions, the MO may have the same impact on the detection coils so that the induced voltage remains close to zero (Fig. 2-11(a)). Thus, the detection of the MO fails.

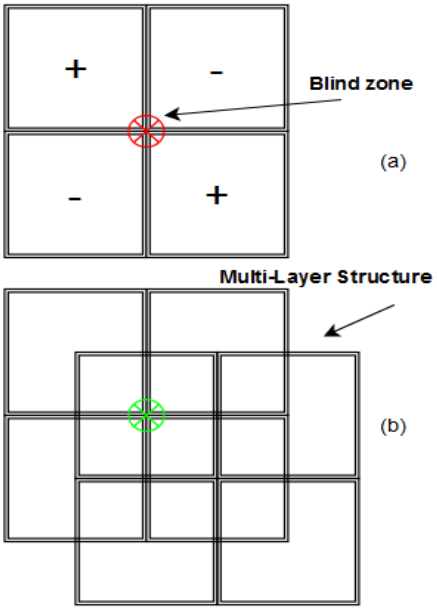

Figure 2-11: Blind zone (a) and Multi-Layer Structure (b).

A solution to solve this problem is to add another detection coil array with an offset, as shown in Fig. 2-11(b). Coming back to the example in [11] this solution is implemented as we can in the in Fig. 2-12.

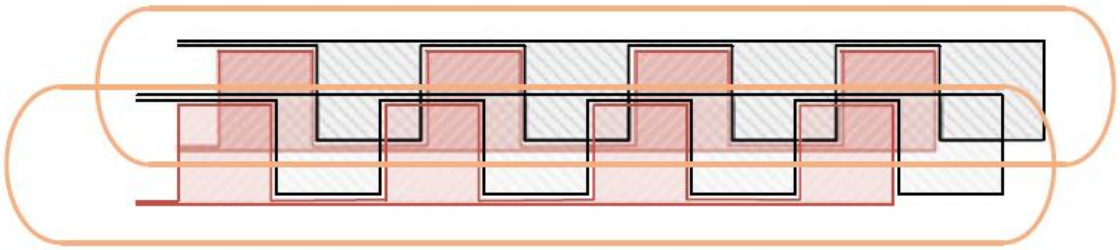

Figure 2-12: Implementation of multiple layers to avoid blind zones [11].

Adding a second layer with an offset, there is a translation of the blind zones. In this way these spots are no longer locations where the MO cannot be detected. More layers are inserted with different offsets in multiple directions, the more the number of blind zones is reduced, however is reasonable to limit the number of layers due to the cost and complexity of the PCB of the detection coil.

Alternately to multi-layer structures, often applied to simple typologies, specific solutions in relation to the characteristics of the sensing pattern must be designed to find out the blind zones and eliminate them.

For instance, in [6], the symmetrical and separate arrangement of the elementary cells allows the elimination of the blind zones without the addition of additional layers:

In Fig. 2-13 (a), if a MO is placed between coil ka and coil (k+1)a, a common blind spot is not such for this topology as the coils connected (blue pair) do not have the same influence as the MO. Fig. 2-13 (b) instead, shows how the absolute center of symmetry is a blind zone as there is no electromagnetic separation between the connected coils (red pair). To eliminate this type of blind zone, the sensing coils of the central channels, are arranged non-symmetrically, as shown in Fig. 2-13(c) eliminating the blind spot.

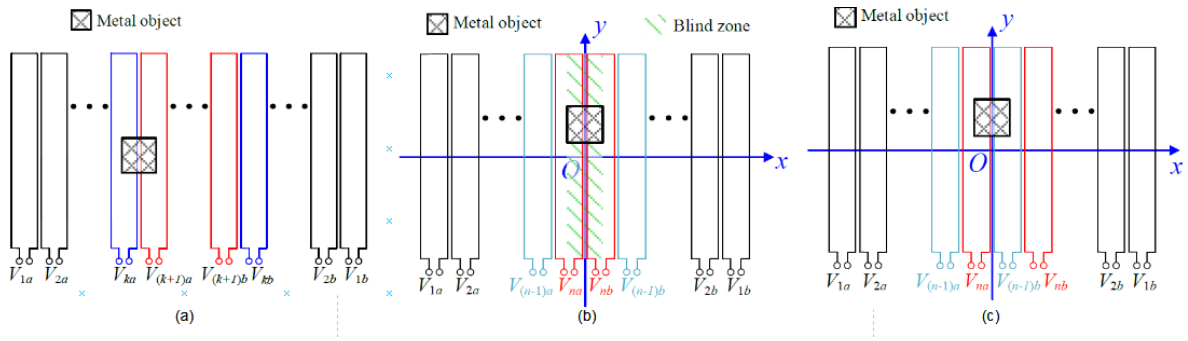

Figure 2-13: Example of blind-zone solution without using multiple layers: Generic blind zone avoided (a), Central blind zone problem (b) and Central blind zone solution (c) [6].

In this example, a simple new arrangement of the coils was enough to eliminate the previously identified blind zones. In general, a multi-layer structure is the most used solution because of its general applicability.

2.1.3 MOD Sensing Circuit and other main stages

The detection coil is often not the only equipment for this method. In fact, different circuits are necessary for the following problems:

- The inductance variation can be limited so an amplifying circuit is needed to increase the effect of the MO. Moreover, measuring a voltage variation is often simpler for practical purposes then an inductance variation. To do this, a resonant circuit is present;
- To detect very small objects and to solve the problem of blind zones the sensing pattern is composed of several elementary cells arranged on several layers. A switching system (Multiplexer), is therefore necessary to test each terminal of the elementary cells.

- In on-line operations it is necessary to design filters to decouple the frequency of power transfer from the frequency of operation of the detection coil.
- A DSP stage controls the Multiplexer and the IPT system to take under control the presence of possible MOs.

The overall configuration of the system is shown in Fig. 2-14.

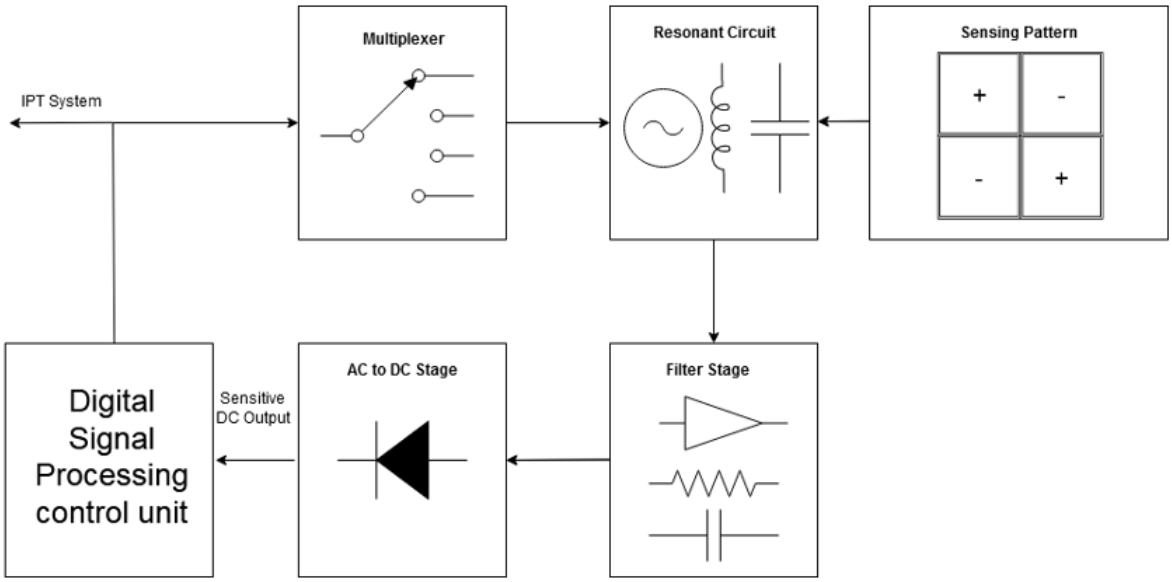

Figure 2-14: General configuration of the entire MOD system.

In chapter 4, a possible resonant sensing circuit, filter and rectifying stages suitable for the proposed method will be proposed in this work. Before that, in this Subsection some examples are proposed which have been useful starting points for the work of this thesis.

Fig. 2-15 shows an example, proposed in [13] of how each stages of Fig 2-14 can be designed.

If instead of measuring the voltage and therefore the inductance to detect the MO, the detection is based on the voltage difference, an example of a structure is shown in Fig. 2-16 [6]. In this structure, two multiplexers per elementary cell are needed instead of one. Furthermore, a digital potentiometer is introduced to subtract the two voltages selected from the two multiplexers.

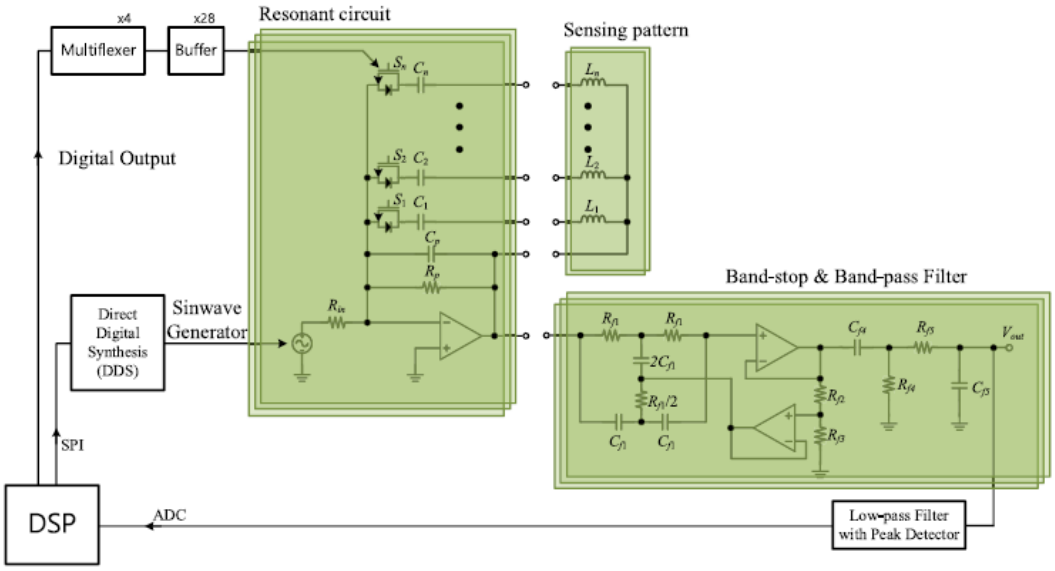

Figure 2-15: Example of MOD stages implementation [13].

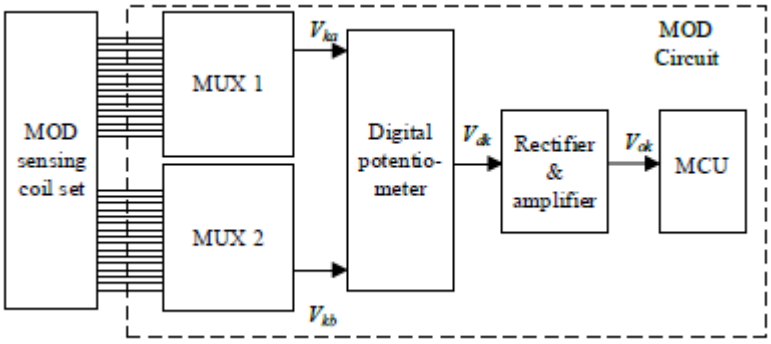

Figure 2-16: Example of MOD stages with voltage difference measurement [6].

In every configuration there is always an AC to DC conversion device for the analog to digital conversion (ADC) (left part of Fig. 2-14). The output voltage should be a dc value considering system performance and cost. If the output voltage is an ac signal, a high-performance ADC is needed to obtain the exact signal, and it is very sensitive to noise.

Each stage, which will then be proposed in the following chapters, is now analysed through some examples of the current state of the art.

1）Resonant Circuit

Resonant circuits are necessary for the MOD system to amplify the impedance/inductance variation. For small MOs, the inductance variation of the detection coil can very small. The resonance condition of the circuit can amplify this variation considerably. Basically, there are two kinds of resonant circuits: series resonance and parallel resonance, as shown in Fig. 2-17.

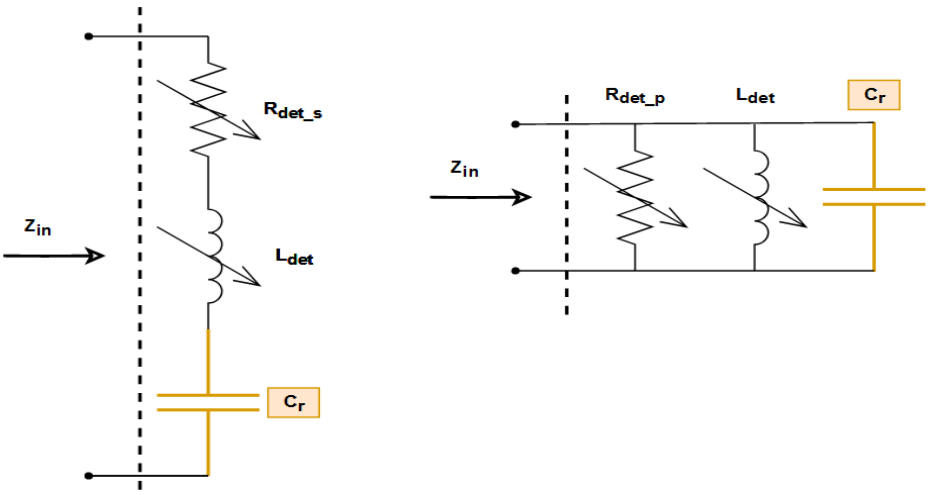

Figure 2-17: Series and Parallel resonant conditions.

The detection coil is represented with its own inductance and equivalent resistance. The modelling of the equivalent resistance of the detection coil is consistent with the type of resonance. Both parameters are represented by variable values in that the presence of an MO will cause an inductance decrease and a resistance increase (Subsection 1.2.1). The resonance condition is created by the insertion of a capacitor in series or in parallel and the angular frequency of both circuits is defined as follows:

$$\omega_r = \frac{1}{\sqrt{L_{det} C_r}} \tag{2.5}$$

In [13] a comparison between these two circuits, in terms of sensitivity to a metal object, is proposed. First, in Fig. 2-18 the input impedance characteristic of both series and parallel resonant are shown.

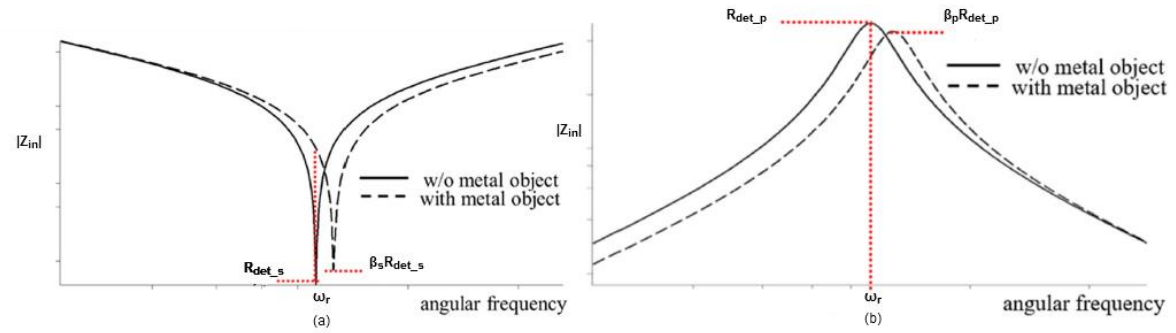

Figure 2-18: Series (a) and Parallel (b) resonant impedance characteristic [13].

Without the presence of any foreign object, the circuit is set to the resonance frequency. By considering ideal the dynamic components, the equivalent impedance has only the resistive part. The series resonance therefore has a very low impedance circuit (resistive short-circuit). On the other hand, parallel resonance results in a high equivalent impedance (resistive open circuit). The presence of an MO creates a new resonance condition as the circuit values vary, while the frequency remains constant. Therefore, the change in equivalent impedance undergoes a strong amplification. This variation is calculated analytically for both types:

$$\Delta Z(\omega_r) = Z_w(\omega_r) - Z_{wo}(\omega_r) = \tag{2.6}$$

$$= \begin{cases} R_{\det\_s}\left(\sqrt{Q_S^2(1-\alpha)^2 + \beta_S^2} - 1\right) \; Series\ Topology \\ R_{\det\_p}\left(1 - \dfrac{\beta_P}{\sqrt{1 + \left(\beta_P Q_P \dfrac{1-\alpha}{\alpha}\right)^2}}\right) = R_{\det\_s} Q_P^2 \left(1 - \dfrac{1}{\sqrt{\dfrac{\beta_S^2}{\alpha^4} + \left(\dfrac{Q_s(1-\alpha)}{\alpha}\right)^2}}\right) \; Parallel\ Topology \end{cases}$$

Where:

- $Q_S = \frac{1}{R_{\det\_s}}\sqrt{\frac{L_{det}}{C_r}}$;
- $Q_P = R_{\det\_p}\sqrt{\frac{C_r}{L_{det}}}$;
- α is the reduction coefficient of the new inductance with the presence of a MO;
- β_S and β_P are the coefficients of resistance increase for the series and parallel circuit with presence of a MO.

Using the series parameters as a reference, in Fig 2-19, the variations in impedance are shown graphically as a function of sensitivity.

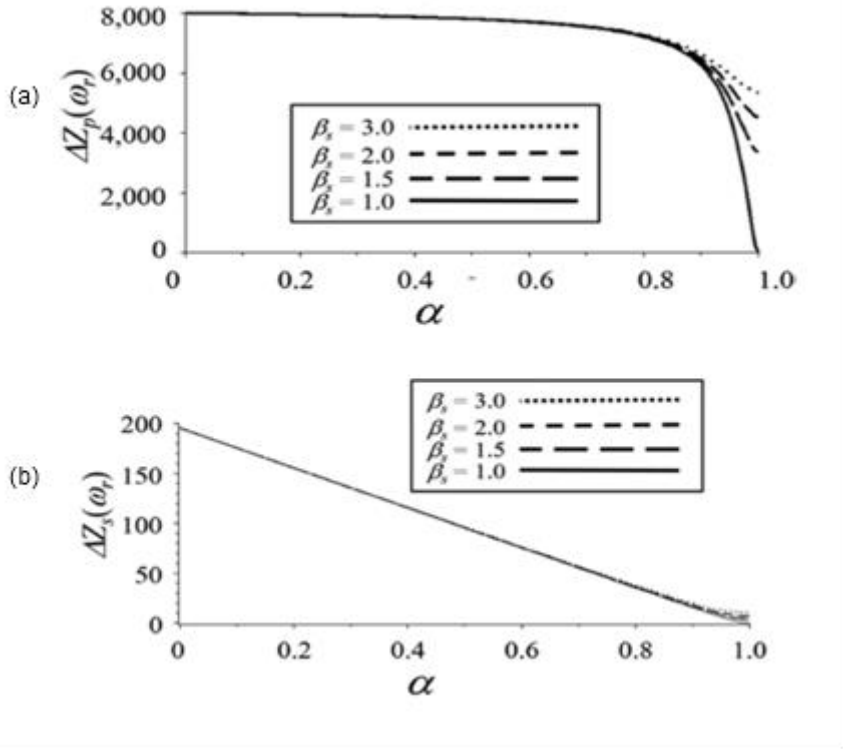

Figure 2-19: Impedance variation at resonant condition sensitivity (α and βs). Parallel resonant topology (a) and Series-resonant topology (b) [13].

Conclusions are:

- For both resonant topologies, impedance variation is more sensitive to the α (inductance variation) than βs (resistance variation);
- Parallel resonant impedance variation is always bigger than series resonant impedance variation.

In other words, the parallel-resonant circuit is more sensitive than the series-resonant circuit. The parallel-resonant circuit is also advantageous in that it is less sensitive to noise than the series topology due to its high value impedance characteristic. Moreover, in [13] it is shown that setting a frequency of the sensing circuit, slightly lower than the resonance frequency, presents a higher sensitivity.

2）Amplification Stage

In addition to the resonant circuit, an operational amplifier (Op-amp) is often added to the circuit by completing the amplification stage. The topology most used is in

inverting configuration. The sensing pattern is connected via the amplifier feedback and the resonant circuit explained in the previous subsection. As active elements are present in the feedback (sensing pattern and resonant circuit), the amplifier can be seen as a generalized integrator. The addition of the amplifier allows the following advantages:

- Increase the variation of impedance / voltage in absolute terms by exploiting the gain of the configuration;
- Electrically decouple the resonant circuit from the other stages. In fact, the impedance of the other circuits (filters, rectification, load etc.) could drastically modify the resonance condition.

Returning to the previous example, Fig 2-20, shows the amplification stage used in [13] where a parallel resonant circuit and a multiple sensing pattern are present.

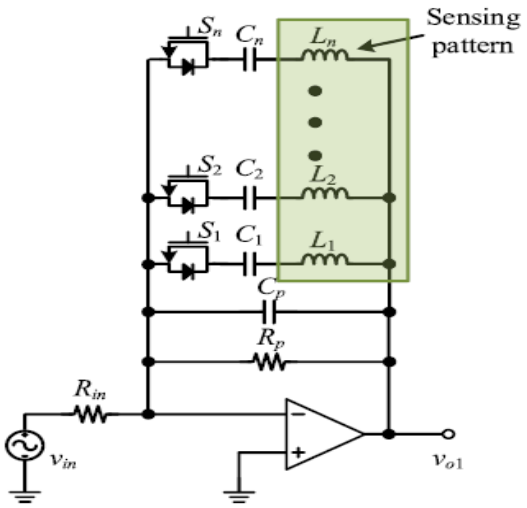

Figure 2-20: Example of a MOD amplification stage [13].

The circuit is composed by different element:

- Each loop of the sensing pattern is represented with its own equivalent inductance $L_1 \dots L_n$; a capacitor sufficiently large is also connected in series to block the dc component (to be not confused with the resonant circuit);
- The switching system, controlled by a multiplexer, is integrated in the configuration with a MOSFET in series with the sensing pattern. In this way, only one pattern at a time is considered to detect if an MO is present;
- A unique capacitor C_p creates the resonant circuit in parallel configuration;
- The resonant circuit, R_p, R_{in}, the Op-amp and a sinusoidal generator complete the amplification stage. R_p combines both the equivalent

resistance of the sensing path loop selected and any resistance added during the design phase. This value is very important as a too small resistance values could affect drastically the resonance and therefore the sensitivity of the system.

The transfer function of voltage gain, neglecting the series block capacitors for sake of simplicity, is given as follows:

$$G_1(s) = \frac{V_{0,1}(s)}{V_{in}(s)} = \frac{R_p||Z_{sens}}{R_{in}} = \frac{R_p}{R_{in}} \frac{sL_i}{s^2\left(L_i R_p C_p\right) + sL_i + R_p} \tag{2.7}$$

Where:

- $Z_{sens} = \frac{sL_i \frac{1}{sC_p}}{sL_i + \frac{1}{sC_p}}$;
- L_i is the inductance of sensing coil considered at that time;
- i stay for the index among 1 and N sensing patterns;
- $s = j\omega$.

When the MO is not present, being in the condition of resonance, the gain results to be only the ratio between the resistance R_p and R_{in}. With the presence of a MO the second term is no longer null since we are no longer in the resonance condition increasing the overall output voltage sensitivity.

In [6] and [11] another topology is adopted. In these cases, the signal from the sensing path is composed of the difference of two voltages measured by a potentiometer. Furthermore, no resonant circuit is adopted. The amplification stage is composed exclusively of an op-amp in a non-inverting configuration. Fig. 2-21 shows the overall circuit.

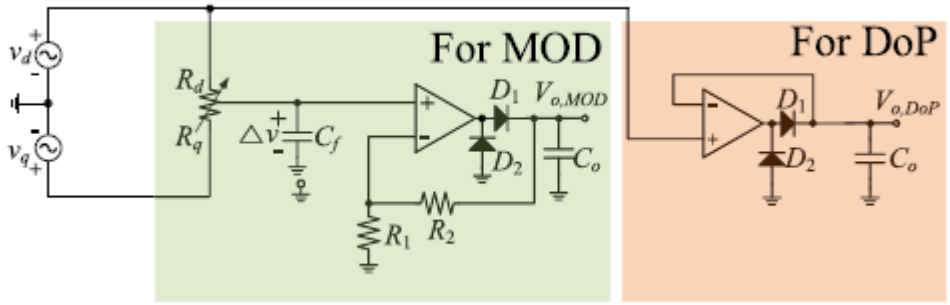

Figure 2-21: Example of MOD and DoP amplification stage without the resonant circuit [11].

The differential output voltage of the MOD sensing circuit is simply determined as follows:

$$V_o = \sqrt{2}(1 + \frac{R_2}{R_1})\Delta V \tag{2.8}$$

The figure allows us to see also an example of the stage rectification composed by a diode D_1, a capacitor C_0 which create a half-wave rectifier and a diode D_2 to avoid negative saturation of the op-amp. In [11] also the vehicle detection is implemented (DoP). In this circuit the amplification stage consists of a unitary gain (follower/buffer configuration) in order to obtaining an uncoupled high impedance circuit. A rectification stage is implemented as in MOD circuit.

3）Filters stage

Filters are often present in the system FOD system. The filters and their functions are analysed using some examples. In this part, the term MOD is replaced by the generic FOD since the following considerations are also valid for the LOD. The main functions of the filters are:

- **Eliminate the harmonic component at the frequency of the IPT system.**
  The standard J2954 sets the frequency of the wireless power transfer for EV's at 85 kHz [14]. The frequency of the FOD system is often set at a frequency about 10 times higher, for example 1 MHz. Therefore, a filter circuit is necessary to cancel out as much as possible the component of the IPT and attenuate the frequency used in the FOD circuit minimally. Typical solutions are a Band-stop filter tuned at 85 kHz or a High-pass filter with the beginning of the pass band well beyond 85 kHz. The second solution may also be useful

to mitigate the DC component of op-amps (if included) that could compromise the system.

- **Eliminate the High-frequency noise.**
  The high frequency components (over 10 MHz) need to be attenuated as they could compromise the sensitivity of the sensing circuit. These components could come from the switching systems present in the IPT power converters (Subsection 1.1.2). In this case, a Low-pass filter with a cut-off frequency higher than the frequency of the sensing circuit could be a simple solution. A solution combined with the previous requirement could lead to the solution of a single Band-pass filter centered on the frequency of the sensing circuit.

In Fig. 2-22 an example of the filter circuit used in [13] is shown. An active type of twin-T band-stop filter is applied to eliminate the IPT 85 kHz frequency component (yellow area). The second stage (green area) is a RC band-pass filter to attenuate the DC component and the high-frequency switching noise. The IPT component is not filtered as it is also used as the frequency of the sensing circuit (no resonant circuit is present).

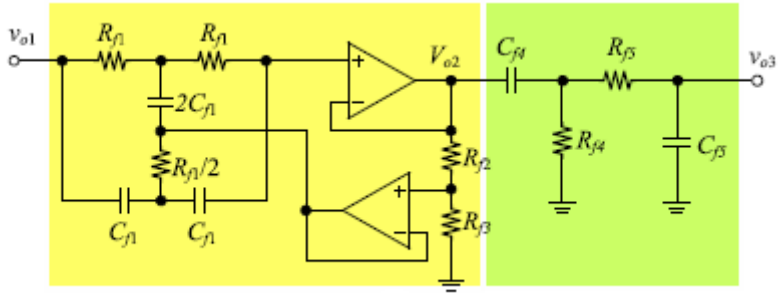

Figure 2-22: Example of filter stage for FOD [13].

The work in [11] instead, is useful to underline as components already present in the sensing circuit for other functions, can also perform filtering operations with the advantage of not adding new components. In fact, in Fig. 2-21, the digital potentiometer, in addition to creating the null-voltage reference condition, together with the capacitor C_f , it creates a first-order RC Low-pass filter in order to reduce the high frequency noise around several megahertz.

Finally, the limited bandwidth of op-amps which could be present in the sensing circuit, can attenuate low or high frequencies.

2.1.4 Active methods

Unlike the cases mentioned above, active methods have auxiliary coils with power supply. Two power supplies are present in the system: The IPT supply and the detection coil power supply. The detection coil is therefore, like the IPT system, consisting of a transmitter coil and a receiver coil.

An Example in presented in [15]. In Fig. 2-23, the detection coil transmitter loop is indicated with solid lines while the receiver loop is indicated with dashed lines.

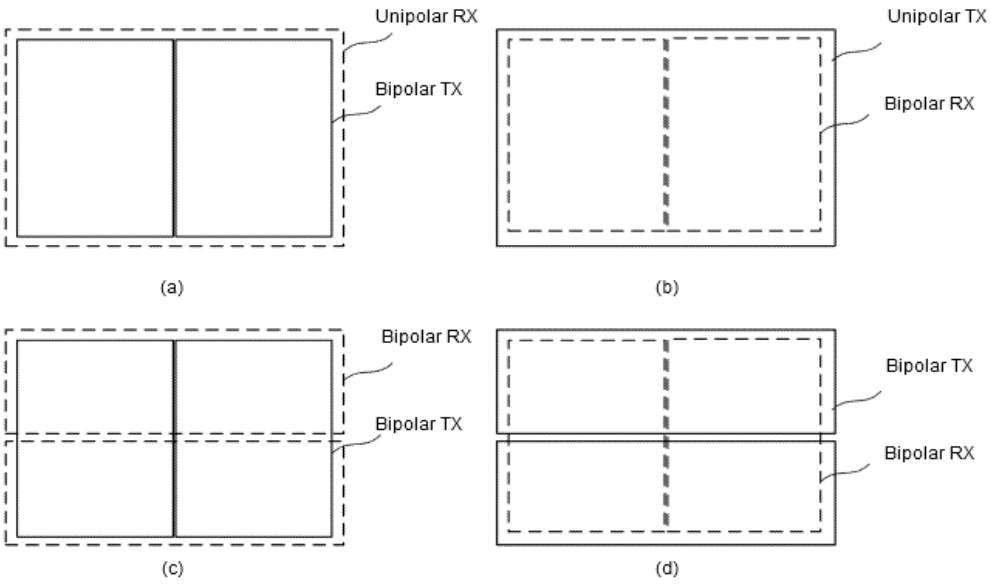

Figure 2-23: Example of Active Field-Based method for MOD. (a) Bipolar TX as transmitter and a unipolar RX. (b) Unipolar TX and a bipolar RX. (c) and (d) Two perpendicular bipolar TX and RX [15].

By using a unipolar and a bipolar detection coils or two perpendicular bipolar coils, the voltage induced to the RX of the detection coil can be set to zero. With the presence of an MO, this condition is missing for the same reasons as passive methods, and detection is possible. The frequency used is between 1 MHz and 10 MHz (similar to the sensing circuit in the passive methods). This method can present good results since the coupling between a TX and a RX can make the detection coil more sensitive. However, the complexity and cost of the MOD method increase. Blind spots could be present.

2.2 Field-Based Detection for LOs

A Living object has a negligible impact on the inductance and equivalent resistance. However, it can affect the capacitance around it. The principle is explained in Fig. 2-24 through the equivalent circuit of the system equipped with detection coil for the LOD. In the circuit we have:

- Z_{TX} is the equivalent impedance of the transmitting coil of the IPT;
- C_{TX-det} is the equivalent capacitance between the TX and the detection coil;
- C_{det-gr} is the equivalent capacitance between the detection coil and the ground;
- C_{det-LO} is the equivalent capacitance between the detection coil and the LO when it is present;
- V_{wo} and V_w is the sensing voltage of the detection coil which is affected by the LO.

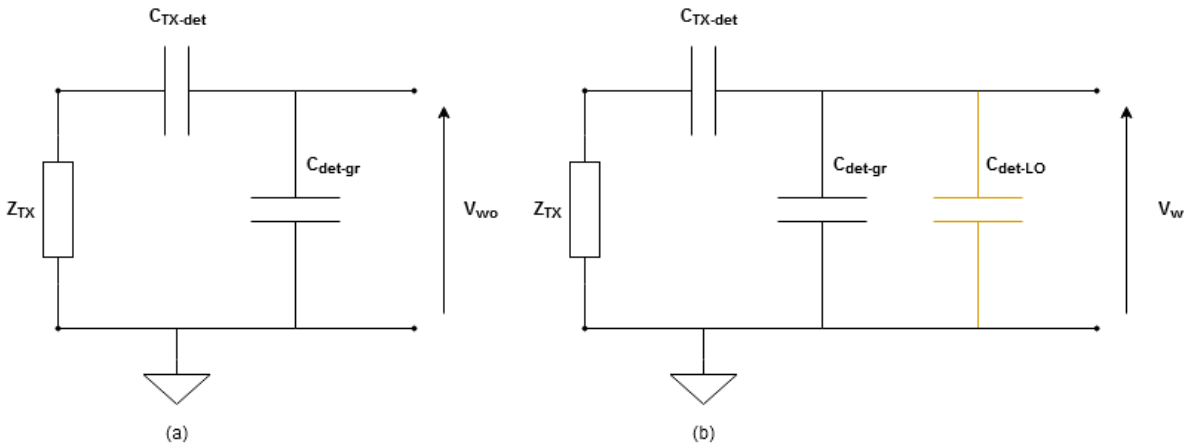

Figure 2-24: Principle of Field-Based LOD system. Equivalent circuit (a) Without an LO. (b) With an LO.

For the detection of metal objects, the various capacitances of the system have not been considered. For LOs, on the other hand, they play a fundamental role in LOD methods. In Fig. 2-24 (b) the presence of a LO causes an increase in the capacitance in the circuit and therefore the voltage induced on the detection coil undergoes a variation. Thus, the LO can be detected.

As a matter of simplicity, in the above circuit the capacitance to the ground of the transmitting coil and of the LO is neglected. However, the ground effect (the coupling to ground of the various components of the system), can decrease the capacitance

variation of the detection coil; it is therefore a fundamental parameter to be taken into the next considerations.

2.2.1 Design of the LOD Sensing Pattern

Similarly to what seen in Section 2.1, for the MOD, in this case, the design of a capacitive sensing pattern of the detection coil is required for the detection of living objects. In this case, however, the goal is to design a circuit with high sensitivity in varying capacitance instead of inductance, using the principle seen in Fig. 2-24. Some examples are reported below.

As a first simple example, in patent [16] instead of a real detection coil there are used eight metal plates around the TX pad, as shown in Fig. 2-25. The equivalent circuit of Fig. 2-24 can also be applied in this case where the detection coil is replaced by the eight metal plates.

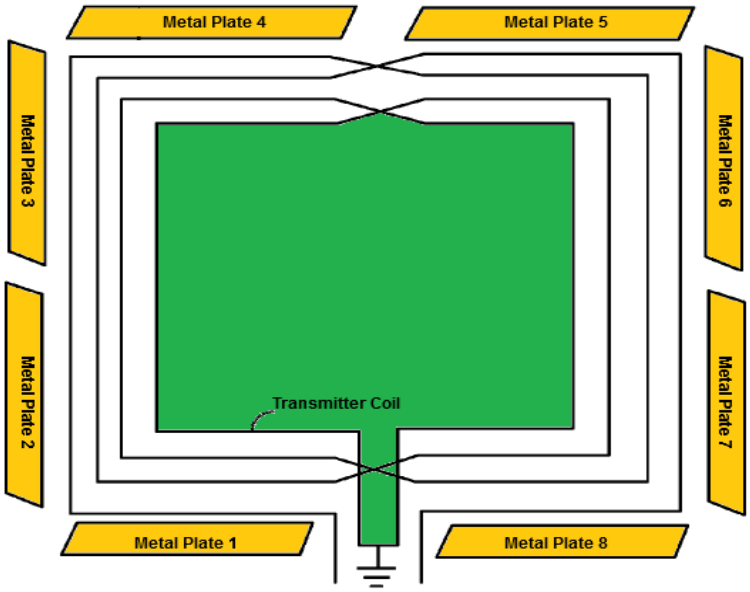

Figure 2-25: LOD with metal plates [16].

Similarly, patent [17] also adopts the capacitive detection method with metal plates, but the location and the shape are different. In Fig. 2-26 we can see how the metal plates are positioned next to the transmitter, covering the sensor which is a sensing circuit designed to detect the voltage variation. The sensor has its own aluminium shield. It is possible to see how a part of the metal plates can be used as a ground conductor to mitigate the ground effect.

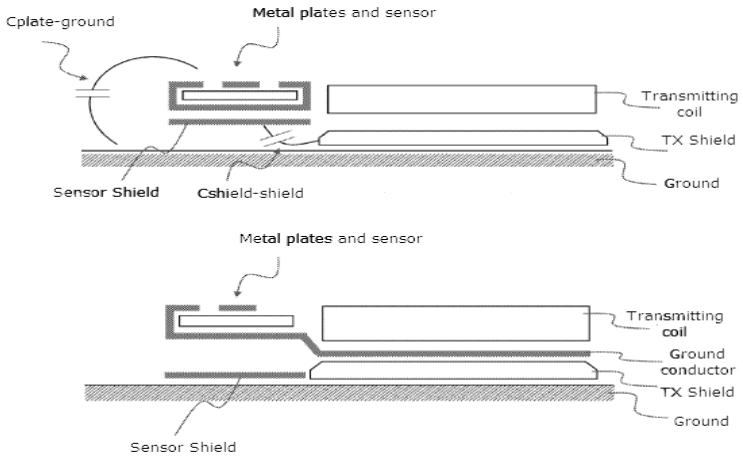

Figure 2-26: Different locations and shapes for metal plates in LOD [17].

In [18] a real detection coil with a capacitive sensing pattern is designed. A comb-shape pattern is used, as shown in Fig. 2-27. When an LO approaches the charging area, the capacitance of the comb pattern sensor would vary since a coupling between the LO and the detection coil is established.

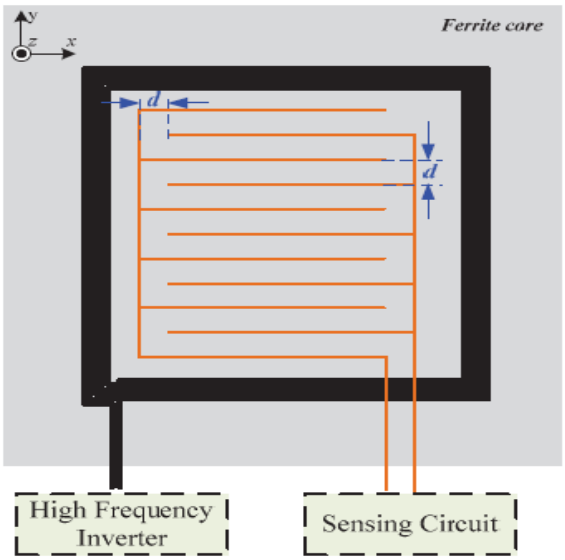

Figure 2-27: LOD with a comb-shape sensing pattern [18].

The sensing path mounted on the TX pad, includes two electrodes with a distance d between which is constant in the whole area of the pad to obtain a uniform capacitance. Unlike the designs of conventional capacitive sensors, the pattern should be as thin as possible to avoid interference with the IPT system. The capacitance per unit length of the sensor can be calculated as follows (all parasitic capacitance is neglected):

$$C_0 = \frac{\pi \varepsilon_r \varepsilon_0}{\ln\left(\frac{d}{2r} + \sqrt{\left(\frac{d}{2r}\right)^2 - 1}\right)} \approx \frac{\pi \varepsilon_r \varepsilon_0}{\ln\left(\frac{d}{r}\right)} \tag{2.9}$$

Where:

- r is the radius of the sensing pattern;
- d is the distance between the two electrodes to create the capacitor;
- ε_r is the relative permittivity of the material;
- $\varepsilon_0 = 8.854 * 10^{-12} \frac{F}{m}$ is the permittivity of vacuum.

The equivalent model considering the effect of the LO and ground effect is shown in Fig. 2-28.

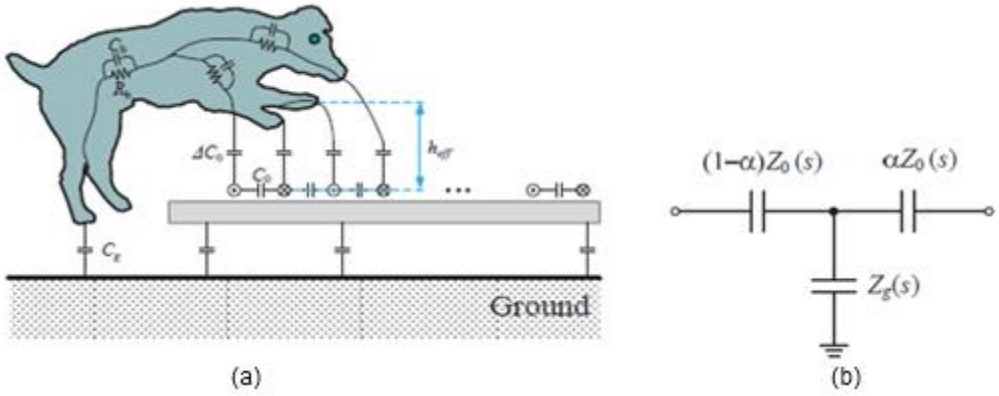

Figure 2-28: (a) Equivalent model for the LOD. (b) Equivalent circuit [18].

From Fig. 2-28 we can notice:

- The parasitic capacitances between the sensing pattern and the ferrite core affect the real mutual capacitance between two electrodes Co when there is no LO;
- ΔCo is the capacitance variation when the living object is placed nearby the sensing pattern. Thus, the new capacitance will be $C' = C_0 + \Delta C_0$;
- C_g is the capacitance that includes the ground effect of the LO, the ferrite core and the detection coil;
- The body capacitance and resistance of the LO are negligible because it has much lower impedance compared with the impedance of Cg and Co in various frequency ranges;

- It is possible to define a coefficient α with a value between 0 and 1; this value indicates how the LO couples with the ground (α = 0.5 would imply symmetrical coupling).

A multiple comb-pattern capacitive sensor is further proposed in [19] to improve the sensitivity as shown in Fig. 2-29.

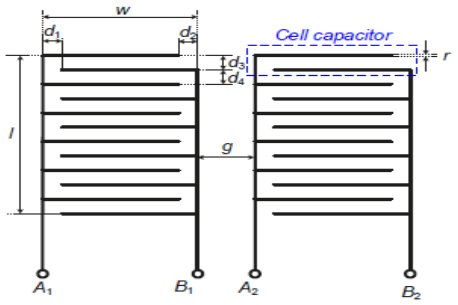

Figure 2-29: Multiple Comb for LOD [19].

In this work, considering the capacitor as a coplanar structure, the capacitance of each comb is calculated as follow:

$$C_0 = n\frac{\epsilon_r(w-2d)}{120v_0\ln\left(\frac{2\left(1+\frac{d-r}{d+r}\right)}{1-\frac{d-r}{d+r}}\right)} \tag{2.10}$$

Where:

- n is the number of cell capacitor inside each comb (Fig. 2-29);
- $v_0 = 300000\ km/s$ is the light speed in vacuum;
- w is the width of each comb;
- $d, r\ and\ \epsilon_r$ are the same parameters used in the single comb detection coil.

The new parameter for the multiple comb structure is the parasitic capacitance C_{par} between the two combs.

In fact, this capacitance can make a capacitance changes even though the LO is on the other comb. Therefore, reducing coupling capacitance between two adjacent coils (a comb-shape coil in this case) is also an important design consideration. C_{par} can be calculate is this way:

$$C_{par} = \frac{\epsilon_r l}{120 v_0 \ln\left(\frac{2\left(1+\frac{g-r}{g+r}\right)}{1-\frac{g-r}{g+r}}\right)} \tag{2.11}$$

Where:

- l is the length of each comb;
- g is the distance between the two combs.

As shown in Eq. 2.11, a decrease of C_{par} caused by increasing g, can decouple two adjacent combs. However, if g is increased too much, a LO placed between the two adjacent coils cannot be detected. Therefore, there is a trade off choice in determination of g.

Eq. 2.9, 2.10 and 2.11 are approximate formulas useful for having an approximate value of the capacitance in question. These values can also be obtained through electrostatic simulations as we will see in Chapter 3. However, the mathematical form of the equation allows us to understand how geometrical parameters affect the capacitance before the software simulation, decreasing the number of simulations necessary for the design of the sensing path.

2.2.2 LOD Sensing Circuit

As for the MOD, a sensing circuit must also be designed for the LOD. In this case, the change in capacitance will have to be amplified in a voltage change. The considerations made in Subsection 2.1.3 regarding the filter and rectification stage remain the same. For the LOD the detection coil is also often made up of multiple capacitive cells making necessary a stage (multiplexer, switching system etc.) which scan each capacitive loop one at a time.

In [18] a first very simple sensing circuit consists of an active op-amp integrator with a DC voltage input, a reset switch and a RC low pass filter as shown in Fig. 2-30.

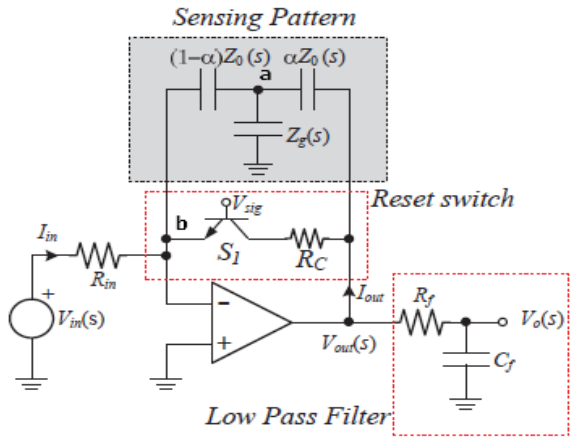

Figure 2-30 : Simple sensing circuit for LOD [18].

The output voltage is derived:

$$V_{out}(s) = \frac{-V_{in}(s)}{sC_0R_{in}} * \left(\frac{\alpha(1-\alpha)C_g + \beta C_0}{\beta^2 C_0}\right) \tag{2.12}$$

Where the coefficient $\beta = \frac{z_0'}{z_0}$ indicates the increment of capacitance when there is a LO. No resonant circuit is used and amplification is carried out exclusively by the op-amp. Furthermore, since we have a DC input generator, a reset switch, it is necessary to avoid saturation of the circuit. In the end, a simple RC low-pass filter is used to eliminate the high frequency components to desired.

Considering the multiple comb structure [19] the sensing circuit can be designed differently as shown in Fig. 2-31.

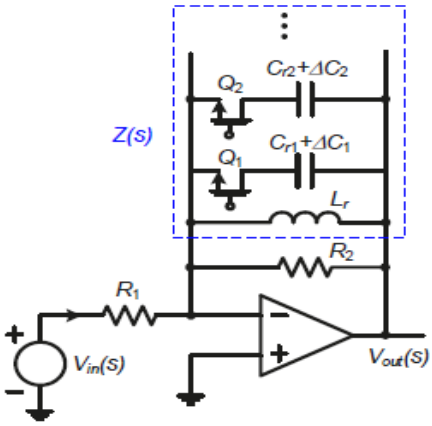

Figure 2-31: Sensing circuit for multiple coil structure in LOD [19].

Each capacitor is connected in series with one switch Q_i in order tomake sure that only one capacitor is scanned in the LOD at one time. An inductor L_r is present to form a parallel resonant circuit, together with an op-amp in inverting configuration (Integrator topology). The overall circuit is identical to the one used in the MOD (subsection 2.1.3). The only difference is that in this case the detection coil is equivalent to a capacitor whereas the resonant element is an inductor (opposite to the MOD). Thus, the voltage gain is:

$$G(s) = \frac{V_{out}(s)}{V_{in}(s)} = \frac{R_2}{R_1} \frac{sL}{s^2(LR_2(C_{ri} + \Delta C_i) + sL + R_2} \tag{2.13}$$

Where i is the index which indicates the comb considered at one time. If there is no living object on the Tx pad, the voltage gain will be kept at $\frac{R_2}{R_1}$ since the active part of the amplifier feedback is in parallel resonance (very high impedance). When a LO is on the sensing pattern, the capacitance is increased by the amount of ΔC_i, which leads to the reduction of the voltage gain. The output voltage V_{out} reduced by an amount of ΔV, can be given as follows:

$$\frac{\Delta V}{V_{out}} = 1 - \frac{1}{\sqrt{1 + \omega_r^2 R_2^2 \Delta C_i^2}} \tag{2.14}$$

Where ω_r is the designed angular frequecy of resonance.

In MOD a the presence of a metal object causes a decrease in the equivalent inductance of the detection coil. On the other hand, in LOD a living object decreases the equivalent capacitance of the circuit. In both cases, the voltage induced on the detection coil decreases.

CHAPTER 3. DESIGN AND SIMULATION OF THE PROPOSED METHOD

After analysing the various methods and problems of the FOD, in this Chapter a Field-Based method is proposed by designing a new detection coil.

The chapter illustrates the idea of method improvement, the detection coil model, the equivalent circuit and the simulation path to validate the method.

To do this, Electrostatic and Electromagnetic simulations will be carried out using the "Ansys Electronic Desktop" software. In addition to defining the geometrical parameters to be designed, each simulation is useful for understanding the operation of the detection coil and the function of the various subsets (single spiral, basic cell and layers). Then, it will be carried out the entire detection coil model in order to verify the effectiveness of the proposed method.

Finally, a prototype of the detection coil was made in the laboratory to verify the results obtained from simulations through real measurements in an IPT system (Section 3.6).

3.1 Background and Objectives of the proposed method

In the previous Chapter we discussed, using examples of the current state of the art for this technology as the Field-based method can detect metal and living objects by designing a sensing pattern present in the detection coil able to detect the coil impedance variation. For the detection of metal objects (MO) it is necessary to design an inductive sensing pattern. On the contrary, the detection of living objects (LO) is carried out via a capacitive pattern. The impedance variation is then converted through a sensing circuit, in a voltage variation. In summary, the component called detection coil consists of a sensing path or pattern which varies its impedance if FOs are present. This sensing pattern is inserted within a sensing circuit which consist also of other elements such as a resonance circuit. Auxiliary components such as filters, rectification and DSP are required as explained in Subsection 2.1.3.

In literature the two types of objects (MO and LO), for the Field-based methods, are analysed separately, focusing on the design of a detection coil only for MO or LO. Wave-Based method can detect both types of objects without additional systems but

is an expensive solution. The Field-based method is an optimal compromise between cost and accuracy of results between the Wave-base method and System parameter methods. It can be also used for both High and Low power application. For these reasons the Field-Based method has been chosen.

In this thesis a new form of detection coil is proposed with the aim of detecting both metallic and living objects with a single detection coil. The idea is to have an equivalent circuit with both inductive and capacitive elements in order to have an equivalent impedance variation for both foreign objects. In the next sections it is explained how this is possible introducing the detection coil model.

3.2 The Detection Coil

The requirements to design a detection coil for the MOD are well defined (Subsection 2.1.1). The common idea in literature is to create an inductive circuit with null induced voltage when any object is present on the detection coil. When a metallic object is present, the magnetic field is distorted so the equivalent inductance has a different value and the induced voltage will be different from zero. For LOD, the variation of the magnetic field is negligible whereas the electric field undergoes a usable variation for the detection. Therefore, starting from the well-known MOD principle, the idea of the proposed detection coil is to internally insert a capacitive circuit in order to have sensitivity of both fields (Magnetic field for MOD and Electric field for LOD). The proposed structure is proposed in Fig. 3-1:

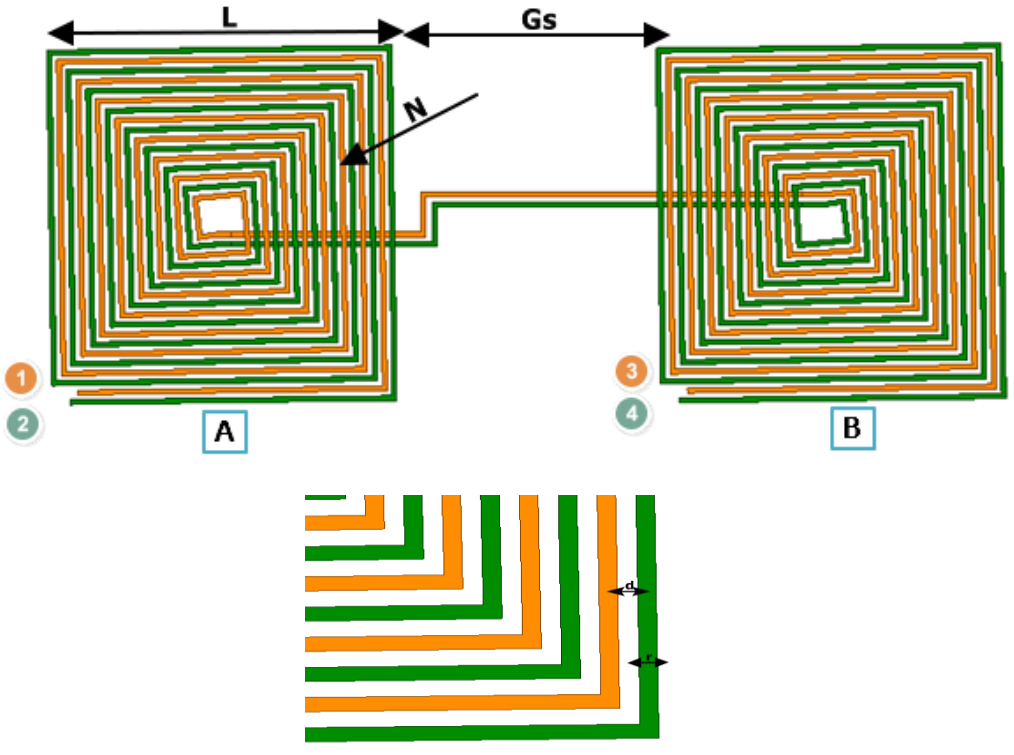

Figure 3-1: Proposed detection coil structure and geometrical parameters.

In the structure there are 4 terminals. Starting from terminal 1 up to terminal 3 (orange part) we note how a non-overlapped inductive circuit is present where the left side (Square spiral A) and the right side (Square spiral B) have two inductive loops in series with opposite directions. In this way, the null induced voltage reference condition is created. In both parts A and B several turns are inserted. Similarly, a second circuit with two inductive loops in series is present from terminal 2 to terminal 4 (green part). Circuit 1-3 and 2-4 present turns at a constant distance from the inner to the outer radius. In this way, a homogeneous capacitive circuit is created between terminals 1-2 and 3-4 which can be considered the electrodes that form a capacitor. Figure 3-1 shows also the different coil design parameters:

- L : size of each square spiral;
- N : Number of turns;
- d: distance between electrodes;
- r : internal size of pattern wires (tracks);
- G_s: Distance between the two spirals connected in series.

To a better understanding of how the structure can be modeled and used for the MOD and LOD it is possible to derive the equivalent circuit (Fig. 3-2). We can divide the circuit in two parts:

- **Inductive part (Magnetic circuit):** starting from the terminal 1 and arriving to the terminal 3 we can model the coil as an inductance that takes into account the contribution of spiral A in series to spiral B (L_{13}). The inductance is modeled with their own resistance in series. Same situation from terminal 2 to terminal 4. A mutual inductance between circuit 1-3 and circuit 2-4 is present to model the magnetic coupling which presents the following relationship according to the transformer theory:

$$L_M = k\sqrt{L_{13}L_{24}} \tag{3.1}$$

  Where k is the coupling coefficient between the two circuit 1-3 and 2-4;

- **Capacitive part (Electric circuit):** Considering the track 1 and the track 2 as two electrodes it is possible to model the structure as a mutual capacitor between terminals 1 and 2. Furthermore, the inductive circuit 1-3 present the capacitance to the ground modeled with the capacitor C_{13g}. Same situation for the spiral B considering tracks 3 and 4 in order to model $C_{34}$and C_{24g}.

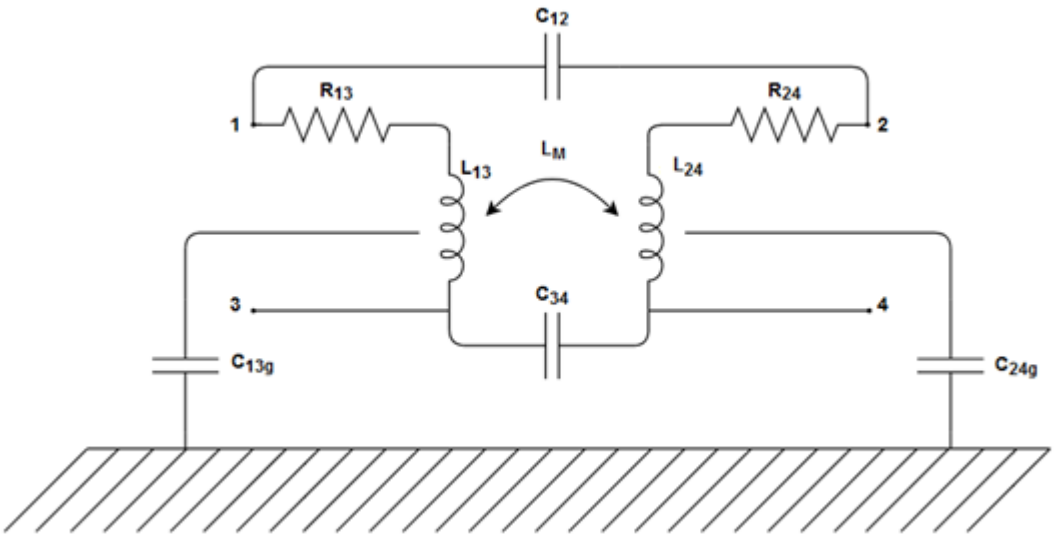

Figure 3-2: Equivalent circuit of the proposed detection coil.

From the equivalent circuit it is immediately possible to see how the equivalent impedance, from any terminal, has both an inductive part and a capacitive part.

By changing the reference terminals, it is possible to have a predominantly inductive or capacitive circuit. In this way both types of objects (MO and LO) can be detected. In fact, by measuring the impedance variation from terminals 1-3 or 2-4, the circuit is predominantly inductive so an MO will cause a high sensitivity of the inductance variation. On the other hand, from the terminals 1-2 or 3-4 the circuit is mainly capacitive, thus presenting a sensitivity for LO. Subsequently, it will also be shown that both circuits have good sensitivity for both MOD and LOD.

Figure 3.2 shows us the structure of what we can call as a "Basic Cell" of the detection coil. In fact, from the previous works in the literature we understand how it is better to create a sensitive path, in this case both inductive and capacitive with a small size to detect object as little as possible. On the other hand, the size of the detection coil must cover the entire area of the power transfer. As a conclusion, the optimal solution to satisfy both factors, consists in duplicating the basic cell several times to form a layer. Each new basic cell will produce four new terminals. In the creation of the layer two new parameters that we can call G_H and G_V must be taken into consideration. These two parameters are the distances between each basic cell of the same layer in horizonal and vertical direction in order to create rows and columns respectively. Furthermore, if we consider the problem of blind zones (Subsection 2.1.2) it is better to consider a multi-layer solution to solve this problem. Considering at least two layers a further parameter to be designed is the distance between the elementary cells of different layers (G_z).

A model of the detection coil was created using the Ansys Electronics Desktop software. First a basic cell is considered for the optimal design of the parameters N, L, d, r and G_s. Subsequently, we consider a second basic cell positioned with a horizontal or vertical offset to simulate the creation of a layer (G_H and G_V parameters) and finally several basic cells with z-axis distance (multi-layer structure) in order to design the G_z parameter.

The geometrical parameters of the coil will be simulated as a function of the impedance variation of the detection coil. For the capacitive circuit, an "Electrostatic" simulation is performed whereas for the inductive circuit a magnetic simulation is carried out called "Eddy Current simulation". Impedance variation is simulated by inserting on the detection coil an object with metal properties or properties similar to a LO into the model.

Once the geometrical parameters and the complete model of the detection coil have been defined. The actual sensitivity both for MO and LO will be verified. The model will include subsequently also a possible IPT structure (Transmitter, Receiver, Shield and ferrite).

3.3 Design of the Basic Cell

This section carries out the design of the geometrical parameters of the basic cell, i.e. the basic element of the detection coil that allows the detection of objects. Since the aim of this thesis is to have a method that detects both the cases of foreign objects (MO and LO), a sensitive variation of both inductance and capacitance is required. To verify this, both an Electrostatic and an Electromagnetic simulation was carried out for each geometrical parameter. The two optimization outputs for each simulation are therefore:

$$S_E\% = \frac{C_w - C_{wo}}{C_{wo}} * 100 \qquad S_M\% = \frac{L_w - L_{wo}}{L_{wo}} * 100 \tag{3.2}$$

Where:

- S_E is the Electric Sensitivity (Capacitance variation);
- S_M is the Magnetic Sensitivity (Inductance variation);
- w and wo stay respectively for “with” and “without” the foreign object.

In fact, since in the simulations individual elements of the detection coil are considered (a spiral, basic cell, a layer) the value of the capacitance or the inductance does not have a great significance while it is better to consider their percentage variation. In Table is listed the path of simulations carried out, starting from the

design of the basic cell and its connection in series to the design of the layer and the entire detection coil. For each simulation, the electrical and geometrical parameter in question and the objective to be achieved are considered. The table refers to the equivalent circuit of Fig. 3-2.

Table 3-1: Simulation path for geometrical parameters of the detection coil.

Electrical Parameter	Geometrical Parameter	Design Optimization
Single Spiral • C_{12} (or C_{34}) • L_{13} $(or$ $L_{24})$	L, N, d	Maximize S_E and S_M
Series connection of two spirals • C_{12} and C_{13g} (or C_{34} and C_{24g}) • L_{13} (or L_{24}) and L_M	G_s	Maximize S_E and S_M
Presence of multiple basic cells (layer): • $C_{H/V}$: Capacitance between basic cells of the same layer in horizontal and vertical directions. • $L_{H/V}$ *:* Mutual Inductance between basic cells of the same layer in horizontal and vertical directions.	G_H, G_V	Decrease $C_{H/V}$ and $L_{H/V}$
Presence of multiple layers: • C_z : Capacitance between basic cells of different layer in the z-axis directions. • L_z : Mutual Inductance between basic cells of different layer in the z-axis directions.	G_z	Decrease C_z and L_z

3.3.1 Size of the Basic Cell

The first fundamental parameter to be defined is the size of the basic cell (L). This parameter is related to the other internal parameters of the basic cell (number of turns, radius and internal size of the tracks). Furthermore, the size of the basic cell will be the fundamental parameter for deciding how many basic cells will be necessary to form a layer and the total size of the detection coil. The simulation is shown in Fig. 3-3. For this simulation a single spiral is taken into consideration (the connection of the second spiral in series will be considered subsequently) and a foreign object of circular shape with diameter L_o and height H_o is positioned on the spiral. To calculate the sensitivity, the capacitance and inductance values with and without the object will be considered.

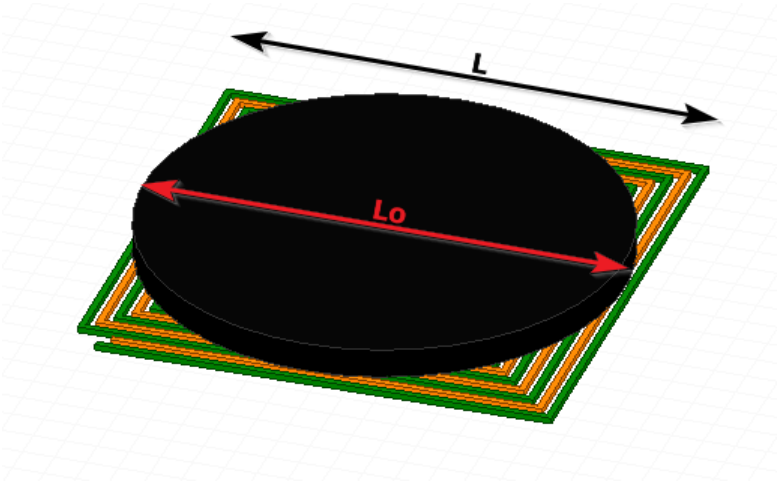

Figure 3-3: Overall Simulation for the Size of the Basic Cell.

For the electric sensitivity the object has properties of the material similar to a LO [20] while for the magnetic sensitivity the chosen material is the copper. The property of the foreign object are listed in Table 3-2 where ϵ_r and σ are respectively the Relative Permittivity and the Conductivity of the material.

Table 3-2: FOs Properties.

Parameter	Value
L_o	$[1-200]\ mm$
H_o	$2\ mm$
LO properties.	$\epsilon_r = 400$
	$\sigma = 4\ s/m$
MO properties	$\epsilon_r = 1$
	$\sigma = 58 * 10^6\ s/m$

In this simulation we want to consider the only effect of the size of the basic cell on sensitivities. By increasing or decreasing the L parameter, the internal parameters (N, d and r) would also undergo variations. For example, doubling L, keeping d and r constant would mean increasing the number of turns or keeping the latter parameter constant but having different values of d or r. Therefore, in order to isolate the effect of L, the simulation is carried out by keeping the this value constant and to vary the diameter of the object L_0, thus analyzing the $\frac{L_o}{L}$ ratio as a function of the sensitivity. The results are shown in Fig. 3-4.

From Fig. 3-4 (a) it is possible to analyze the Electric Sensitivity: starting from a small LO, the new capacitance is directly proportional to the size of the object then, there is a peak of the value of the capacitance when the size of the object coincides with the size of the detection coil ($\frac{L_o}{L} = 1$). Using the capacitance value without the presence of the object it is possible to calculate the sensitivity of the detection coil; By continuing to increase the size of the object, the capacitance decreases until it reaches an asymptotic value; This is justified by the ground effect (subsection 2.2.1). In fact, as long as $\frac{L_o}{L}$ is less than one (the foreign object is smaller than the spiral), the circuit capacitance increases proportionally to the portion of the object electrically coupled with the spiral. On the other hand, if the object is larger than the spiral ($\frac{L_o}{L} > 1$), there is also the coupling to the ground of the object (in addition to the coupling to the ground of the detection coil present in any case). This coupling significantly decreases the electric sensitivity (from 18 to 8%).

As for magnetic sensitivity (Fig. 3-4 (b)) it is possible to note that the variation of inductance is simply directly proportional to the size of the object, since a larger MO causes a larger interference of the magnetic field. In this case, the magnetic sensitivity is negative as the inductance tends to decrease compared to the case with no foreign object (MO). Furthermore, it is possible to outline a minimum limit below which the variation of inductance is negligible. In fact, a good sensitivity is noticed when the object turns out to be at least half of the spiral ($\frac{L_O}{L} > 0.5$).

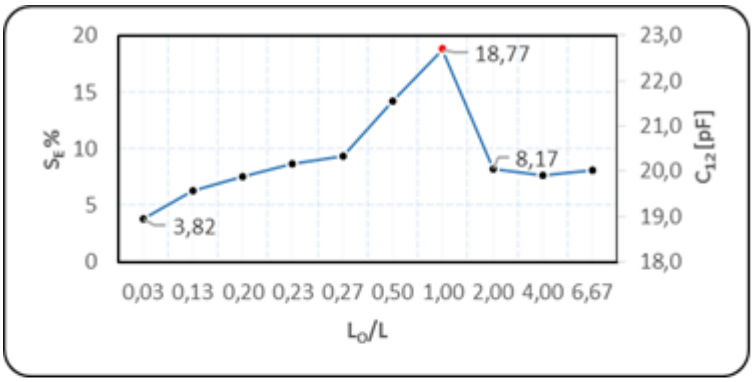

(a)

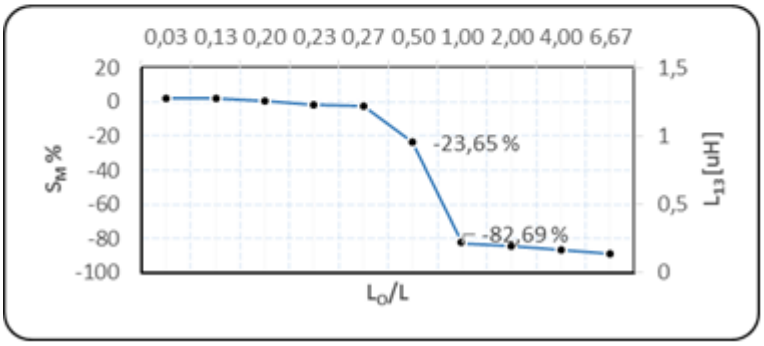

(b)

Figure 3-4: Size of the FO/Size of the Basic Cell vs Electric Sensitivity (a) and Magnetic Sensitivity (b).

In conclusion, the Magnetic simulation recommends decreasing the detection coil size as much as possible in order to detect the smallest possible MO. On the other hand, the capacitance simulation demonstrates that small detection coils are much more easily subject to the ground effect (higher possibility of a LO larger than the detection coil). A compromise choice between LOD and MOD is necessary in the design of the detection coil size. Considering the results of this simulation, from this point, the size of the basic cell L is set at 30 mm.

3.3.2 Internal Parameters

Once the size of the cell bases has been defined, it is necessary to define the internal parameters of the sensitive path. These parameters (Fig. 3-1) are three:

The number of turns N, the distance between the tracks d (the distance between the inductive circuits that creates the capacitive circuit) and finally the internal radius of the tracks r.

In the following simulation we focus on the first two. Since L is now a fixed parameter, parameters N and d are correlated. In fact, a greater distance between the traces causes a decrease of N and vice-versa. Thus, we define the "Dense factor", as the ratio of these two parameters, which values for the simulation are shown in the Tab. 3-3 and Fig. 3-5 shows graphically the effect of this parameter from an high value (left) to a low value (right).

Table 3-3: Internal Parameter Simulation Parameters.

N	d [mm]	N/d (Dense Factor)
16	0.2	80
10	0.5	20
8	0.8	10
6	1.2	5
4	2	2

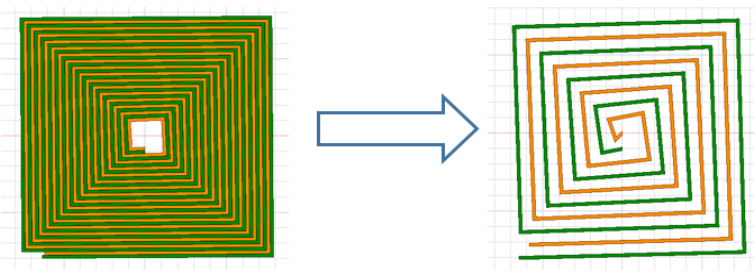

Figure 3-5: Dense Factor graphical effect.

According to the values shown in the table, also in this case the magnetic and electric sensitivity is observed by simulating the presence and absence of an MO or LO. The characteristics of the objects are the same as those of the tab, in this case, however, we have $L = L_0 = 30\ mm$. Even in this case the capacitance and the inductance we consider are respectively C_{12} and L_{13}.

The result is shown if Fig. 3-6, where it was considered the absolute value of Magnetic sensitivity, as it is always negative in this simulation. If the Dense Factor decreases the Electric sensitivity becomes positive and increases with the increase of this coefficient; On the other hand, the Magnetic sensitivity decreases with decreasing $\frac{N}{d}$. To increase magnetic sensitivity, a high dense factor is required, while Electric sensitivity requires a small dense factor.

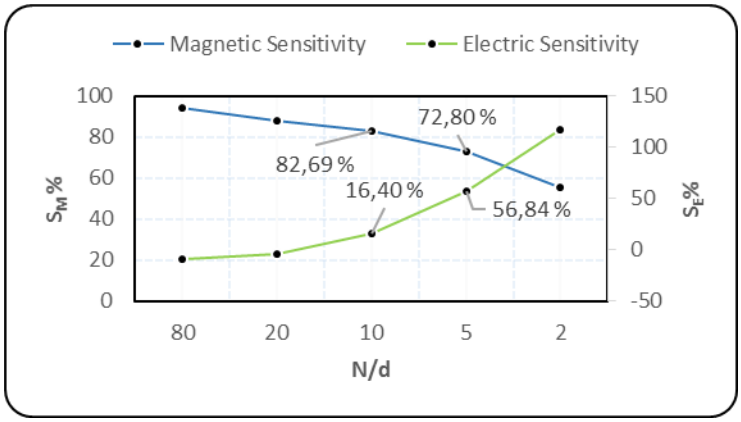

Figure 3-6: Dense Factor Vs Electric and Magnetic Sensitivity.

In fact, varying this coefficient means having a sensitive path attributable mainly to an inductor ($\frac{N}{d}$ high) or a capacitor ($\frac{N}{d}$ small) and consequently an increase or a reduction of the relative sensitivity. If we have $\frac{N}{d} < 10$, a good compromise of sensitivity is noted and the "less dense" basic cells ($\frac{N}{d} = 5\ or\ \frac{N}{d} = 2$) seem the best compromise. However, the value 10 was chosen as the final design choice for the following reasons:

Too low values of $\frac{N}{d}$ have a very small capacitance which could be subject to noise disturbances in online applications. Furthermore, with the choice of $L = 30\ mm$, it is better to remain more conservative on Magnetic sensitivity than the Electric as it is much more likely to occur in real MO with a size lower than 30 mm compared to realistic LO. Consequently, with this choice we have $d = 0.8\ mm$ and $N = 8$.

Finally, $r = 0.4\,mm$ was chosen as considering the trade-off among low eddy-current caused by electromagnetic field, low equivalent resistance and realistic dimensions of a PCB.

3.3.3 Series Connection

Once the optimal parameters of the single spiral have been defined, the second spiral is connected in series to obtain the complete "Basic Cell". In fact, the series of two spirals will be the element to be reproduced to obtain the detection coil layers. The simulation conducted is shown in Fig. 3-7 The object is the same as the previous simulations (MO and LO) and it is positioned on the first spiral. In this case, the geometrical variable as a function of the sensitivity is the distance of the series connection G_S.

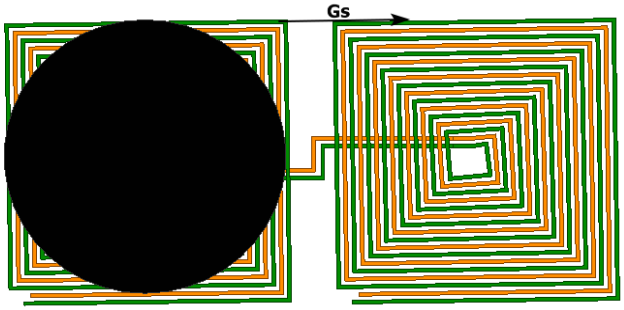

Figure 3-7: Series Connection of the Basic Cells.

The reasons for choosing this series connection are as follows:

- As seen in the subsection 2.1.1, it is preferable to have a null (or very close to zero) induced voltage on the detection coil as a reference condition (absence of MO). The series connection of two spirals with opposite current flow direction guarantees this condition on the basic cell since the two voltages induced on the spirals have opposite sign;
- The series connection of the second spiral increases the space covered by the detection coil without increasing the number of basic cells as it is a single element.
- The two spirals being connected are dependent on each other so the actual size of the basic cell L doubles meeting the requirements of the LOD. For the purposes of sensitivity, however, since both sensitivities are based on the interference of the FO on the Magnetic or Electric field, the single spiral is

enough for the detection of the object. Thus, the size of the basic cell it could be seen again as only L (useful for the small MOD requirements). In practice, a single spiral can detect small MO individually while both spirals can work to detect LO by mitigating the ground effect.

The simulation results are shown in Fig. 3-8. As we have the complete basic cell of the equivalent circuit showed in Fig. 3-2 The parameters to be analyzed are three for each sensitivity. In fact, we have C_{13g}, C_{24g} and C_{12} (since the circuit is reciprocal we do not consider C_{34}) for Electric sensitivity and L_{13}, L_{24} and L_M for the Magnetic sensitivity. However, for the purpose of this simulation all the electrical or magnetic parameters follow the same trend, therefore it is enough to analyze one by type.

First, it is important to notice there is a reduction of the Magnetic sensitivity after the addition of the series connection. This is reasonable because of the null induced voltage condition but also the object is positioned on a single spiral and not on both, therefore in this simulation the detection is not optimal as the previous ones. However, the reduction in sensitivity is justified by the increase of the range of detectable LO and MO as explained above. Thus, the choice to be more conservative on the MOD turns out to be right.

The electrostatic simulation shows how the capacitance value is the double compared to the simulations with only one spiral. In fact, looking at the equivalent circuit, the series connection of the spirals, considering a low impedance inductive circuit, involves a parallel connection of the capacitors C_{12} and C_{34}. The Electric Sensitivity does not undergo large decreases after series connection.

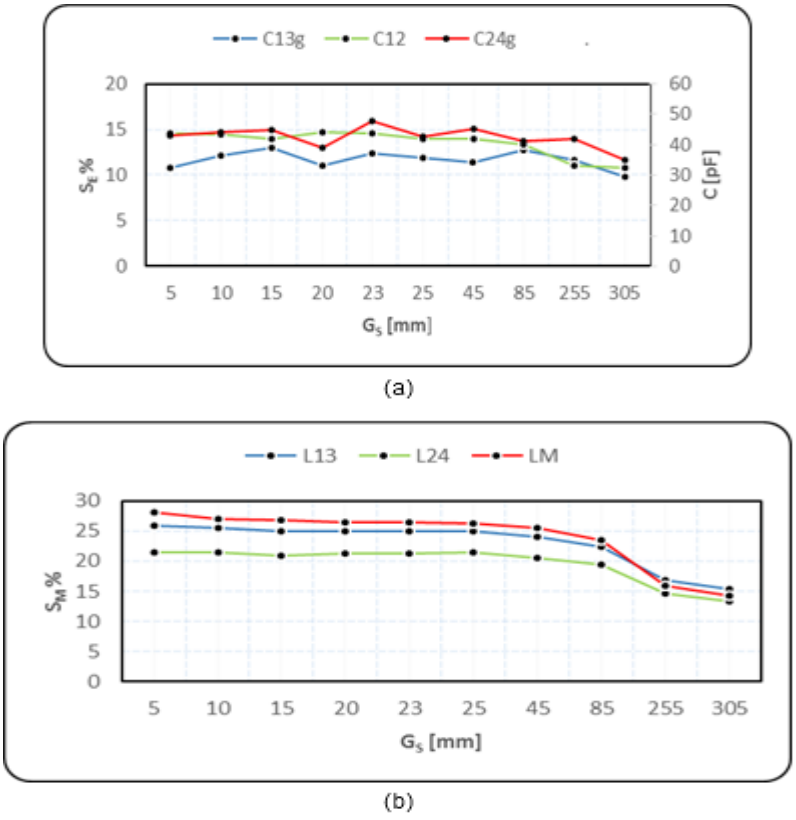

Figure 3-8: Distance of the Series Connection Vs Electric Sensitivity (a) and Magnetic Sensitivity (b).

Finally, the geometrical parameter G_S does not seem to cause strong S_E variations. While in Magnetic Sensitivity, for high G_S values, S_M decreases significantly. This is caused by the fact that a long series connection causes a not negligible increase in the equivalent impedance of the circuit making the sensing path less sensitive.

Thus, it was chosen $G_S = 23\,mm$ which is also useful for making homogeneous layers. In fact, this value allows to insert a spiral of a basic cell between the two spirals of another one with an offset of $7\,mm$. A lower value of G_S it was not chosen also due to the fact the total number of basic cells it cannot be too high. In section 3.5 this will be shown better.

3.4 The Layer Structure

Once all the parameters of the basic cell have been defined, the next step is to create a layer. In fact, a layer structure (of multiple elements) as explained in sections 2.1.1 and 2.2.1 is the optimal solution to cover as much space as possible with good sensitivity values. In order to create a layer structure, it is necessary to reproduce the basic cell several times along the horizontal and/or the vertical axis. Subsequently, a multi-layer structure will also be considered (reproduction of the basic cell along the transverse z axis).

The basic cells will be electrically and magnetically coupled to each other. It is therefore essential to keep the coupling coefficients under control, obtain their lowest possible value and then check that the various couplings do not cause a high reduction in the sensitivity and selectivity of the detection coil.

Furthermore, in the following subsections, the system variables are introduced in matrix form, both in a single layer (1-Layer, 2 Basic cells) and with multiple layers (1 Basic cells, 2 or 4 Layers).

3.4.1 Single-Layer Structure

The first step is to consider the detection coil formed by a single layer. In Fig. 3-9 the layer creation is shown where the traces of the terminals have also been created. The horizontal distance G_H and the vertical distance G_V of the basic cells must be defined.

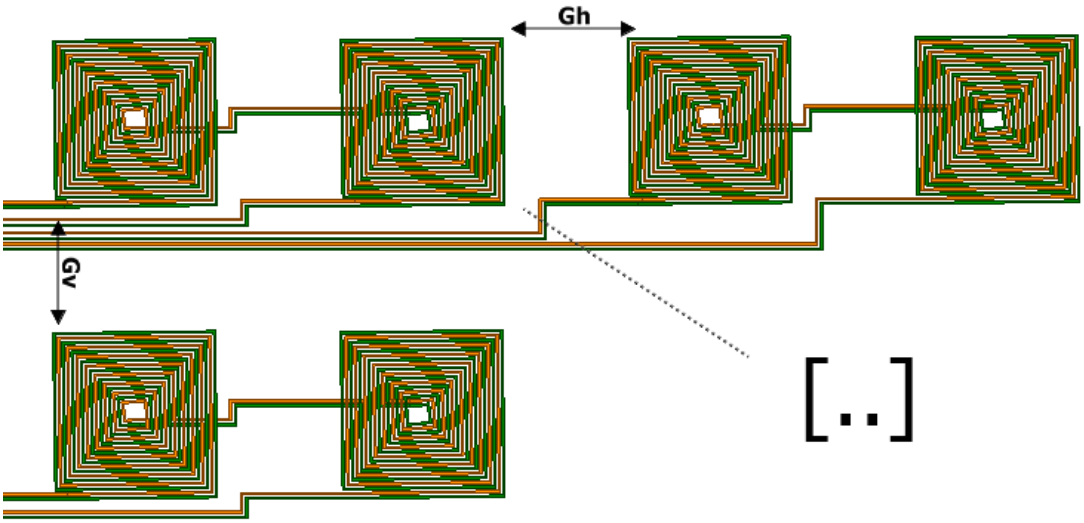

Figure 3-9: Detection coil Layer Structure.

In the simulations a conservative case is considered $G_H = G_V = 1\,mm$ (greater distances imply smaller couplings). Considering first the horizontal alignment as example, we define matrix $\hat{C}_H$ of two basic cells where $C_{12} = C_{34}$:

$$\hat{C}_H = \begin{bmatrix} C_{13g} & C_{12} & \cdots & \cdots \\ C_{12} & C_{24g} & \cdots & \cdots \\ \cdots & \cdots & C_{13g,H} & C_{12,H} \\ \cdots & \cdots & C_{12,H} & C_{13g,H} \end{bmatrix} \tag{3.3}$$

The matrix in Eq. 3.3 presents the following elements:

- C_{13g} and C_{24g} are the Self-Capacitance (Capacitance to the ground) of the first basic cell;
- $C_{13g,H}$ and $C_{24,H}$ are the Self-Capacitance (Capacitance to the ground) of the second basic cell placed along the horizontal axis;
- C_{12} and $C_{12,H}$ are the mutual-Capacitance of the second basic cells;
- All the other elements marked with [..], are parasitic capacitances caused by the coupling between the basic cells.

The coupling coefficient matrix $\widehat{K}_{C,H}$ can also be defined in Eq. 3.4:

$$\widehat{K}_{C,H} = \begin{bmatrix} 1 & K_{12} & .. & .. \\ K_{12} & 1 & .. & .. \\ .. & .. & 1 & K_{12,H} \\ .. & .. & K_{12,H} & 1 \end{bmatrix} \tag{3.4}$$

In Fig. 3-10 are showed the Electrostatic simulation values. In the first matrix the values are in pF; in the second matrix there are the coupling coefficient.

	C13	C24	C13H	C24H
C13	42.015	-41.588	-0.15583	-0.27059
C24	-41.588	42.54	-0.27721	-0.67476
C13H	-0.15583	-0.27721	39.723	-39.29
C24H	-0.27059	-0.67476	-39.29	40.235

(a)

	C13	C24	C13H	C24H
C13	1	-0.98372	-0.0038145	-0.0065812
C24	-0.98372	1	-0.0067436	-0.01631
C13H	-0.0038145	-0.0067436	1	-0.98278
C24H	-0.0065812	-0.01631	-0.98278	1

(b)

Figure 3-10: Capacitance (a) and Coupling coefficient (b) of 1-Layer, 2 Horizontal Basic Cells Structure.

The Coupling percentage can be computed with Eq. 3.5:

$$Coupling_{\%} = \frac{\max(C_{parasitic})}{C} * 100 = \left(1 - \max\left(K_{parasitic}\right)\right) * 100 \tag{3.5}$$

Where C is the capacitance relative to the maximum parasitic capacitance taking as reference the first basic cell.

In the conservative case of $G_H = 1\,mm$ we have $Coupling_{\%} < 1.63\%$.

Similarly, as for the magnetic coupling we define:

$$\hat{L}_H = \begin{bmatrix} L_{13} & L_M & \cdot\cdot & \cdot\cdot \\ L_M & L_{24} & \cdot\cdot & \cdot\cdot \\ \cdot\cdot & \cdot\cdot & L_{13,H} & L_{M,H} \\ \cdot\cdot & \cdot\cdot & L_{M,H} & L_{24,H} \end{bmatrix} \qquad \hat{K}_{L,H} = \begin{bmatrix} 1 & K_{12} & \cdot\cdot & \cdot\cdot \\ K_{12} & 1 & \cdot\cdot & \cdot\cdot \\ \cdot\cdot & \cdot\cdot & 1 & K_{12,H} \\ \cdot\cdot & \cdot\cdot & K_{12,H} & 1 \end{bmatrix} \tag{3.6}$$

Where:

- L_{13}, L_{24}, $L_{13,H}$ and $L_{24,H}$ are the Self-Inductance of the basic cells;
- L_M and $L_{M,H}$ are the Mutual Inductance of the basic cells;
- $\hat{K}_{L,H}$ is the matrix of the inductive coupling coefficients which elements satisfy Eq. 3.7 with $i \neq j$

$$L_{ij} = K_{ij}\sqrt{L_i L_j} \tag{3.7}$$

- Elements marked with [..] are the coupling inductances for $\hat{L}_H$ and the coupling coefficient for $\hat{K}_{L,H}$ between the two basic cells.

In the conservative case of $G_H = 1\,mm$, using Eq. 3.5 but with the inductive elements, we obtain $Coupling_{\%} < 3.47\%$ (Fig. 3-11 (b)). In Fig. 3-11, in the first matrix the inductances are in μH, in the second matrix we have the coupling coefficients.

	L13	L24	L13H	L24H
L13	1.6668	1.3689	0.0486	0.046525
L24	1.3689	1.8832	0.064186	0.066856
L13H	0.0486	0.064186	1.8203	1.4571
L24H	0.046525	0.066856	1.4571	2.0379

(a)

	L13	L24	L13H	L24H
L13	1	0.77265	0.027901	0.025244
L24	0.77265	1	0.034667	0.034128
L13H	0.027901	0.034667	1	0.75653
L24H	0.025244	0.034128	0.75653	1

(b)

Figure 3-11: Inductance (a) and Coupling coefficient (b) of 1-Layer, 2 Horizontal Basic Cell Structure.

With the same procedure it is possible to obtain the couplings along the vertical axis through the matrices $\hat{C}_V$, $\hat{K}_{C,V}$, $\hat{L}_V$, $\hat{K}_{L,V}$.

To make the detection homogeneous over the entire layer it was chosen $G_H = G_V = G_S = 23\,mm$. In this case, we have $Coupling_{\%} < 1.08\,\%$ for the capacitance and $Coupling_{\%} < 3.47\%$ for the inductance. It has been noticed how the vertical coupling is worse for the capacitance, while the horizontal one for the inductance. Furthermore, the magnetic coupling does not vary by increasing the distance, in the simulated range of the basic cells.

In section 3.5, it will be tested if these values are sufficient to guarantee the Sensitivity and the Selectivity of the detection coil.

3.4.2 Multi-Layer Structure

In Subsection 2.1.2, it has been explained how in general, a sensing path can suffer from the so-called “Blind zones”, which are areas where the presence of an FO is not detected. This phenomenon is present in the detection of metallic objects (MOD). The typical example of a blind zone is the center of a symmetrical sensing path; in fact, in this case the contributions of the magnetic field distortion are equivalent around the area in order to obtain a null resultant. The most used solution is to utilize a multi-layer structure as a sensing path. In this way, offsets are created along the horizontal and vertical directions which mitigate the blind zones. In this thesis this solution is also used. A 4-layer structure is chosen and a simulation to

analyse the coupling between the various layers is necessary. In the simulation four layers are used, each with one basic cell as shown in Fig. 3-12.

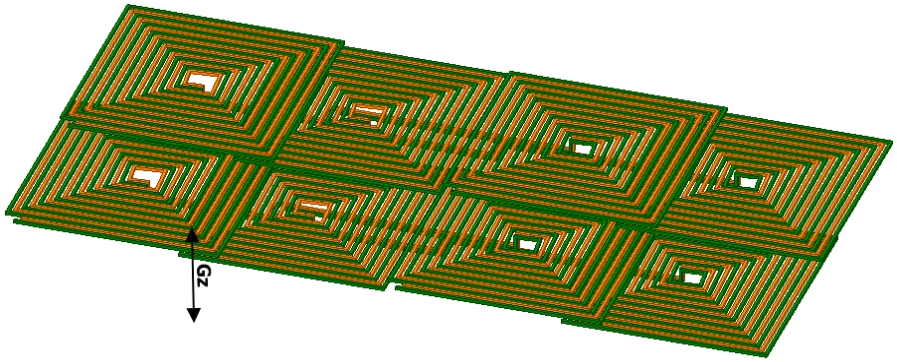

Figure 3-12: 4-Layer detection coil structure.

From the previous simulations the choices of having $L = 30\,mm$ and $G_H = G_V = G_S = 23\,mm$, achieve a vertical and horizontal offset of $7\,mm$. Additionally, the parameter G_z, i.e. the distance between the various layers along the z-axis is set at $0.25\,mm$ to have a realistic value of the height (thickness) of the detection coil. Similarly, to the previous section, the simulation will output the matrices:

$$\hat{C}_Z = \begin{bmatrix} C_{13g,1} & C_{12,1} & \cdots & \cdots & \cdots & \cdots & \cdots & \cdots \\ C_{12,1} & C_{24g,1} & \cdots & \cdots & \cdots & \cdots & \cdots & \cdots \\ \cdots & \cdots & C_{13g,2} & C_{12,2} & \cdots & \cdots & \cdots & \cdots \\ \cdots & \cdots & C_{12,2} & C_{24g,2} & \cdots & \cdots & \cdots & \cdots \\ \cdots & \cdots & \cdots & \cdots & C_{13g,3} & C_{12,3} & \cdots & \cdots \\ \cdots & \cdots & \cdots & \cdots & C_{12,3} & C_{24g,3} & \cdots & \cdots \\ \cdots & \cdots & \cdots & \cdots & \cdots & \cdots & C_{13g,4} & C_{12,4} \\ \cdots & \cdots & \cdots & \cdots & \cdots & \cdots & C_{12,4} & C_{24g,4} \end{bmatrix} \quad \hat{K}_{C,Z} = \begin{bmatrix} 1 & K_{12,1} & \cdots & \cdots & \cdots & \cdots & \cdots & \cdots \\ K_{12,1} & 1 & \cdots & \cdots & \cdots & \cdots & \cdots & \cdots \\ \cdots & \cdots & 1 & K_{12,2} & \cdots & \cdots & \cdots & \cdots \\ \cdots & \cdots & K_{12,2} & 1 & \cdots & \cdots & \cdots & \cdots \\ \cdots & \cdots & \cdots & \cdots & 1 & K_{12,3} & \cdots & \cdots \\ \cdots & \cdots & \cdots & \cdots & K_{12,3} & 1 & \cdots & \cdots \\ \cdots & \cdots & \cdots & \cdots & \cdots & \cdots & 1 & K_{12,4} \\ \cdots & \cdots & \cdots & \cdots & \cdots & \cdots & K_{12,4} & 1 \end{bmatrix} \tag{3.8}$$

$$\hat{L}_Z = \begin{bmatrix} L_{13,1} & L_{M,1} & \cdots & \cdots & \cdots & \cdots & \cdots & \cdots \\ L_{M,1} & L_{24,1} & \cdots & \cdots & \cdots & \cdots & \cdots & \cdots \\ \cdots & \cdots & L_{13,2} & L_{M,2} & \cdots & \cdots & \cdots & \cdots \\ \cdots & \cdots & L_{M,2} & L_{24,2} & \cdots & \cdots & \cdots & \cdots \\ \cdots & \cdots & \cdots & \cdots & L_{13,3} & L_{M,3} & \cdots & \cdots \\ \cdots & \cdots & \cdots & \cdots & L_{M,3} & L_{24,3} & \cdots & \cdots \\ \cdots & \cdots & \cdots & \cdots & \cdots & \cdots & L_{13,4} & L_{M,4} \\ \cdots & \cdots & \cdots & \cdots & \cdots & \cdots & L_{M,4} & L_{24,4} \end{bmatrix} \quad \hat{K}_{L,Z} = \begin{bmatrix} 1 & K_{12,1} & \cdots & \cdots & \cdots & \cdots & \cdots & \cdots \\ K_{12,1} & 1 & \cdots & \cdots & \cdots & \cdots & \cdots & \cdots \\ \cdots & \cdots & 1 & K_{12,2} & \cdots & \cdots & \cdots & \cdots \\ \cdots & \cdots & K_{12,2} & 1 & \cdots & \cdots & \cdots & \cdots \\ \cdots & \cdots & \cdots & \cdots & 1 & K_{12,3} & \cdots & \cdots \\ \cdots & \cdots & \cdots & \cdots & K_{12,3} & 1 & \cdots & \cdots \\ \cdots & \cdots & \cdots & \cdots & \cdots & \cdots & 1 & K_{12,4} \\ \cdots & \cdots & \cdots & \cdots & \cdots & \cdots & K_{12,4} & 1 \end{bmatrix}$$

Where:

- A generic element $A_{ij,x}$ indicate:

  $A = L, C\ or\ K$ (Inductance, Capacitance or coupling coefficient element);

ij indicate which inductance or capacitance of the basic cell is considered (self or mutual);

x indicates which layer the element belongs to.

- Elements marked with [..] are the coupling coefficients between different basic cells of different layers.

The numerical values, both for a 2-layer and a 4-layer structure are shown in Appendix A. The couplings result to be:

$$Capacitive\ Coupling_{\%} < 16.685\ \%\ (2\ Layers)$$

$$Capacitive\ Coupling_{\%} < 15.308\ \%\ (4\ Layers)$$

$$Inductive\ Coupling_{\%} < 6.067\ \%\ (2\ Layers)$$

$$Inductive\ Coupling_{\%} < 10.98\ \%\ (4\ Layers)$$

These couplings cause an overall increase of the impedance of the detection coil. In addition, in the following Section the sensitivity and selectivity of the detection coil will be tested to also analyze their effect.

3.5 Full Detection Coil Model

In the previous sections, all the geometrical parameters of the detection coil were analysed according to the Electric and Magnetic sensitivity in order to obtain a good detection of both MOs and LOs. It is therefore possible to present in this section the complete model of the detection coil.

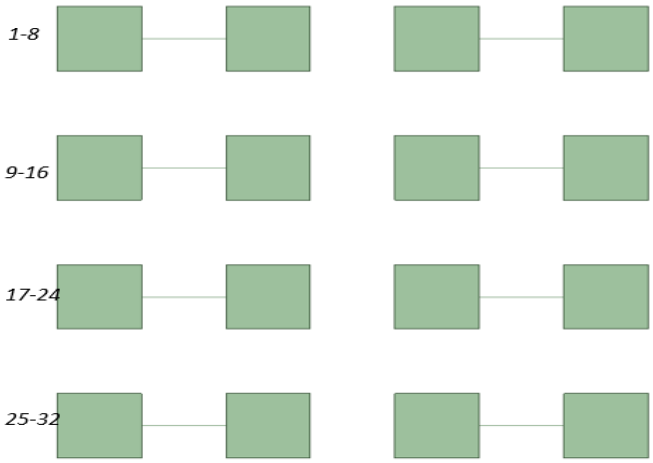

Figure 3-13: 1-Layer schematic of the Detection Coil.

In Fig. 3-13, for the sake of simplicity, each spiral is represented with a square and the connection in series with a horizontal line. Two squares and a line form the previously called “Basic cell”. In the formation of the layer it was chosen to insert two basic cells per row and four per column.

As explained in Fig. 3.2 each basic cell has 4 terminals therefore each row has 8. There is therefore a total of 32 terminals per layer. In Fig. 3-14 instead the whole detection coil is shown including all four layers. In total there are 128 terminals, 32 per layer. The green areas symbolize the offset zones created by the multi-layer structure.

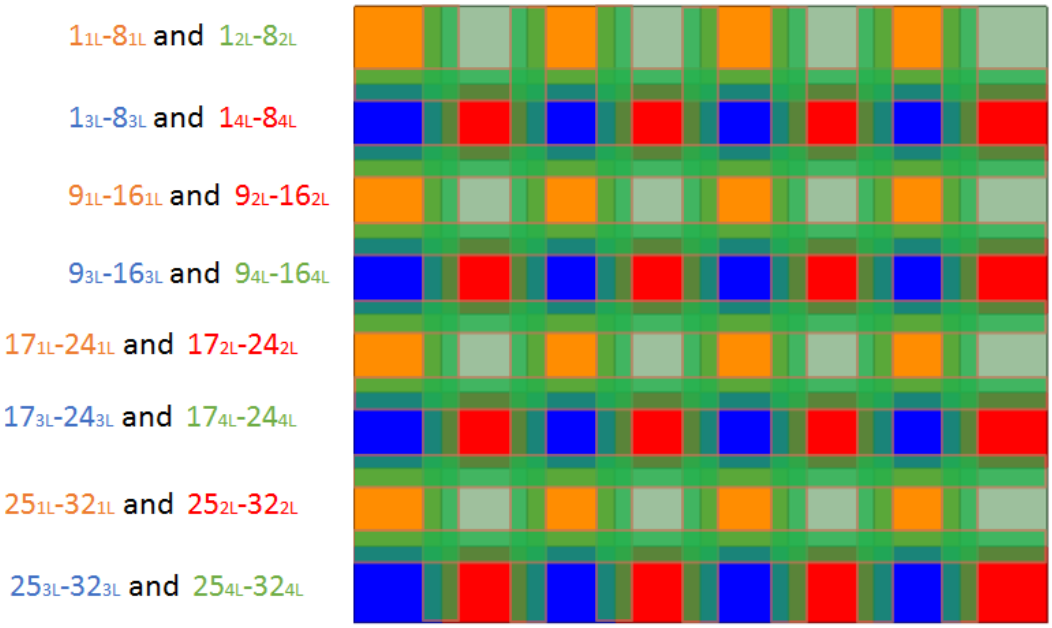

Figure 3-14: 4-Layer schematic of the detection coil.

Finally, in the Tab 3-4, all the geometrical specifications of the detection coil are shown:

Table 3-4: Geometrical Specification of the Detection Coil.

Parameter	Value
L	30 mm
N	8
d	0.8 mm
r	0.4 mm
G_S	23 mm
G_H	23 mm
G_V	23 mm
G_Z	0.25 mm
Number of Basic Cells per layer	8
Number of layers	4
Vertical/Horizontal layers Offset	7 mm
Tracks Thickness	0.1 mm
Detection coil (PCB) Thickness	1.15 mm
Detection coil total dimension	*230 x 230 x 1.15 mm*

3.5.1 The Simulation Model

Now that the entire detection coil has been designed, it is possible to create the complete model using the Ansys software and verify its effectiveness. Specifically, four simulations will be carried out:

1. Offline Electrostatic Simulation;
2. Offline Eddy Current (Electromagnetic) Simulation;
3. Online Electrostatic Simulation;
4. Online Eddy Current (Electromagnetic) Simulation;

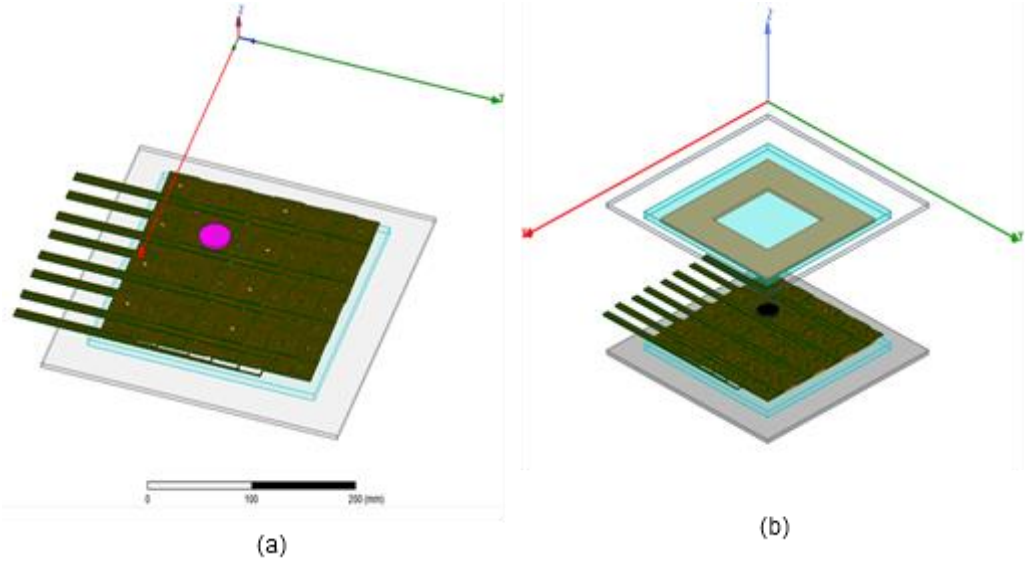

Figure 3-15: Full Simulation Model. Offline model (a) and Online model (b).

In Fig. 3-15, the simulation models are shown. Fig. 3-15 (a) shows the offline model while the Online model is shown in Fig. 3-15 (b). In the offline model, in addition to the detection coil, it was added the transmitter coil (TX), a ferrite structure and a mechanical glass structure. In the online configuration, the receiver structure has also been added with a misalignment of $2.5\ mm$ for a sake of generality.

Tab. 3-5 instead, show the specifications of the model.

Table 3-5: Simulation Model specifications.

Offline Parameters	**Value**
Transmitter coil dimensions	$200\ x\ 200\ x\ 5\ mm$
Transmitter ferrite dimensions	$230\ x\ 230\ x\ 5\ mm$
Detection coil dimensions	$230\ x\ 230\ x\ 1.15\ mm$
Transmitter glass dimensions	$300\ x\ 300\ x\ 3\ mm$

Online Parameters	Value
Transmitter coil dimensions	$200\ x\ 200\ x\ 5\ mm$
$I_{tx} = I_{rx}$	$10\ A$
$I_{tx}\ Phase$	$0°$
$I_{rx}\ Phase$	$90°$
$N_{tx} = N_{rx}$	12
IPT Frequency	$85\ kHz$
$L_{tx} = L_{rx}$	$50\ uH$
k_{IPT}	0.2
$M_{IPT} = k_{IPT}\sqrt{L_{tx}L_{rx}}$	$10\ uH$
$V_{tx} = j\omega M_{IPT} I_{tx} = V_{rx} = j\omega M_{IPT} I_{rx}$	$53.4\ V$
IPT Power Level	$0.5\ kW$
Transmitter ferrite dimensions	$230\ x\ 230\ x\ 5\ mm$
Detection coil dimensions	$230\ x\ 230\ x\ 1.15\ mm$
Transmitter glass dimensions	$300\ x\ 300\ x\ 3\ mm$
Receiver coil dimensions	$200\ x\ 200\ x\ 5\ mm$
Receiver ferrite dimensions	$230\ x\ 230\ x\ 5\ mm$
Receiver glass dimensions	$300\ x\ 300\ x\ 3\ mm$
Airgap	$100\ mm$
Horizontal/Vertical Misalignment	$2.5\ mm$

The above parameters have been chosen in order to simulate a realistic and reproducible IPT structure as explained later in the next section.

Furthermore, in order to analyze the sensitivity of the detection coil, a FO is inserted in the model (a LO for simulations 1 and 3 and a MO for simulations 2 and 4).

The object specifications are the same as those used in Section 3.3 listed in the Tab. 3-1 considering the case $L_O = L$.

3.5.2 LOD Simulation

Once the simulation model is defined, it is important to define the output that the simulation will give us. To do this, as in the Section 3.4, the variables are defined in a matrix form. In the Electrostatic simulation, only the first layer is considered as output, however the other 3 layers are also included in the model. Thus, it provides us the matrix $\hat{C}_{Tot}$ with size 18 x 18 for the Online simulation and 16 x 16 for the Offline simulation. As the number of basic cells is high, the separator _ between the terminals of the basic cells has been included.

$$\hat{C}_{Tot} = \begin{bmatrix} \begin{bmatrix} C_{1\_3g} & C_{1\_2} \\ C_{1\_2} & C_{2\_4g} \end{bmatrix} & \cdots & \cdots & \vdots \\ \vdots & \ddots & \begin{bmatrix} C_{29\_31g} & C_{31\_32} \\ C_{31\_32} & C_{30\_32g} \end{bmatrix} & \begin{bmatrix} C_{txg} & C_{tx\_rx} \\ C_{tx\_rx} & C_{rxg} \end{bmatrix} \end{bmatrix} \tag{3.9}$$

In Eq. 3.9:

- Each basic cell forms on the diagonal a 2 x 2 matrix including the Self-capacitance (Capacitance to the ground) and the Mutual capacitance. The entire layer, containing 8 basic cells, forms a 16 x 16 matrix;
- The last two rows and columns are composed by the IPT system. Thus, the Transmitter and the Receiver also form a 2 x 2 matrix. This part is not present in the Offline simulation as the IPT system is not powered.
- All the elements, marked with [..], are parasitic capacitances caused by the coupling between the basic cells and the basic cells with the IPT system.

Numeric values are shown in Appendix B. However, in order to test the effectiveness of the detection coil in FOD, only the elements on the diagonal are necessary. It is therefore possible to obtain a more intuitive 8 x 4 positional matrix $\hat{C}$.

$$\hat{C} = \begin{matrix} Position \\ 1 \\ 1 \\ 2 \\ 2 \\ 3 \\ 3 \\ 4 \\ 4 \end{matrix} \begin{matrix} \\ 1 \\ 2 \\ 1 \\ 2 \\ 1 \\ 2 \\ 1 \\ 2 \end{matrix} \begin{bmatrix} C_{1\_3g} & C_{1\_2} & C_{5\_7g} & C_{5\_6} \\ C_{1\_2} & C_{2\_4g} & C_{5\_6} & C_{6\_8g} \\ C_{9\_11g} & C_{9\_10} & C_{13\_15g} & C_{13\_14} \\ C_{9\_10} & C_{10\_12g} & C_{13\_14} & C_{14\_16g} \\ C_{17\_19g} & C_{17\_18} & C_{21\_23g} & C_{21\_22} \\ C_{17\_18} & C_{18\_20g} & C_{21\_22} & C_{22\_24g} \\ C_{25\_27g} & C_{25\_26} & C_{29\_31g} & C_{29\_30} \\ C_{25\_26} & C_{26\_28g} & C_{29\_30} & C_{30\_32g} \end{bmatrix} \quad (3.10)$$

As in the previous cases, since the circuit is reciprocal, we have $C_{1\_2} = C_{3\_4}$. Same for each basic cell.

In addition to selecting the only elements of interest, this matrix turns out to be a positional matrix since the numbers 1 to 4 of the rows and columns of the matrix indicate the position of the basic cell in the detection coil. In Fig. 3-16 the first numbered layer is shown.

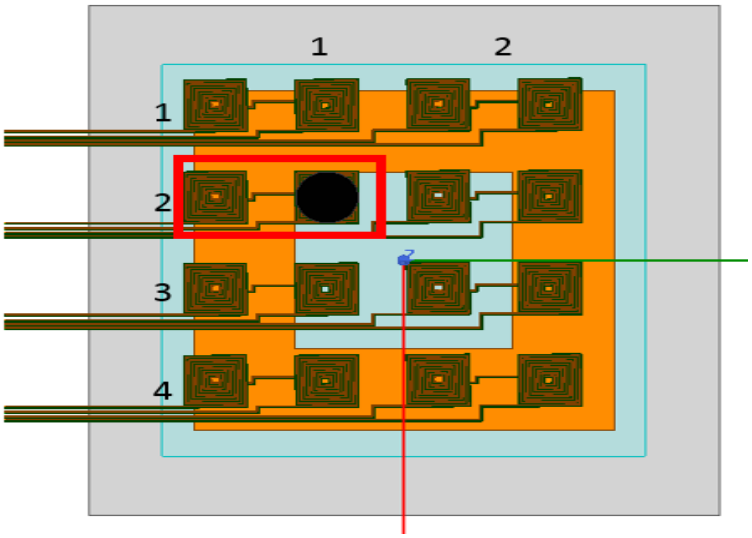

Figure 3-16: Positional Matrix and Simulation Model.

Furthermore, it is possible to consider a single sensitive element per basic cell further reducing the size of the matrix. For instance, if we only consider the mutual capacitance of the basic cells, we obtain the 4 x 2 matrix $\hat{C}_M$. From the results (Appendix B) the mutual capacitance is more sensitive than the capacitance to the ground.

$$\hat{C}_M = \begin{matrix} Position \\ 1 \\ 2 \\ 3 \\ 4 \end{matrix} \begin{matrix} 1 & 2 \end{matrix} \begin{bmatrix} C_{1\_2} & C_{5\_6} \\ C_{9\_10} & C_{13\_14} \\ C_{17\_18} & C_{21\_22} \\ C_{25\_26} & C_{29\_30} \end{bmatrix} \tag{3.11}$$

As the last step, the Electric Sensitivity Matrix is calculated by analyzing the presence of a LO as shown in Fig. 3-16. Each element of the matrix is computer in this way:

$$\hat{S}_E\% = \left| [S_{ij} = \frac{C_{ij(w)} - C_{ij(wo)}}{C_{ij(wo)}} * 100] \right| \tag{3.12}$$

Where ij is the index of each element of the matrices listed above while w and wo indicate whether the simulation was performed "with" or "without" the LO.

All the numerical values are reported in Appendix B. Considering the only the mutual capacitance, the results for the Electric Sensitivity in both the offline and online cases are shown below:

$$\hat{S}_{E,Offline}\% = \begin{matrix} Position \\ 1 \\ 2 \\ 3 \\ 4 \end{matrix} \begin{matrix} 1 & 2 \end{matrix} \begin{bmatrix} 0.314 & 0.327 \\ \mathbf{22.410} & 0.327 \\ 0.288 & 0.316 \\ 0.290 & 0.284 \end{bmatrix} \tag{3.13}$$

(3.14)

$$\hat{S}_{E,Online}\% = \begin{matrix} Position \\ 1 \\ 2 \\ 3 \\ 4 \end{matrix} \begin{matrix} 1 & 2 \end{matrix} \begin{bmatrix} 9.538 & 8.089 \\ \mathbf{38.168} & 20.847 \\ 10.120 & 9.969 \\ 8.671 & 5.826 \end{bmatrix}$$

The position, i.e. the basic cell where the LO has been positioned, is indicated in bold. Referring to fig we therefore mean the base cell of the second row, first column and therefore the variation of the capacitance C_{9_10}.

In offline simulation, there is an excellent LOD sensitivity and selectivity (DoP). In fact, in the position where the LO is positioned there is a variation in capacitance of 22.4 % while in the other positions there are no measurable capacitance variations. The fact that the detection coil is also selective offline is an excellent result as in addition to detecting the object, it is also possible to define its position.

The IPT system, (Online operation), makes the detection coil even more sensitive to LOs. in fact, it is possible to observe an increase in sensitivity from 22.4 to 38.2 %.

However, Online, the other basic cells also have a variation in capacitance, even if less than the position where the LO is present. There are two ways to approach this result:

- Guarantee the Selectivity by designing a sensing circuit with high minimum sensitivity (for instance, more than 25%)
- Do not consider online selectivity as a target anymore. Since the level of danger is higher online, only sensitivity is assumed as a priority parameter to be monitored. In this case, this partial selectivity of the detection coil could be an advantage in that less scans of the detection coil may occur making Online LOD faster than Offline. In fact, thinking about the detection coil combined with a switching system which scans the various terminals of the detection coil, Offline the system detects the object only when the basic cell containing the object is scanned. Online, on the other hand, as the other basic cells are sensitive too, detection could occur earlier. It should be remembered that the simulation is quite conservative as the object is small.

The second option seems the most reasonable one since selectivity was not a primary objective of the project.

Returning to the Offline configuration, since a strong selectivity is noted, a further simulation is carried out as shown in Fig. 3-17.

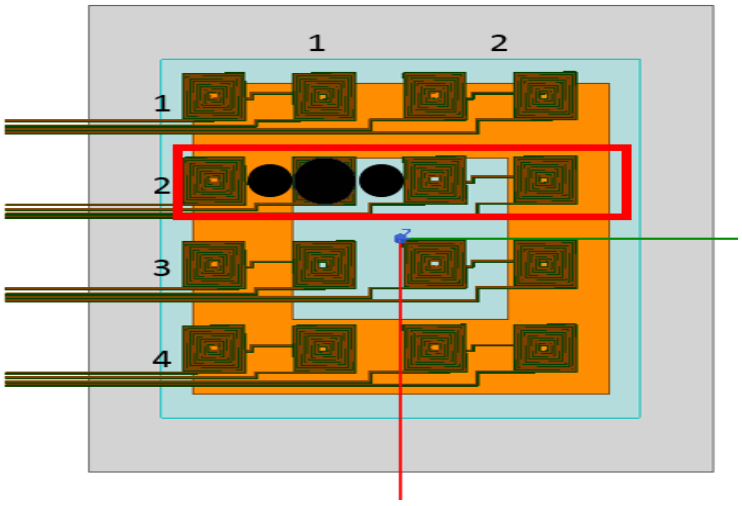

Figure 3-17: LOD Simulation to test layers coupling.

The LO is now positioned in two new positions which are part of areas covered by the other layers. Results are listed here:

$$\hat{S}_{E,Offline}\% = \begin{matrix} Left\ Position \\ 1 \\ 2 \\ 3 \\ 4 \end{matrix} \begin{matrix} 1 & 2 \end{matrix} \begin{bmatrix} 0.386 & 0.415 \\ 0.370 & 0.426 \\ 0.379 & 0.409 \\ 0.379 & 0.380 \end{bmatrix} \tag{3.15}$$

$$\hat{S}_{E,Offline}\% = \begin{matrix} Right\ Position \\ 1 \\ 2 \\ 3 \\ 4 \end{matrix} \begin{matrix} 1 & 2 \end{matrix} \begin{bmatrix} 0.396 & 0.419 \\ 0.367 & 0.411 \\ 0.369 & 0.398 \\ 0.376 & 0.384 \end{bmatrix} \tag{3.16}$$

We note how the first layer does not undergo perceptible changes in capacitance. By combining these two simulations with the first Offline simulation we can conclude that:

The first simulation confirm that a layer detects the object if positioned on it with selectivity over the surface of the layer. The second and third simulations, on the other hand, prove selectivity even between the layers since the LO is positioned in positions not covered by the first layer and is not detected. The values of the coupling coefficients calculated in Subsection 3.4.1 and 3.4.2 are of a sufficiently low value to decouple the layers; otherwise in the last two simulations, the parasitic capacitances between the layers would have caused a change in capacitance. A complete Offline Selectivity is therefore confirmed.

3.5.3 MOD Simulation

Following the same procedure of the previous section, the Sensitivity and the Selectivity of the detection coil to the MOs is now verified by an Electromagnetic simulation (Eddy Current simulation) obtaining in this case the various inductances of the system as output.

In this case, the simulation provides us in addition to the inductance values also the resistance values. It is therefore appropriate to define the 18 x 18 $\hat{Z}_{Tot}$ matrix:

$$\hat{Z}_{Tot} = \begin{bmatrix} \begin{bmatrix} R_{1\_3}, L_{1\_3} & R_{1\_2}, L_{1\_2} \\ R_{1\_2}, L_{1\_2} & R_{2\_4}, L_{2\_4} \end{bmatrix} & \cdots & \cdots & \cdots \\ \vdots & \ddots & \vdots & \vdots \\ \cdots & \cdots & \begin{bmatrix} R_{29\_31}, L_{29\_31} & R_{31\_32}, L_{31\_32} \\ R_{31\_32}, L_{31\_32} & R_{30\_32}, L_{30\_32} \end{bmatrix} & \cdots \\ \vdots & \vdots & \vdots & \begin{bmatrix} R_{tx}, L_{tx} & R_{tx\_rx}, L_{tx\_rx} \\ R_{tx\_rx}, L_{tx\_rx} & R_{rx}, L_{rx} \end{bmatrix} \end{bmatrix} \tag{3.17}$$

Where we have:

- Each basic cell forms on the diagonal a 2 x 2 matrix including the Self-Inductance and the Mutual inductance (previously called L_M). The entire layer, containing 8 basic cells, forms a 16 x 16 matrix;
- The last two rows and columns are composed by the IPT system. Thus, the Transmitter and the Receiver also form a 2 x 2 matrix. This part is not present in the Offline simulation as the IPT system is not powered.
- All the elements, marked with [..], are parasitic inductances caused by the coupling between the basic cells and the basic cells with the IPT system.
- Same goes for resistance values. These values have been reported for completeness, however from now on, these values will no longer be considered as they are not useful for the purpose of testing the Magnetic Sensitivity.

Numeric values are shown in Appendix C. As in the LOD simulation, it is useful to switch to the 8 x 4 positional matrix $\hat{L}$:

$$\hat{L} = \begin{matrix} Position \\ 1 \\ 1 \\ 2 \\ 2 \\ 3 \\ 3 \\ 4 \\ 4 \end{matrix} \begin{matrix} \begin{matrix} 1 & 1 & 2 & 2 \end{matrix} \\ \begin{bmatrix} L_{1\_3} & L_{1\_2} & L_{5\_7} & L_{5\_6} \\ L_{1\_2} & L_{2\_4} & L_{5\_6} & L_{6\_8} \\ L_{9\_11} & L_{9\_10} & L_{13\_15} & L_{13\_14} \\ L_{9\_10} & L_{10\_12} & L_{13\_14} & L_{14\_16} \\ L_{17\_19} & L_{17\_18} & L_{21\_23} & L_{21\_22} \\ L_{17\_18} & L_{18\_20} & L_{21\_22} & L_{22\_24} \\ L_{25\_27} & L_{25\_26} & L_{29\_31} & L_{29\_30} \\ L_{25\_26} & L_{26\_28} & L_{29\_30} & L_{30\_32} \end{bmatrix} \end{matrix} \tag{3.18}$$

Even for the inductance $L_{1\_2} = L_{3\_4}$ l is valid. Same for each basic cell.

From Appendix C the Mutual Inductance is slightly more sensitive than the Self Inductance to the ground. Thus, we can obtain the 4 x 2 matrix $\hat{L}_M$:

$$\hat{L}_M = \begin{matrix} Position \\ 1 \\ 2 \\ 3 \\ 4 \end{matrix} \begin{matrix} \begin{matrix} 1 & 2 \end{matrix} \\ \begin{bmatrix} L_{1\_2} & L_{5\_6} \\ L_{9\_10} & L_{13\_14} \\ L_{17\_18} & L_{21\_22} \\ L_{25\_26} & L_{29\_30} \end{bmatrix} \end{matrix} \tag{3.19}$$

Finally, the Magnetic Sensitivity Matrix is calculated by analyzing the presence of a MO as in Fig.3-16. Therefore, each element of the matrix is computed:

$$\hat{S}_M\% = \left| [S_{ij} = \frac{L_{ij(w)} - L_{ij(wo)}}{L_{ij(wo)}} * 100] \right| \tag{3.20}$$

Where ij is the index of each element of the matrices listed above while w and wo indicate whether the simulation was performed "with" or "without" the MO.

Magnetic Sensitivity matrices are obtained for both Offline and Online configuration:

$$\hat{S}_{M,Offline}\% = \begin{matrix} Position \\ 1 \\ 2 \\ 3 \\ 4 \end{matrix} \begin{matrix} 1 \quad 2 \\ \begin{bmatrix} 0.018 & 0.104 \\ \mathbf{-57.719} & 0.123 \\ 0.140 & 0.042 \\ -0.138 & -0.139 \end{bmatrix} \end{matrix} \tag{3.21}$$

$$\hat{S}_{M,Online}\% = \begin{matrix} Position \\ 1 \\ 2 \\ 3 \\ 4 \end{matrix} \begin{matrix} 1 \quad 2 \\ \begin{bmatrix} -0.061 & -0.215 \\ \mathbf{-57.752} & 0.016 \\ -0.216 & -0.090 \\ 0.098 & 0.059 \end{bmatrix} \end{matrix} \tag{3.22}$$

Online and Offline simulations show similar results; in both cases the Magnetic Sensitivity is confirmed (more than 57.7% of Inductance variation). A strong Selectivity (DoP) is also present since only the basic cell under the surface of the MO undergoes detectable variations.

3.6 Experimental Verification

A real PCB shown in Fig. 3-18, designed with the parameters chosen in the previous sections, was created in order to confirm the results of the previous simulations. To do this, real impedance measurements will be made to verify the effectiveness of the detection coil for real FOs.

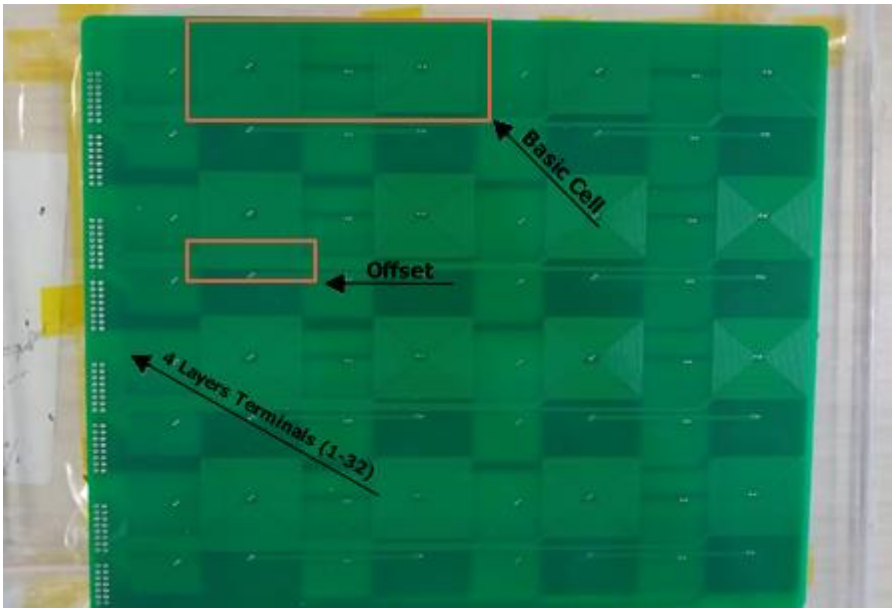

Figure 3-18: PCB of the proposed detection coil.

In the experiment, the detection coil is positioned over a typical transmitter of an IPT system shown in Fig. 3-19. The characteristics of the transmitter are shown in Tab. 3-6.

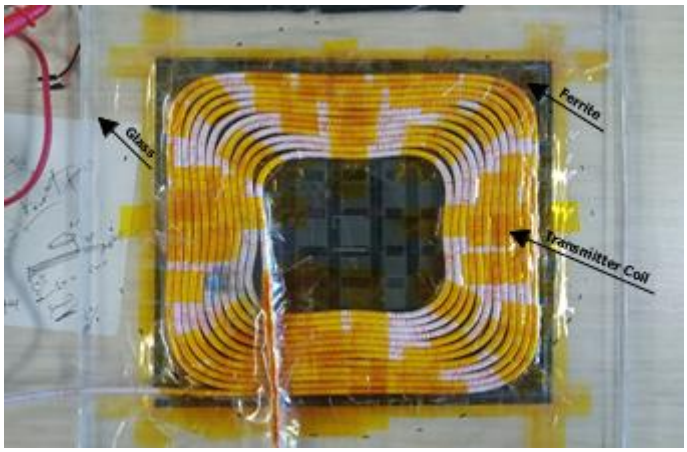

Figure 3-19: IPT Transmitting pad used in the experiment.

Table 3-6: Laboratory IPT Parameters.

Component	Value
Transmitter coil dimensions	$200\ x\ 200\ x\ 5\ mm$

Transmitter ferrite dimensions	$230\ x\ 230\ x\ 5\ mm$
Detection coil dimensions	$230\ x\ 230\ x\ 1.15\ mm$
Transmitter glass dimensions	$300\ x\ 300\ x\ 3\ mm$
N_{tx}	12

We note that:

- The structure has the same parameters used in the Ansys simulation model to have consistent results between the simulations and the real measurement.
- The Detection coil completely covers the surface of the IPT system.
- Even though the measurements will be taken Offline, the number of turns of the transmitter coil is 12.

3.6.1 Measurement of the Impedance

As a first validation step of the proposed method, the impedance measurements of the detection coil are carried out in various circumstances.

Several objects are positioned on the detection coil to check both the MOD and the LOD (Fig. 3-20 and Tab 3-7).

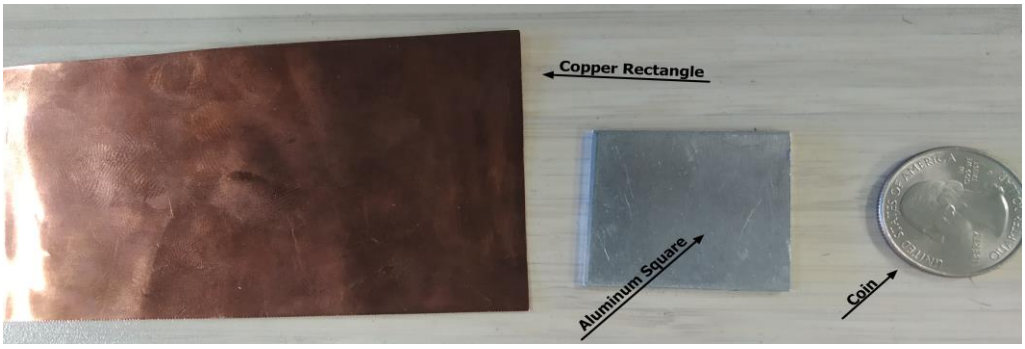

Figure 3-20: Real MOs used.

Table 3-7: FOs specifications for both MOD and LOD validation.

Object	FO type	Physical Dimension
USA quarter dollar coin	MO	$Diameter = 23\ mm$
Aluminum square	MO	$30\ x\ 30\ mm$
Copper Rectangle	MO	$90\ x\ 50\ mm$
Human fingertip	LO	$Diameter = 7\ mm$

To verify the Magnetic and the Electric Sensitivity, the Impedance of the basic cell from its terminals will be measured. Measurements are set up on different base cells and from different terminals. The previously simulated Inductance and Capacitance variations, when a MO or a LO will be positioned, will cause an impedance variation through the relationships constituted by the equivalent circuit of the basic cell.

The impedance measurement is carried out though a signal generator with frequency of 300 kHz and $1V$ of amplitude.

As a first measurement, the mainly inductive terminals and the mainly capacitive terminals were tested separately. From the inductive terminals the variation of inductance is verified with the presence of different MOs while from the capacitive terminals the variation of capacitance is tested with the presence of a LO. The results of four different basic cells (Fig. 3-21) are shown in Tab. 3-8 and Tab 3-9.

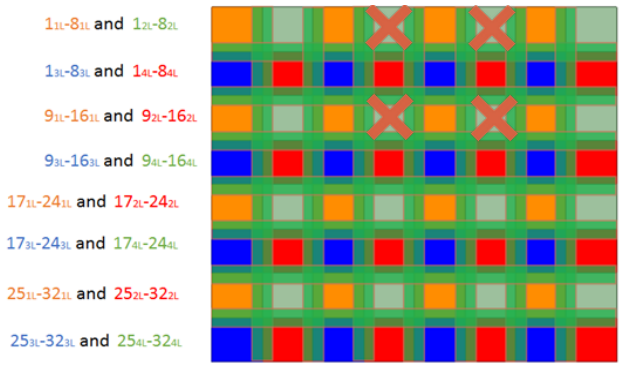

Figure 3-21: Basic Cells Tested.

Table 3-8: Inductance variation for MOD.

Terminals	Without MOs $[\mu H]$	With Coin $[\mu H]$	With Aluminum square $[\mu H]$	With Copper Rectangle $[\mu H]$
L_{2_4}	3.710	2.854 (−23.07%)	2.281 (−38.51%)	2.375 (−35.98%)
L_{5_7}	3.376	2.582 (−23.51%)	2.220 (−34.24%)	2.379 (−29.53%)
L_{10_12}	3.690	2.947 (−20.135%)	2.320 (−37.12%)	2.415 (−34.55%)
L_{13_15}	3.377	2.637 (−21.91%)	2.179 (−35.47%)	2.336 (−30.82%)

Table 3-9: Capacitance variation for LOD.

Terminals	Without LO $[pF]$	With Human Fingertip $[pF]$
C_{3_4}	96.44	> 112 (> 16%)
C_{5_6}	108.924	> 130 (> 19.26%)
C_{9_10}	100.978	> 130 (> 28.71%)
C_{13_14}	111.910	> 124 (> 10.71%)

All the basic cells tested have a good sensitivity to the positioned objects. As expected, MOs decrease inductance while LOs increase capacitance.

In the MOD it is noted that the aluminum square has the greatest sensitivity since the condition $L = L_O$ applies.

In the LOD the variation in capacitance is a function of the pressure exerted by the fingertip; the conservative case with as small pressure as possible is reported.

Subsequently, the sensitivity of the inductive (or capacitive) circuit is tested for both types of objects (MOs or LOs). Since we will have both the inductive and the capacitive contribution, in this case the impedance at the terminals of the basic cell is measured. Considering in this case only one basic cell, the impedance for both circuits measured without any object is:

$$Z_{34} = R_{34} + jX_{34} = R_{34} + j(\omega L_{34} - \frac{1}{\omega C_{34}}) = 0.1 - j5.43\ k\Omega\ \ (Capacitive\ Terminals) \tag{3.23}$$

$$Z_{24} = R_{24} + jX_{24} = R_{24} + j(\omega L_{24} - \frac{1}{\omega C_{24}}) = 2.61 + j6.88\ \Omega\ (Inductive\ Terminals) \tag{3.24}$$

The resistance value, also in this case, is not considered as it presents a difficult measurement repeatability also according to the room temperature.

Numerical values confirm the mainly capacitive nature (negative reactance less and high impedance value) for the first circuit and the predominantly inductive nature for the second circuit (positive reactance and low impedance circuit). The sensitivity results are shown in Tab 3-10:

Table 3-10: Impedance variation for both MOD and LOD.

Terminals	Without FO	With Coin	With Aluminum square	With Copper Rectangle	Human Fingertip
X_{3_4} $[k\Omega]$	−5.43	−5.19 (−4.42%)	−4.69 (−13.63%)	−5.37 (−1.10%)	> −5.12 (−5.71%)
X_{2_4} $[\Omega]$	6.88	5.12 (−25.58%)	4.11 (−40.26%)	4.24 (−38.37%)	> 7.01 (1.89%)

As expected, the capacitive circuit has better results for LOs and the inductive circuit is more sensitive to MOs. However, both types can be detected by both circuits. This is an excellent result as it is possible to choose only one type of circuit to be used in order to decrease the terminals to be scanned during detection. Furthermore, using only one type of circuit, only one type of resonant circuit (sensing circuit) will be needed. In conclusion, a compromise choice is needed between the effectiveness (in terms of sensitivity to the FOs) of the detection coil and the complexity and costs of the system (speed of the switching system and the number of resonant circuits).

In the next chapter, as a sensing circuit for the designed detection coil will be proposed, the hypothesis to use only the capacitive circuit will be adopted. In fact, the circuit will be designed to resonate with the parameters measured by the capacitive terminals. However, the choice to use the inductive circuit remains valid. The choice was made because, for this thesis, priority is given to LOD as in literature it has been less thorough. Furthermore, the capacitive circuit has the advantage that the impedance value decreases for both types of detection; therefore, the voltage variation will always be negative, simplifying the design of the sensing circuit. However, even the MOs are detected with good results thus confirming the project goal of having a Field-Based method for both types of detection. The idea is to present a general proposal that can be modified based on the application and on the type and size of the FOs which must be detected.

3.6.2 Measurement of the Voltage

As further confirmation of the good results obtained from the impedance measurements, the voltage on the detection coil is measured in this Subsection.

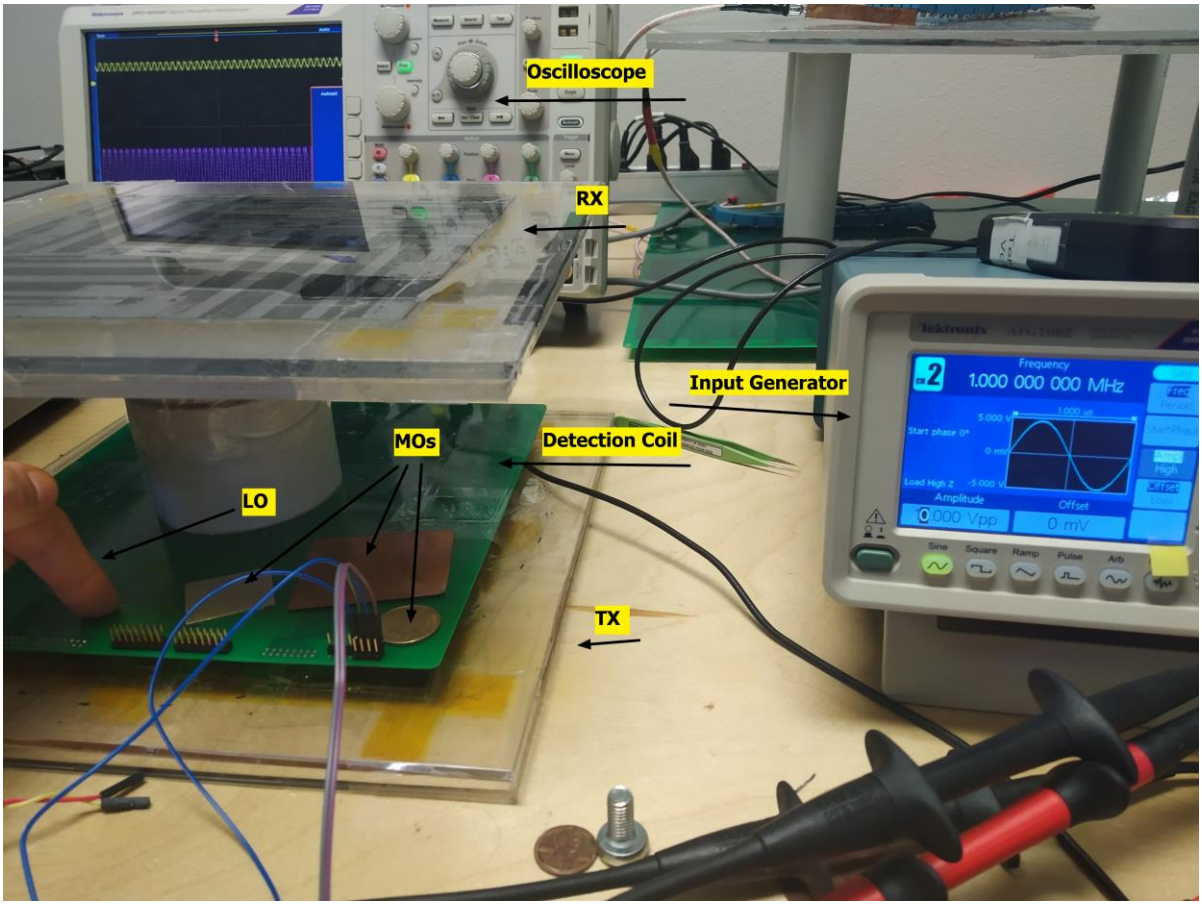

Figure 3-22: Experimental Setup.

Fig. 3-22 shows how the measurement was performed. The IPT structure is composed by the transmitting structure (TX, ferrite and Glass) and the receiving structure (RX, ferrite and glass). Both structures have identical geometrical parameters with reference to Tab. 3-6. The detection coil is inserted above the TX to carry out the FOD. The measurement is performed offline (no power transfer) thus, a voltage generator supplies the detection coil with a reference voltage. The frequency is set at $1MHz$ while the amplitude is made to vary from 2 to $10\,V$.

A digital oscilloscope measures the output voltage on the basic cell of the detection coil. MOs and the fingertip as LO (Tab. 3-7) are positioned over the detection coil to carry out the measurement with and without the foreign object. For the MOD the inductive terminals are tested. Capacitive terminals are instead selected for LOD.

First, in Fig. 3-23 it can be seen how the voltage on the detection coil varies (decreases) its amplitude in the moment the foreign object is added.

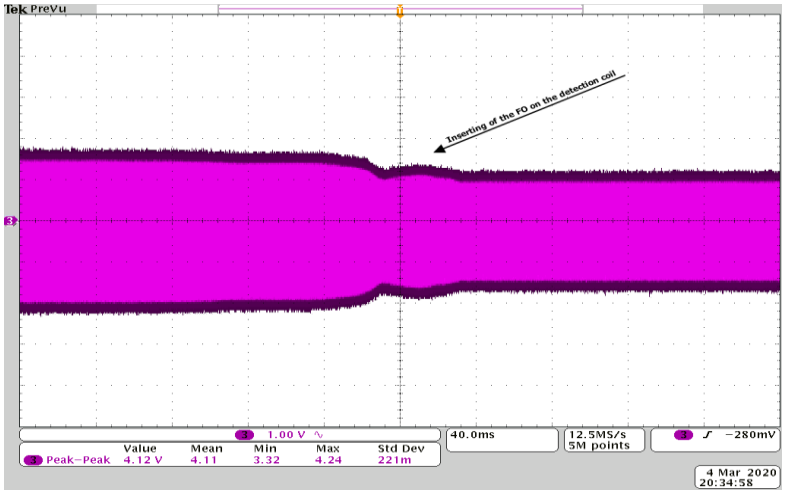

Figure 3-23: Voltage vs Time when a FO is placed.

In Fig. 3-24 the voltage on the detection coil is shown with the insertion of metal objects. The voltage decrease from a value of $2.08\,V$ to $1.46\,V$ with the presence of the aluminum square (29.8%), to $1.68\,V$ (19.23%) with the coin and $1.88\,V$ (9.6%) with copper rectangle.

The three objects, being made of metallic materials, cause a good voltage sensitivity in coherence with the decrease of inductance measured previously. The aluminum square has the best sensitivity since the dimensions of the basic cell and the object coincide. This result is in accordance with the simulation of Subsection 3.3.1 where it is shown that in this condition the inductive circuit is entirely involved and the capacitive circuit does not undergo the ground effect. The coin and the copper rectangle present intermediate situations where, in the first case, the object is smaller than the basic cell, in the second case it is larger. The not whole stress of the inductive circuit and the ground effect cause a slightly lower sensitivity.

In Fig. 3-25 the voltage on the detection coil is shown with the insertion of the human fingertip (living object). The voltage decreases from a value of $2.00\,V$ to $1.60\,V$ (20%) with the presence of the LO. This result is consistent with the previously measured capacitance increase. In this case the sensitivity is also a function of the pressure exerted by the fingertip.

For both MOD and LOD the results are consistent with the simulations of Section 3.5 and the previous measure of the impedance.

Finally, it is possible to state that the voltage and frequency values used are effective for testing the sensitivity of the detection coil.

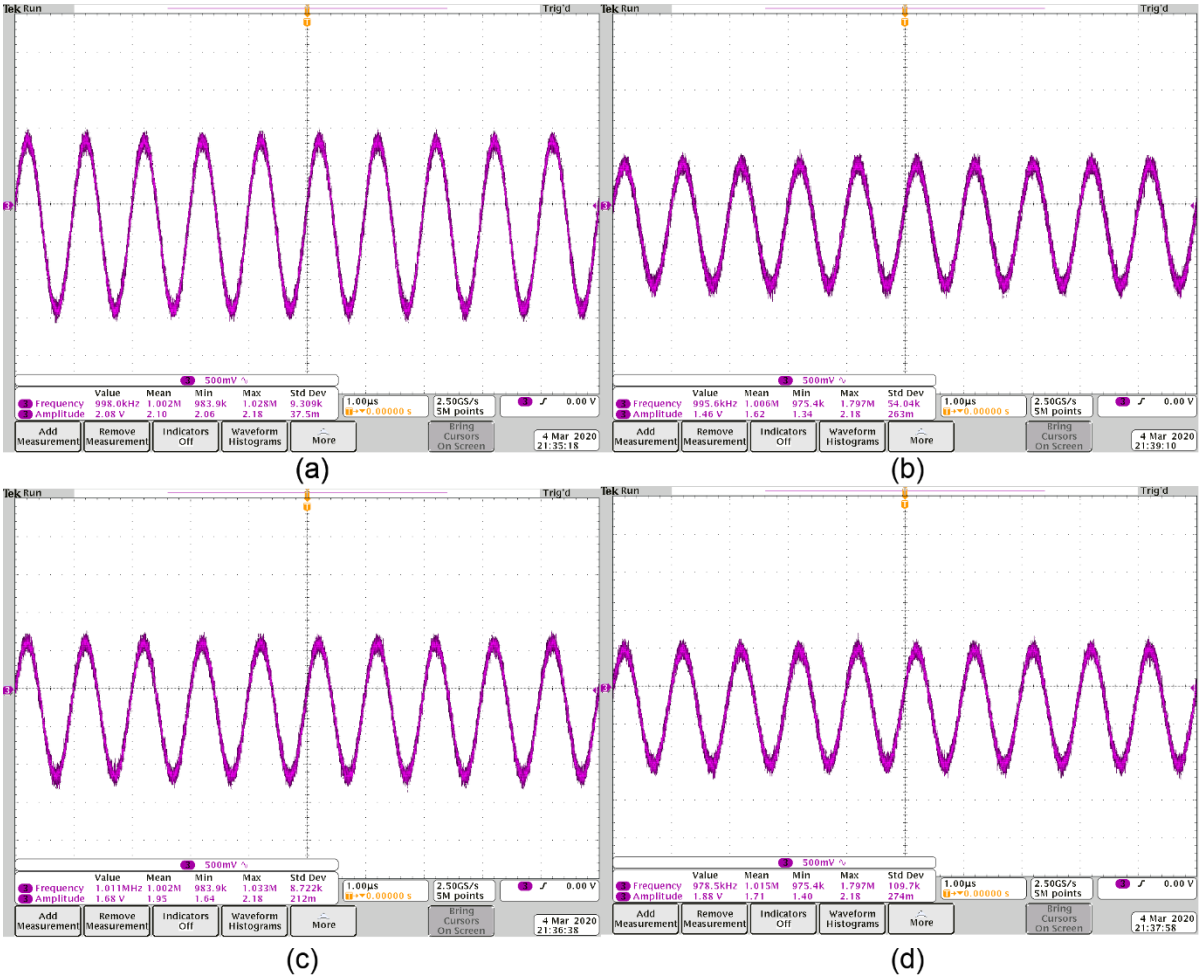

Figure 3-24: Voltage variation in MOD. Detection Coil Voltage without MOs (a), with the Aluminum Square (b), with the coin (c) and with the Copper Rectangle (d).

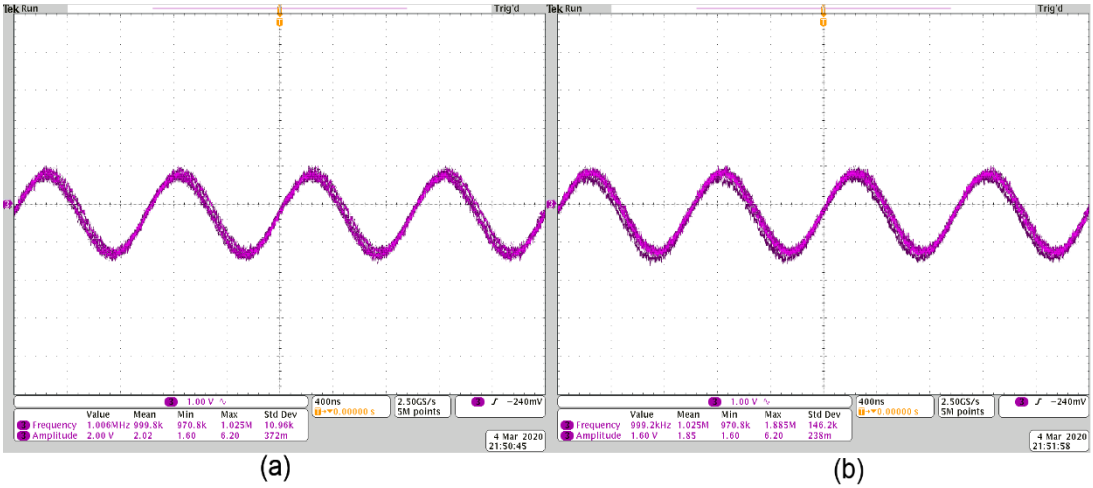

Figure 3-25: Voltage variation in LOD. Detection coil Voltage without the LO (a) and with the LO (fingertip) (b).

CHAPTER 4.
SENSING CIRCUIT DESIGN

As explained in the subsections 2.1.3 and 2.2.2, both for the MOD and for the LOD, the design of a Sensing Circuit is necessary to improve the Field-Based method. Therefore, as a completion of the work of this thesis, after having designed the detection coil, it is associated a proposal of sensing circuit in coherence with the parameters and characteristics of the equivalent circuit of the coil. In the chapter, simulations will be carried out using the software LTspice, first analysing the equivalent circuit of the detection coil and then with the design of the sensing circuit. In all the simulations only one basic cell is considered.

4.1 Equivalent Circuit Analysis

An analysis of the equivalent circuit of the basic cell is necessary to understand the electrical characteristics of the circuit in order to design a suitable sensing circuit.

According to the equivalent circuit of Fig. 3-2, in Fig. 4-1, the equivalent simulation model used in LTspice is shown:

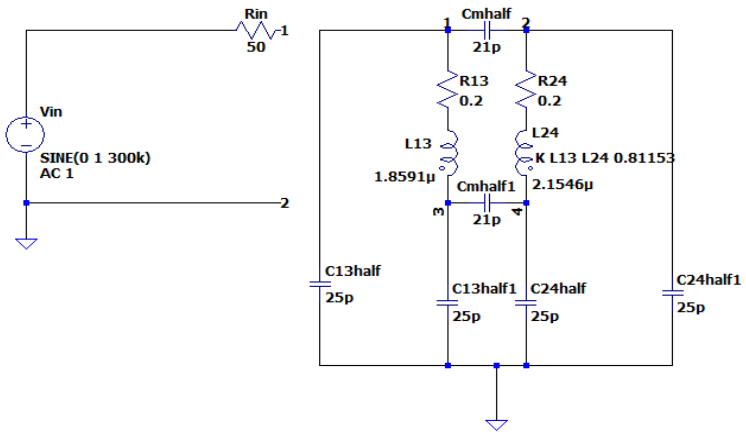

Figure 4-1: Basic Cell Equivalent circuit on LTspice.

In the simulation model we can observe:

- The numerical values of the circuit were taken from the electromagnetic simulations in Appendix B and C. The reference is the first basic cell of the first layer (terminals 1 to 4) with the simulation without FOs Offline.
- **Capacitive Circuit:**

  From Appendix B, Matrix $\hat{C}_{tot}$ of Eq. 3.9 without the LO, Offline, the positions $(C_{13.1}, C_{13.1})$ and $(C_{24.1}, C_{24.1})$ represent the capacitance to the ground (Self Capacitance) C_{13g} and C_{24g}. In both cases the value is approximated to 50 pF and it is divided in half between the terminals $(C_{13half}, C_{13half1}, C_{24half}, C_{24half1})$.

  The value in the position $(C_{13.1}, C_{24.1})$ represent the Mutual Capacitance $C_m = C_{12} = C_{34}$. The value is approximated to 42 pF and it is divided in half between the terminals (C_{mhalf}, C_{mhalf1}).

- **Inductive circuit:**
  From Appendix C, Matrix $\hat{Z}_{tot}$ of Eq. 3.17 without the MO, Offline, the positions $(Z_{13.1}, Z_{13.1})$ and $(Z_{24.1}, Z_{24.1})$ contain the values of the Self Resistance and Self Inductance R_{13}, L_{13} and R_{24}, L_{24}. For the inductances the exact value of the simulation is considered while for the resistances the value is approached to $0.2\ ohm$.
  The mutual inductance in position $(Z_{13.1}, Z_{24.1})$ calculated by the Ansys software is considered in the LTspice simulation via the parameter K with the relation of Eq. 4.1 which is also confirmed by the coupling coefficient matrix. The Mutual resistance is neglected.

$$K = \frac{L_M}{\sqrt{L_{13} L_{24}}} = 0.81153 \tag{4.1}$$

- A voltage generator with amplitude of $1V$, frequency of $300\ kHz$ and equivalent series resistance of $50\ ohm$ is added, consistently with the measurements of subsection 3.6.1.

Both for the analysis of the circuit and for the subsequent design of the sensing circuit, the capacitive terminals (1 and 2) will be considered. In fact, in subsection 3.6.1,

through laboratory measurements, it is concluded that the detection coil, seen from the capacitive terminals, has good results both for the MOD and for the LOD.

To analyze the circuit, the impedance from the capacitive terminals is simulated in the frequency domain in Fig. 4-2.

The Low-Frequency response (Fig. 4-2 (a)) is useful to make a comparison between the laboratory measured impedance value and that obtained from the LTspice simulation:

$$Z_{12}^{dB}(\omega = 2\pi * 300 * 10^3) = 75.2\ dB \tag{4.2}$$

$$|Z_{12}| = 5.754\ kohm \tag{4.3}$$

$$\left|Z_{12,measured}\right| = 5.431\ kohm \text{ (from Eq. 3.23 in 3.6.1)} \tag{4.4}$$

We see how the values are very close (mismatch of 6%) thus confirming the equivalent circuit model adopted. The difference is caused by two factors; the resistance values are difficult to measure. Furthermore, the coupling coefficients between the basic cells are not considered in the LTspice simulation.

Instead, from the High-Frequency behavior (Fig. 4-2 (b)) we can see:

- A Capacitive circuit trend (Low pass filter with slow decay):

  As expected, an inductive element will have to be used to create the resonance.

- Very High Self-Resonant frequencies: 16, 18, 31, 41 MHz:

  These frequencies, being very high, lead to the exclusion of the possibility of using the self-resonance of the detection coil as they would make the circuit too sensitive to high frequency noise.

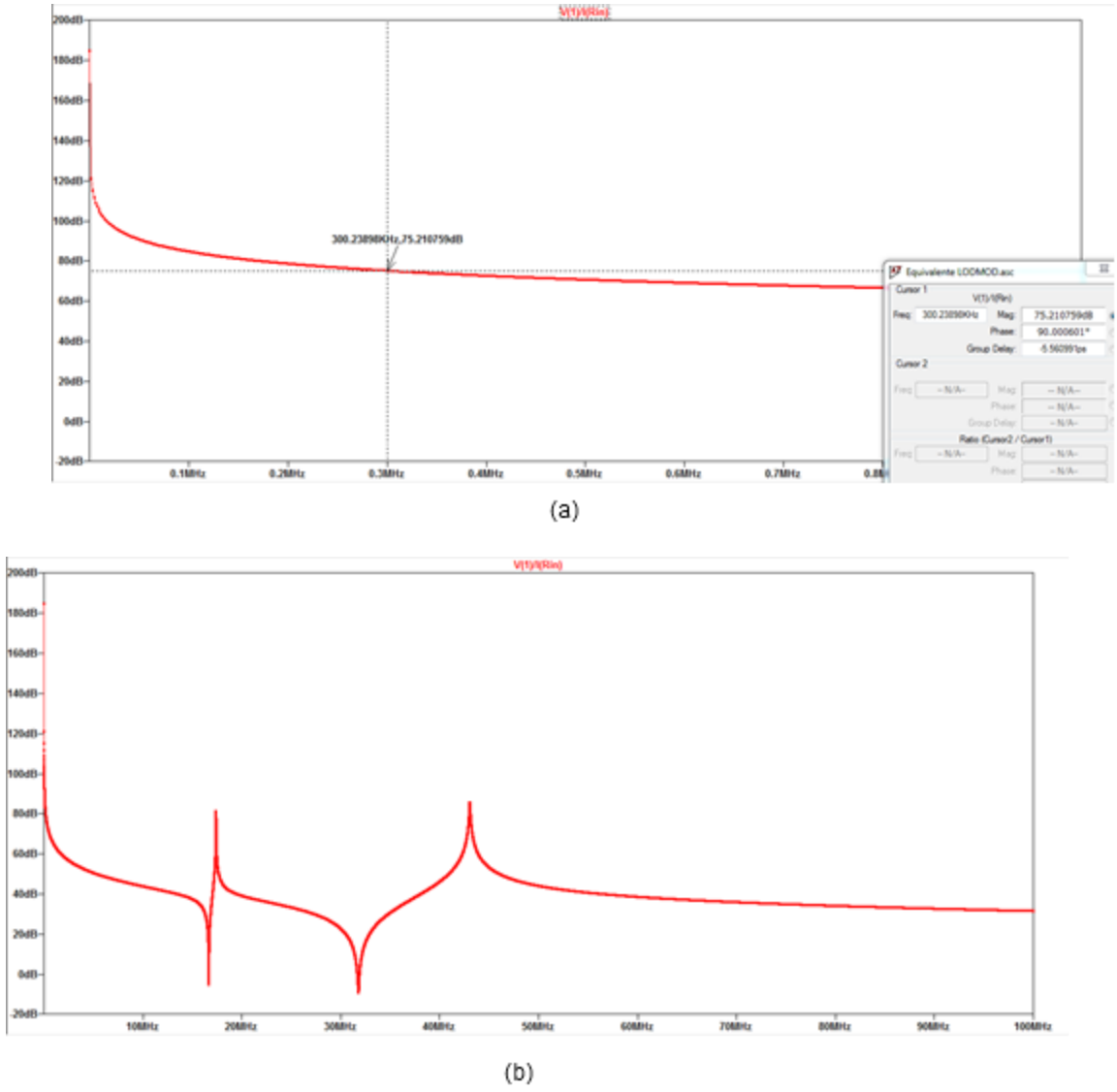

Figure 4-2: Low-Frequency (a) and High-Frequency (b) Impedance Characteristic of the Basic Cell equivalent circuit.

4.2 Proposed Sensing Circuit

In this section we propose a suitable sensing circuit for the previously designed detection coil.

The block diagram of the system is shown in Fig. 4-3. The Basic Cell, seen from the capacitive terminals 1 and 2, is connected to a resonant circuit in order to increase its sensitivity. The circuit is powered by an AC generator and a calibration circuit. These three blocks define the so-called “Sensing Circuit”. To get a project with practical implementation, the filtering, decoupling and rectifying stages of the signal is added thinking of an online application and a signal that can be sent to a digital system. In Fig. 4-4 the simulation model used is shown.

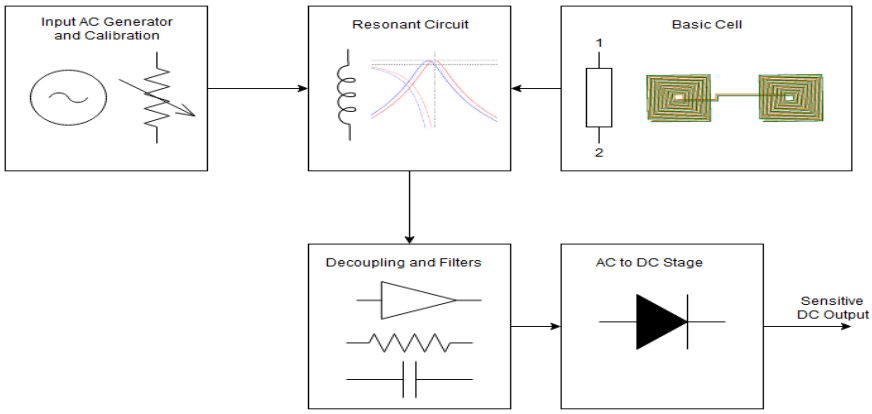

Figure 4-3: Block Diagram of the proposed Sensing Circuit.

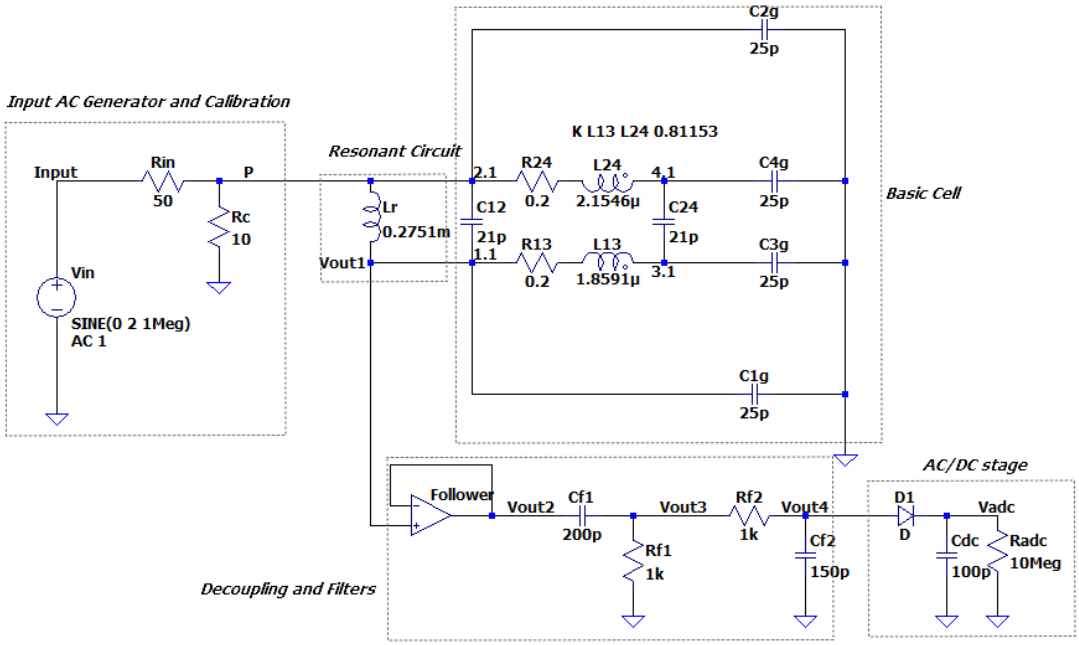

Figure 4-4: LTspice model of the Sensing Circuit.

Resonant Circuit:

The resonant circuit is composed of an inductor connected in parallel between the capacitive terminals 1 and 2. To design the inductor, the impedance and the equivalent capacitance of the basic cell are measured by choosing a resonance frequency $f_r = 1\ MHz$. Thus, we have:

$$Z_{12}^{dB}(\omega = 2\pi * 1 * 10^6) = 64.75\ \text{dB} \tag{4.5}$$

$$|Z_{12}| = 1.727\ kohm \tag{4.6}$$

$$C_{12} = \frac{1}{\omega |Z_{12}|} = 92.16\ pF \tag{4.7}$$

Consequently, the value of the inductance can be calculated:

$$L_r = \frac{1}{(2\pi f_r)^2 C_{12}} = 275{,}1\ uH \tag{4.8}$$

Since a high value is obtained, for practical implications the option of several Air Core inductors connected in series is evaluated.

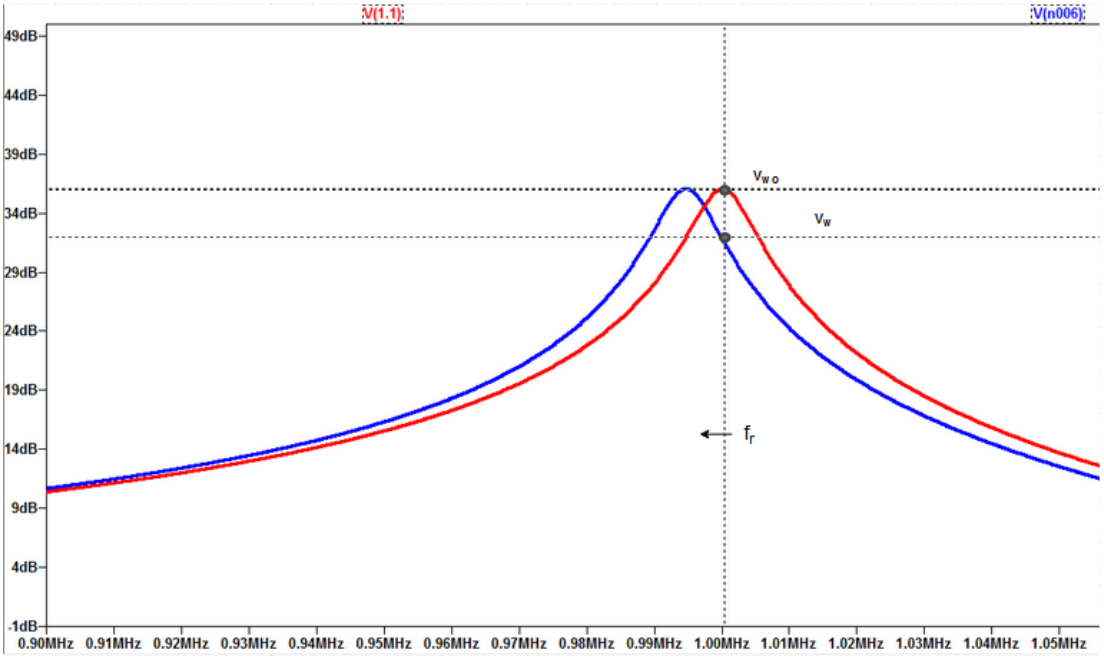

Figure 4-5: Resonant circuit voltage characteristic.

Fig. 4-5 shows the operating principle of the resonant circuit: by setting the circuit to the resonance condition, the circuit has a high impedance and voltage value (red line). A change in the operating point (red points) causes a sharp decrease in voltage making the circuit very sensitive. The presence of a FO causes the variation of the impedance of the circuit, thus losing the resonance condition. The working frequency remains $1\ MHz$ but a new resonance condition is established (blue line). It is therefore also possible to see the variation of impedance as a variation of the resonance frequency of the circuit.

Input AC Generator and Calibration:

To obtain the resonance condition between the inductor and the basic cell, an AC generator supplies the circuit with a sinusoidal signal of $2V$ amplitude and frequency equal to the resonance frequency ($1MHz$).

A sensitivity calibration is possible by inserting the resistance R_C. In fact, together with the internal resistance of the generator $R_{in} = 50\ \Omega$, it forms a voltage divider with ratio $\frac{R_C}{R_{in}}$ which allows to set the sensitivity of the circuit. In Fig. 4-6 we can see how by changing the R_C value it is possible to make the resonance peak flatter or more accentuated by observing two extreme cases of R_C very large and very small. In practice, the amplitude and width of the resonance peak can be adjusted by R_C or in general the ratio $\frac{R_C}{R_{in}}$ and the input voltage V_{in}. The steepness of the resonance peak is reflected in the sensitivity of the change in the output voltage.

This adjustment is very useful because based on the application it is possible to adjust the circuit according to the possible detectable FOs. For example, the need to detect small MOs requires a very steep peak while for large LOs (animals or children) a smooth resonance could be enough for the detection.

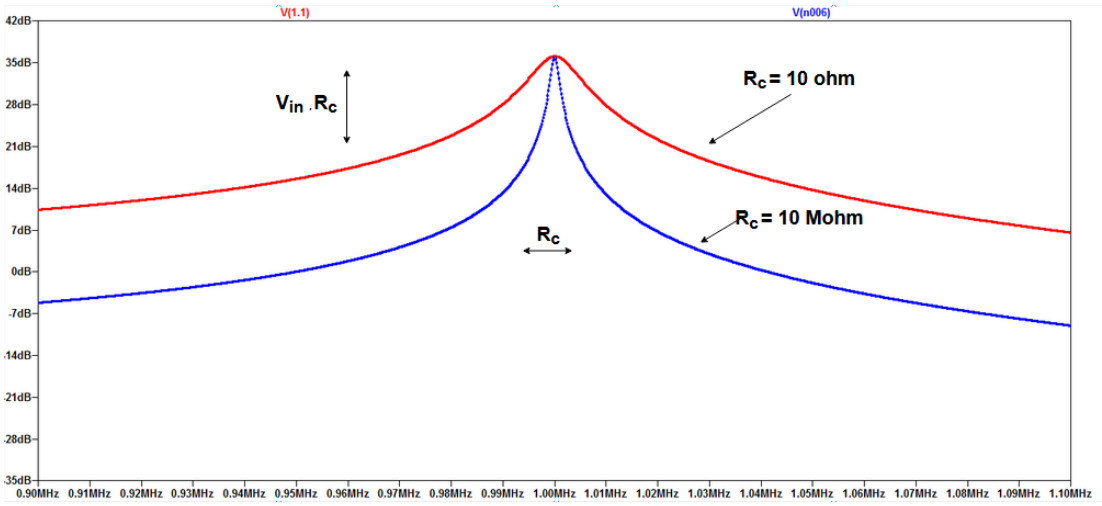

Figure 4-6: Input Calibration of the resonance peak.

The case ($R_C = 10\ \Omega$ with steep peak) is taken into consideration from this point.

Once the calibration has been set, it is possible to define the sensitivity of the resonance peak. To do this, in coherence with the measurements obtained in Tab. 3-10 from the capacitive terminals, we consider the cases of impedance variation of 1% and 13%. Tab. 4-1 and Fig. 4-7 shows the variation of impedance with equivalent

variation of capacitance (added in the simulation circuit). ΔdB indicates the variation in amplitude of the output signal while Δf shows the variation in the resonance frequency both caused by the variation in impedance.

Table 4-1: Impedance variation cases considered in the Sensing Circuit

$\Delta Z\%$	Equivalent ΔC	ΔdB	Δf
1%	$1\ pF$	$4.4\ dB$	$6\ kHz$
13%	$15\ pF$	$28.65\ dB$	$73\ kHz$

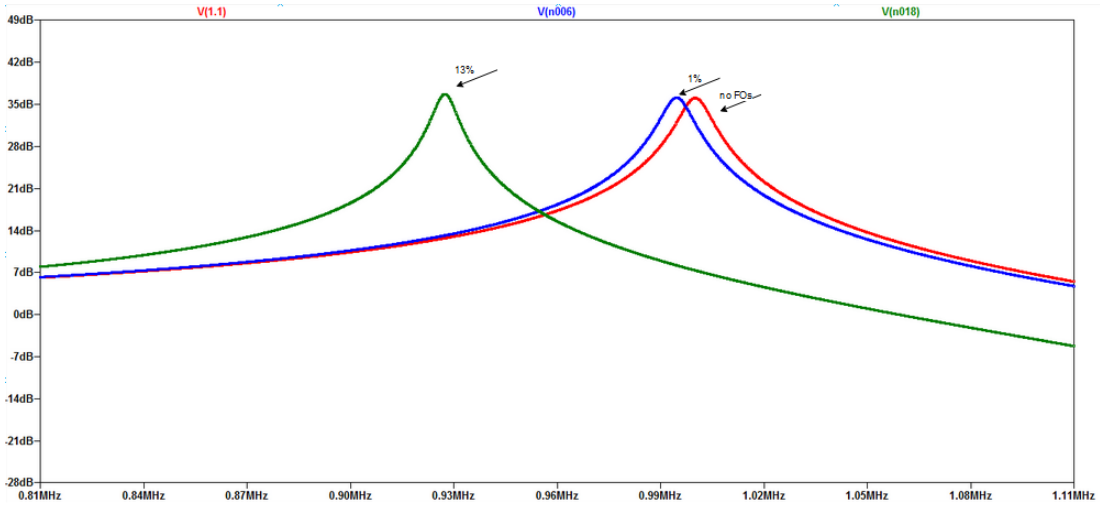

Figure 4-7: Voltage Characteristic with different variation of the impedance.

Decoupling, filters and AD/DC stage:

To complete the circuit, the main stages required are added to the simulation.

First of all, as filters must be added to the circuit an op-amp in follower configuration (unit gain) is added to decouple the resonance circuit from the rest of the circuit. In fact, the impedance of the filters and the load without the decoupling would dramatically affect the resonance peak.

Subsequently, the stage of the filters is designed; the harmonic components to be filtered are the IPT frequency (assumed as $85\ kHz$[14]) and the high frequency noise. To do this, a connection in series of two simple RC high and low pass filters is

implemented to obtain a band pass filter with poles $\frac{1}{R_{f1}C_{f1}} = 5\ MHz$ and $\frac{1}{R_{f2}C_{f2}} = 6.67\ MHz$. The harmonic component of the IPT system is attenuated at $35\ mV$ (0.7 %) while all components with frequency greater than $10\ MHz$ have amplitude less than $56\ mV$ ($>$ 1.1 %).

Finally, the AC to DC conversion is carried out with a half-wave rectifier (Diode and Capacitor) with a measured output voltage ripple of $\pm\ 0.2\ V$ ($<$ 4%).

Putting all the stages together, in Fig. 4-8 the characteristic of the circuit in the frequency domain is shown where the red line indicates the output voltage before the filter and the blue one after the filters.

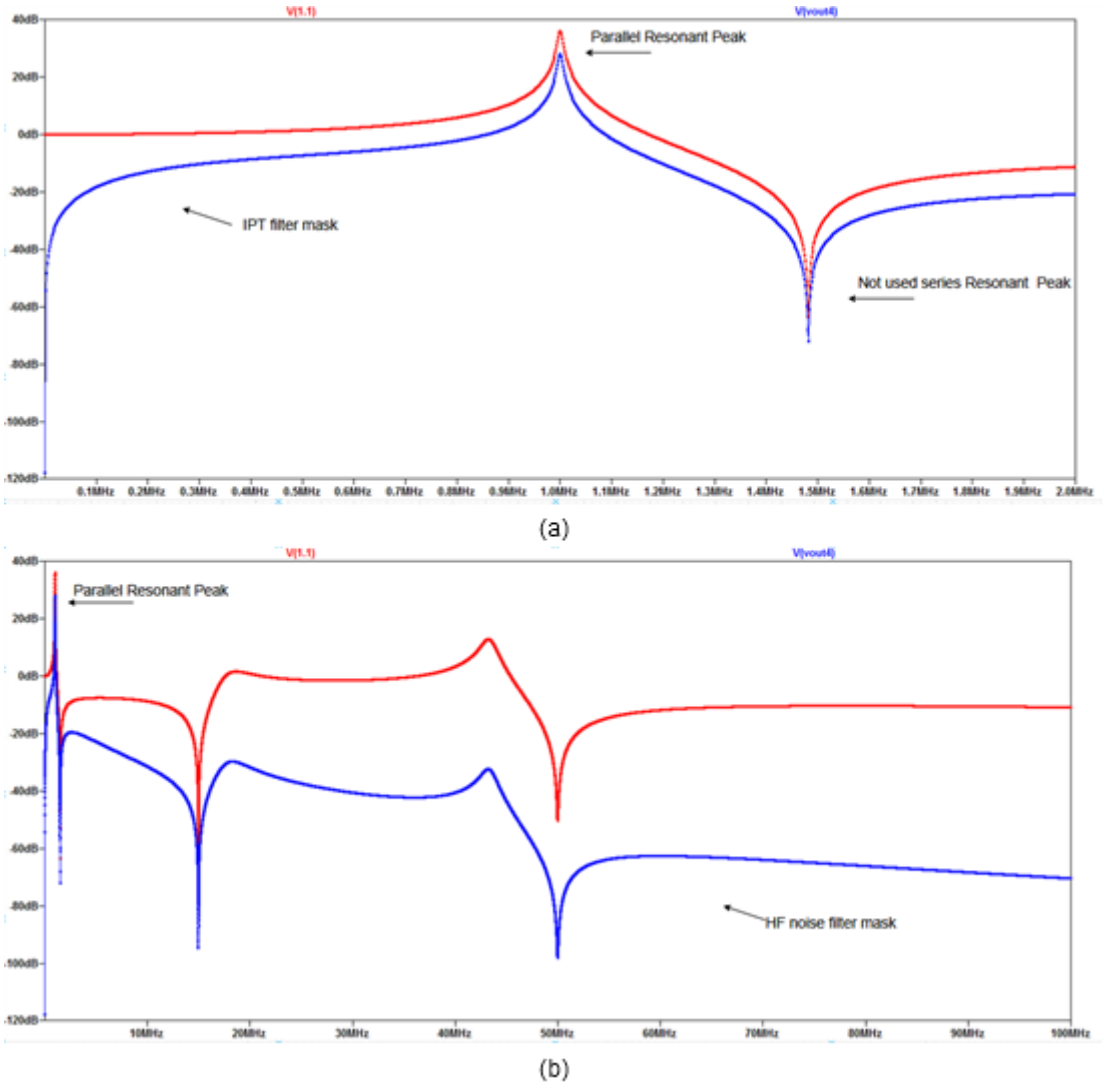

Figure 4-8: Low-Frequency (a) and High-Frequency (b) Sensing circuit output voltage characteristic.

From Fig. 4-8 (a) it can be noted that in addition to the resonance peak used (parallel resonance) also a series resonance peak is present. However, it is not used because

parallel resonance is more sensitive to variations. Furthermore, it is noted how the designed filter eliminates the low harmonic components including the IPT frequency. The high frequency graph (Fig. 4-8 (b)) shows the attenuation of the high frequencies including the Self-resonances of the detection coil (Section 4.1).

Finally, the circuit waveforms are plotted in Fig. 4-9. Considering the 1% impedance variation the DC output voltage goes from $4.97\,V$ to $2.56\,V$. Therefore an impedance variation of 1% is transduced and amplified into a voltage variation of 48.5%. Higher impedance variations (more easily detectable objects) further reduce the voltage and sensitivity of the circuit. The simulation shows the example of the variation of 13% which leads to a voltage of $147\,mV$. Larger variations therefore bring the output voltage closer to zero making the objects easy to detect.

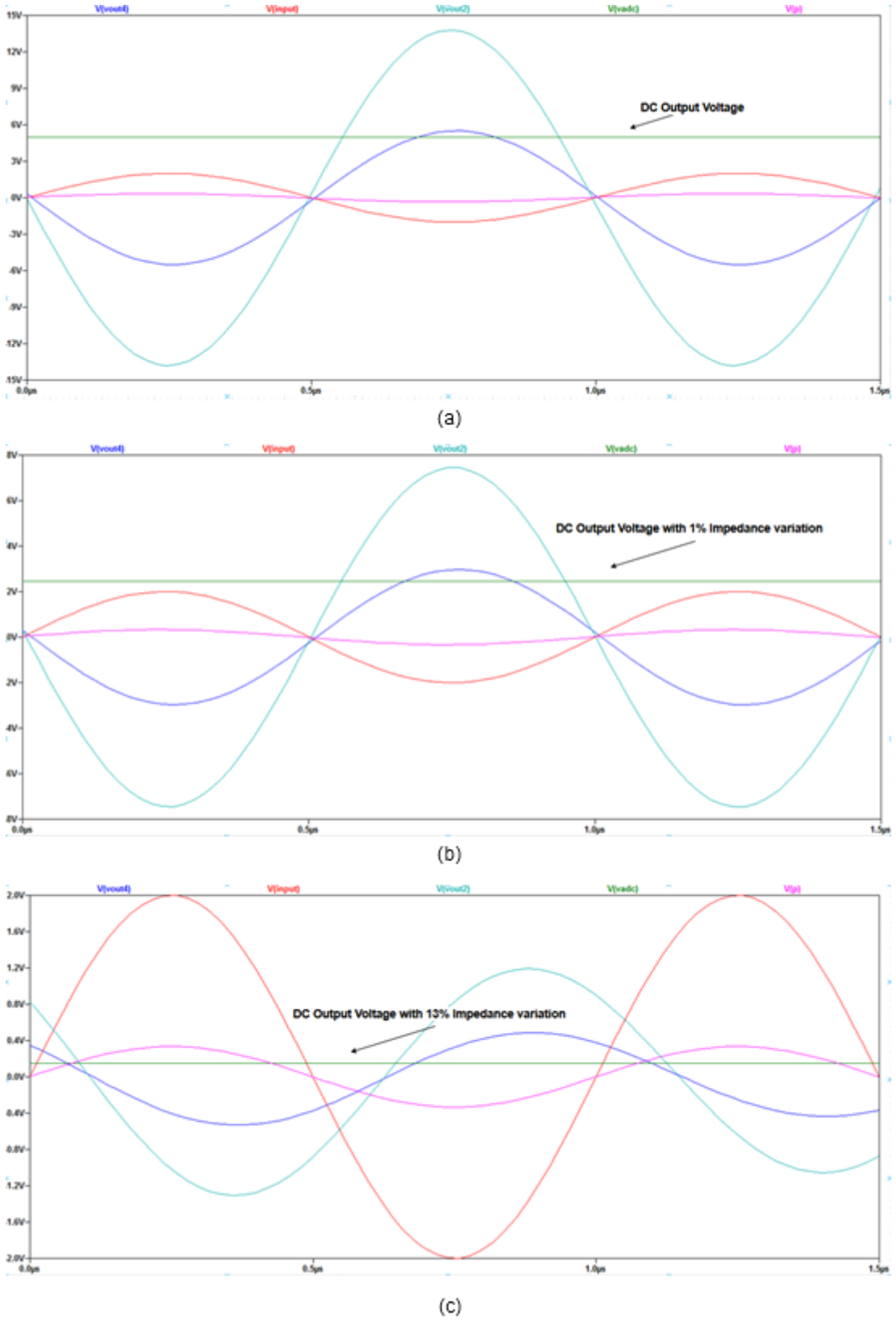

Figure 4-9: Sensing circuit output voltage waveforms without impedance variation (a), with 1% (b) and with 13% of variation (c).

CHAPTER 5.
CONCLUSIONS AND FUTURE WORKS

5.1 Conclusions

Wireless Power Transfer applied to EV charging, has numerous benefits which can contribute to the expansion of electric mobility.

Among the various challenges of the wireless charging, it is relevant to consider the problem of foreign objects in the charging area in order to contrive an appropriate detection method.

The conclusions of this work can be summarized in the following points:

1. The Field-Based method, through a literature research of the current state of the art, was considered in comparison with other methods. Advantages and challenges were highlighted. This method was assessed the most advantageous from the point of view of compromising the accuracy of the results, cost and complexity of the system regarding the foreign object detection in the wireless power transfer for EV recharging systems. The two components characterizing the method are particularly evaluated: the detection coil and the sensing circuit;
2. An innovative detection coil model was developed. The electromagnetic simulations using the software platform ANSYS, have led to an optimization of the sensing pattern parameters which defines the detection coil. Then, a complete model has confirmed excellent results for the detection of both metal objects and living objects with a single coil;
3. An experimental validation was carried out by faithfully recreating the simulated coil and inserting the component in a real IPT structure. Impedance and voltage measurement values are consistent with the results obtained from the simulations and confirm a practical use of the coil;
4. A sensing circuit design is proposed. The simulations were carried out, using the software LTspice, adapting the features of the proposed coil with the circuit. The results confirm the practicability of the detection coil inserted in a sensing circuit and the overall sensitivity of the method has been improved;
5. The aim of creating a unique Field-Based method for the detection of both metal and living objects was achieved with consistent simulation

results and laboratory measurements. Furthermore, the detection of position (DoP) of the object is also feasible in this method.

5.2 Future works

This work has demonstrated the validity of the proposed method. As possible future works, the detection coil could be adapted to some specific case of wireless charging (High-power or Low-power level, static recharge, dynamic recharge, recharge of buses, bicycles etc.). Thus, a case study can be applied to the proposed method defining the power level and the properties of foreign objects to be detected. In this way, some design parameters such as the geometrical parameters of the sensing path, the number of terminals to be scanned or the number of sensing circuits, could be adapted to the specifications of the charging system.

Furthermore, a switching system suitable for the proposed work could be planned by defining the scanned terminals of the detection coil based on what sensitivity results are desired and which possible foreign objects must be detected in a specific application. For example, in low-power structures or in the dynamic charging, the detection of living objects may not be necessary. In this case, therefore, preference could be given to the inductive circuits of the proposed method in order to increase the magnetic sensitivity at the expense of the electric one. On the other hand, in other cases, safety towards the user could be fundamental and the capacitive circuits are more essential; therefore, the geometrical parameters, switching and sensing circuits could be adapted. In general, the idea proposed in this work is flexible to the various applications of IPT in EVs.

REFERENCES

[1] Li S, Mi C. “Wireless power transfer for electric vehicle applications”. IEEE J. Emerg. Select. Topics Power Electron. 2015

[2] W. Chwei-Sen, O. H. Stielau, and G. A. Covic, “Design considerations for a contactless electric vehicle battery charger,” IEEE Trans. Ind. Electron., 2005.

[3] ICNIRP: Guidelines for limiting exposure to time-varying electric and magnetic fields (1 Hz to 100 kHz). Health Phys., 99 (2010), 818–836.

[4] IEEE Standard for Safety Levels with Respect to Human Exposure to Radio Frequency Electromagnetic Fields, 3 kHz to 300 GHz, IEEE Std C95.1-2005 (Revision of IEEE Std C95.1-1991), New York, USA, 2006, 1–238.

[5] Lijuan Xiang, Ze Zhu, Jindong Tian, Yong Tian,”Foreign Object Detection in a Wireless Power Transfer System Using Symmetrical Coil Sets”, IEEE Access, March 2019.

[6] Van X. Thai, Gi C. Jang, Seog Y. Jeong, Jun H. Park, Y.-S. Kim, and Chun T. Rim, “Symmetric Sensing Coil Design for the Blind-zone Free Metal Object Detection of a Stationary Wireless Electric Vehicles Charger”, IEEE Power Electronics Regular Paper, Aug.,2019.

[7] Yiming Zhang, Zhengchao Yan, Jiaqi Zhu, Siqi Li, Chris Mi. “A review of foreign object detection (FOD) for inductive power transfer systems”, ScienceDirect, eTransportation 2019.

[8] Jeong J, Ryu S, Lee B, Kim H. “Tech tree study on foreign object detection technology in wireless charging system for electric vehicles”. In: IEEE international telecommunications energy conference (INTELEC); 2015.

[9] Poguntke T, Schumann P, Ochs K. “Radar-based living object protection for inductive charging of electric vehicles using two-dimensional signal processing”. Wireless Power Transfer 2017.

[10] Simon Verghese, Morris P. Kesler, Katherine L. Hall, and Herbert Toby Lou, “Foreign object detection in wireless energy transfer systems,” Patent US20130069441 A1, (Witricity Corporation), 2011.

[11] S. Y. Jeong, H. G. Kwak, G. C. Jang, S. Y. Choi and C. T. Rim, “Dual-Purpose Nonoverlapping Coil Sets as Metal Object and Vehicle Position Detections for Wireless Stationary EV Chargers,” IEEE Transactions on Power Electronics, 2018.

[12] Chopra S, Percebon LA, Werner M. “Sense coil geometries with improved sensitivity for metallic object detection in a predetermined space.” Aug. 18, 2016. U.S. Patent 2016/0238731 A1.

[13] Jeong SY, Thai VX, Park JH, Rim CT. “Self-inductance based metal object detection with mistuned resonant circuits and nullifying induced voltage for wireless EV chargers”. IEEE Trans Power Electron Jan. 2019.

[14] Wireless Power Transfer for Light-Duty Plug-In / Electric Vehicles and Alignment Methodology, http://standards.sae.org/wip/j2954/.

[15] Chopra S, Percebon L. “Dynamic mutual sensing foreign object detection loops. Mar. 15, 2018”. U.S. Patent 2018/0076671 A1.

[16] Von Novak WH, Monat P, Kallal E. “Wireless power system with capacitive proximity sensing”. Oct. 6, 2015. U.S. Patent 9,154,189 B2.

[17] Katz N, Roy AM, Jonas JR, Kesler MP. Object detection for wireless energy transfer systems. Aug. 20, 2015. U.S. Patent 2015/0233988 A1.

[18] Jeong SY, Kwak HG, Jang GC, Rim CT. “Living object detection system based on comb pattern capacitive sensor for wireless EV chargers.”, IEEE 2nd annual southern power electronics conference (SPEC); 2016.

[19] Thai Van X, Park JH, Jeong SY, Rim CT. “Multiple comb pattern based living object detection with enhanced resolution design for wireless electric vehicle chargers.”, PCIM europe; 2018.

[20] T. Karacolak, R. Cooper, E. S. Unlu and E. Topsakal, “Dielectric Properties of Porcine Skin Tissue and In Vivo Testing of Implantable Antennas Using Pigs as Model Animals,” in IEEE Antennas and Wireless Propagation Letters, 2012.

APPENDIX A

1 Basic cell, 2-Layers Structure: Capacitance and Coupling Coefficients:

Matrix $\hat{C}_Z$ of Eq. 3.8.

Capacitance [pF]				
	C13.1	C24.1	C13.2	C24.2
C13.1	45.255	-36.942	-5.154	-3.1585
C24.1	-36.942	48.048	-3.2166	-7.8893
C13.2	-5.154	-3.2166	43.852	-35.481
C24.2	-3.1585	-7.8893	-35.481	46.529

Matrix $\hat{K}_{C,Z}$ of Eq. 3.8.

Capacitive Coupling Coefficients				
	C13.1	C24.1	C13.2	C24.2
C13.1	1	-0.79223	-0.1157	-0.068832
C24.1	-0.79223	1	-0.070075	-0.16685
C13.2	-0.1157	-0.070075	1	-0.78549
C24.2	-0.068832	-0.16685	-0.78549	1

1 Basic cell, 4-Layers Structure: Capacitance and Coupling Coefficients: Matrix $\hat{C}_Z$ and $\hat{K}_{C,Z}$ of Eq. 3.8.

Capacitance [pF]

	C13.1	C24.1	C13.2	C24.2	C13.3	C24.3	C13.4	C24.4
C13.1	46.672	-36.437	-5.0278	-2.8913	-0.84958	-1.3029	-0.066612	-0.096873
C24.1	-36.437	50.053	-3.0145	-7.4903	-1.3623	-1.5064	-0.099838	-0.14327
C13.2	-5.0278	-3.0145	45.915	-33.963	-0.66752	-1.0559	-0.85337	-1.3327
C24.2	-2.8913	-7.4903	-33.963	49.653	-1.051	-1.4559	-1.3065	-1.4954
C13.3	-0.84958	-1.3623	-0.66752	-1.051	45.278	-33.468	-4.9607	-2.9193
C24.3	-1.3029	-1.5064	-1.0559	-1.4559	-33.468	49.076	-2.918	-7.3698
C13.4	-0.066612	-0.099838	-0.85337	-1.3065	-4.9607	-2.918	44.077	-33.872
C24.4	-0.096873	-0.14327	-1.3327	-1.4954	-2.9193	-7.3698	-33.872	47.229

Capacitive Coupling Coefficients

	C13.1	C24.1	C13.2	C24.2	C13.3	C24.3	C13.4	C24.4
C13.1	1	-0.75387	-0.10861	-0.060061	-0.018481	-0.027224	-0.0014687	-0.0020633
C24.1	-0.75387	1	-0.062882	-0.15025	-0.028615	-0.030394	-0.0021256	-0.0029466
C13.2	-0.10861	-0.062882	1	-0.7113	-0.01464	-0.022245	-0.018969	-0.028619
C24.2	-0.060061	-0.15025	-0.7113	1	-0.022165	-0.029494	-0.027928	-0.03088
C13.3	-0.018481	-0.028615	-0.01464	-0.022165	1	-0.70998	-0.11105	-0.063129
C24.3	-0.027224	-0.030394	-0.022245	-0.029494	-0.70998	1	-0.06274	-0.15308
C13.4	-0.0014687	-0.0021256	-0.018969	-0.027928	-0.11105	-0.06274	1	-0.74238
C24.4	-0.0020633	-0.0029466	-0.028619	-0.03088	-0.063129	-0.15308	-0.74238	1

1 Basic cell, 2-Layers Structure: Inductance and Coupling Coefficients: Matrix $\hat{L}_Z$ and $\hat{K}_{L,Z}$ of Eq. 3.8.

Inductance [μH]

	L13.1	L24.1	L13.2	L24.2
L13.1	1.6535	1.3593	-0.063997	-0.010819
L24.1	1.3593	1.8675	-0.071216	-0.065447
L13.2	-0.063997	-0.071216	1.7033	1.3932
L24.2	-0.010819	-0.065447	1.3932	1.9233

Inductive Coupling Coefficients

	L13.1	L24.1	L13.2	L24.2
L13.1	1	0.77356	-0.03813	-0.06067
L24.1	0.77356	1	-0.03993	-0.03453
L13.2	-0.03813	-0.03993	1	0.76974
L24.2	-0.06067	-0.03453	0.76974	1

1 Basic cell, 4-Layers Structure: Inductance and Coupling Coefficients: Matrix $\hat{L}_Z$ and $\hat{K}_{L,Z}$ of Eq. 3.8.

Inductance [μH]

	I13.1	I24.1	I13.2	I24.2	I13.3	I24.3	I13.4	I24.4
L13.1	1.9246	1.6617	-0.072816	-0.1205	-0.2075	-0.22458	-0.033755	-0.03897
L24.1	1.6617	2.195	-0.075814	-0.072411	-0.22703	-0.24043	-0.045707	-0.051162
L13.2	-0.072816	-0.075814	1.9663	1.6908	-0.08155	-0.088511	-0.20856	-0.22571
L24.2	-0.1205	-0.072411	1.6908	2.2409	-0.085474	-0.089616	-0.22817	-0.24161
L13.3	-0.2075	-0.22703	-0.08155	-0.085474	1.9463	1.688,2	-0.073642	-0.12145
L24.3	-0.22458	-0.24043	-0.088511	-0.089616	1.6882	2.2224	-0.076469	-0.072981
L13.4	-0.033755	-0.045707	-0.20856	-0.22817	-0.073642	-0.076469	1.9751	1.6983
L24.4	-0.03897	-0.051162	-0.22571	-0.24161	-0.12145	-0.072981	1.6983	2.2527

Inductive Coupling Coefficients

	L13.1	L24.1	L13.2	L24.2	L13.3	L24.3	L13.4	L24.4
L13.1	1	0.80847	-0.03743	-0.05802	-0.10721	-0.10859	-0.01731	-0.01872
L24.1	0.80847	1	-0.03649	-0.03265	-0.10984	-0.10886	-0.02195	-0.02301
L13.2	-0.03743	-0.03649	1	0.80546	-0.04169	-0.04234	-0.10583	-0.10724
L24.2	-0.05802	-0.03265	0.80546	1	-0.04093	-0.04016	-0.10845	-0.10753
L13.3	-0.10721	-0.10984	-0.04169	-0.04093	1	0.81172	-0.03756	-0.058
L24.3	-0.10859	-0.10886	-0.04234	-0.04016	0.81172	1	-0.0365	-0.03262
L13.4	-0.01731	-0.02195	-0.10583	-0.10845	-0.03756	-0.0365	1	0.80513
L24.4	-0.01872	-0.02301	-0.10724	-0.10753	-0.058	-0.03262	0.80513	1

APPENDIX B

Offline LOD Simulation:

- Red elements are the Self Capacitance (Capacitance to the ground) and relative Sensitivity;
- Green elements are the Mutual Capacitance and relative Sensitivity;
- The Black boxes indicate the elements for the positional matrices $\hat{C}$ and $\hat{C}_M$;
- The Yellow box indicate the basic cell with the presence of the LO.

Matrix $\hat{C}_{tot}$ of Eq. 3.9 without the LO, Offline.

Capacitance [pF] without the LO	C13.1	C24.1	C57.1	C68.1	C911.1	C1012.1	C1315.1	C1416.1	C1719.1	C1820.1	C2123.1	C2224.1	C2527.1	C2628.1	C2931.1	C3032.1
C13.1	49.286	-41.862	-1.5175	-1.6561	-0.50141	-0.65292	-0.34297	-0.42084	-0.21399	-0.24945	-0.2652	-0.31741	-0.25039	-0.28776	-0.3441	-0.40337
C24.1	-41.862	51.302	-2.3785	-2.1093	-0.58486	-0.76151	-0.40096	-0.49227	-0.24875	-0.29007	-0.30854	-0.36927	-0.29125	-0.33473	-0.4004	-0.46938
C57.1	-1.5175	-2.3785	57.643	-46.979	-0.90764	-1.0837	-0.71978	-0.92101	-0.29755	-0.34913	-0.36066	-0.43293	-0.32991	-0.37929	-0.45401	-0.53235
C68.1	-1.6561	-2.1093	-46.979	58.821	-1.0876	-1.2995	-0.86057	-1.101	-0.35433	-0.41572	-0.42902	-0.51505	-0.3918	-0.45043	-0.53936	-0.63246
C911.1	-0.50141	-0.58486	-0.90764	-1.0876	50.416	-40.776	-1.5768	-1.8062	-0.49721	-0.64701	-0.34797	-0.42638	-0.25023	-0.28939	-0.32987	-0.38744
C1012.1	-0.65292	-0.76151	-1.0837	-1.2995	-40.776	52.914	-2.4213	-2.2234	-0.57695	-0.75037	-0.4059	-0.49747	-0.29141	-0.33706	-0.38453	-0.45162
C1315.1	-0.34297	-0.40096	-0.71978	-0.86057	-1.5768	-2.4213	58.212	-46.665	-0.91296	-1.09	-0.72165	-0.92414	-0.31816	-0.37054	-0.40727	-0.48001
C1416.1	-0.42084	-0.49227	-0.92101	-1.101	-1.8062	-2.2234	-46.665	59.88	-1.092	-1.3055	-0.86081	-1.1017	-0.38154	-0.44425	-0.48831	-0.57553
C1719.1	-0.21399	-0.24875	-0.29755	-0.35433	-0.49721	-0.57695	-0.91296	-1.092	50.422	-40.785	-1.5754	-1.805	-0.51312	-0.66055	-0.40491	-0.48474
C1820.1	-0.24945	-0.29007	-0.34913	-0.41572	-0.64701	-0.75037	-1.09	-1.3055	-40.785	52.905	-2.4151	-2.2186	-0.59361	-0.76397	-0.46965	-0.56244
C2123.1	-0.2652	-0.30854	-0.36066	-0.42902	-0.34797	-0.4059	-0.72165	-0.86081	-1.5754	-2.4151	58.222	-46.657	-0.93771	-1.1116	-0.81059	-1.0152
C2224.1	-0.31741	-0.36927	-0.43293	-0.51505	-0.42638	-0.49747	-0.92414	-1.1017	-1.805	-2.2186	-46.657	59.892	-1.1207	-1.3304	-0.96657	-1.2098
C2527.1	-0.25039	-0.29125	-0.32991	-0.3918	-0.25023	-0.29141	-0.31816	-0.38154	-0.51312	-0.59361	-0.93771	-1.1207	50.514	-40.818	-1.9051	-2.1214
C2628.1	-0.28776	-0.33473	-0.37929	-0.45043	-0.28939	-0.33706	-0.37054	-0.44425	-0.66055	-0.76397	-1.1116	-1.3304	-40.818	52.899	-2.7853	-2.5355
C2931.1	-0.3441	-0.4004	-0.45401	-0.53936	-0.32987	-0.38453	-0.40727	-0.48831	-0.40491	-0.46965	-0.81059	-0.96657	-1.9051	-2.7853	57.975	-47.285
C3032.1	-0.40337	-0.46938	-0.53235	-0.63246	-0.38744	-0.45162	-0.48001	-0.57553	-0.48474	-0.56244	-1.0152	-1.2098	-2.1214	-2.5355	-47.285	59.146

Matrix $\hat{C}_{tot}$ of Eq. 3.9 with the LO, Offline.

Capacitance [pF] with the LO	C13.1	C24.1	C57.1	C68.1	C911.1	C1012.1	C1315.1	C1416.1	C1719.1	C1820.1	C2123.1	C2224.1	C2527.1	C2628.1	C2931.1	C3032.1
C13.1	49.159	-41.731	-1.5127	-1.651	-0.47767	-0.62473	-0.3438	-0.42207	-0.21577	-0.25139	-0.26622	-0.31882	-0.25061	-0.28802	-0.34403	-0.40329
C24.1	-41.731	51.178	-2.3731	-2.1045	-0.5567	-0.7281	-0.40201	-0.4938	-0.25075	-0.29226	-0.30971	-0.37088	-0.29146	-0.33498	-0.40029	-0.46924
C57.1	-1.5127	-2.3731	57.478	-46.826	-0.87486	-1.0455	-0.71682	-0.91749	-0.29883	-0.35047	-0.36228	-0.4351	-0.33011	-0.37953	-0.45424	-0.53264
C68.1	-1.651	-2.1045	-46.826	58.657	-1.0477	-1.2532	-0.857	-1.0967	-0.35592	-0.41739	-0.43105	-0.51776	-0.39205	-0.45073	-0.53967	-0.63284
C911.1	-0.47767	-0.5567	-0.87486	-1.0477	56.722	-33.311	-1.5214	-1.7465	-0.48024	-0.62446	-0.339	-0.41558	-0.24508	-0.28331	-0.32277	-0.3791
C1012.1	-0.62473	-0.7281	-1.0455	-1.2532	-33.311	58.845	-2.3548	-2.1546	-0.55739	-0.72442	-0.39546	-0.4849	-0.2853	-0.32986	-0.37615	-0.44178
C1315.1	-0.3438	-0.40201	-0.71682	-0.857	-1.5214	-2.3548	58.047	-46.513	-0.9102	-1.0866	-0.7188	-0.92035	-0.31893	-0.37138	-0.40872	-0.48176
C1416.1	-0.42207	-0.4938	-0.91749	-1.0967	-1.7465	-2.1546	-46.513	59.714	-1.0889	-1.3018	-0.85762	-1.0974	-0.38267	-0.44549	-0.4903	-0.57793
C1719.1	-0.21577	-0.25075	-0.29883	-0.35592	-0.48024	-0.55739	-0.9102	-1.0889	50.299	-40.668	-1.5693	-1.7974	-0.51252	-0.65924	-0.40683	-0.48709
C1820.1	-0.25139	-0.29226	-0.35047	-0.41739	-0.62446	-0.72442	-1.0866	-1.3018	-40.668	52.779	-2.4077	-2.2103	-0.59283	-0.76237	-0.47179	-0.56505
C2123.1	-0.26622	-0.30971	-0.36228	-0.43105	-0.339	-0.39546	-0.7188	-0.85762	-1.5693	-2.4077	58.054	-46.51	-0.93365	-1.1067	-0.80827	-1.0121
C2224.1	-0.31882	-0.37088	-0.4351	-0.51776	-0.41558	-0.4849	-0.92035	-1.0974	-1.7974	-2.2103	-46.51	59.723	-1.1164	-1.3251	-0.96438	-1.2069
C2527.1	-0.25061	-0.29146	-0.33011	-0.39205	-0.24508	-0.2853	-0.31893	-0.38267	-0.51252	-0.59283	-0.93365	-1.1164	50.371	-40.7	-1.8948	-2.1089
C2628.1	-0.28802	-0.33498	-0.37953	-0.45073	-0.28331	-0.32986	-0.37138	-0.44549	-0.65924	-0.76237	-1.1067	-1.3251	-40.7	52.751	-2.7732	-2.5221
C2931.1	-0.34403	-0.40029	-0.45424	-0.53967	-0.32277	-0.37615	-0.40872	-0.4903	-0.40683	-0.47179	-0.80827	-0.96438	-1.8948	-2.7732	57.826	-47.151
C3032.1	-0.40329	-0.46924	-0.53264	-0.63284	-0.3791	-0.44178	-0.48176	-0.57793	-0.48709	-0.56505	-1.0121	-1.2069	-2.1089	-2.5221	-47.151	58.995

Matrix Offline $\hat{S}_E\%$ of Eq. 3.12 and Matrix $\hat{S}_{E,Offline}\%$ of Eq. 3.13.

Total Sensitivity

	1	1	2	2
1	0.258345369	0.313915315	0.287066356	0.326741554
1	0.313915315	0.24229161	0.326741554	0.279591524
2	11.1173795	22.41001471	0.284252416	0.32679036
2	22.41001471	10.07902116	0.32679036	0.277991761
3	0.244537665	0.287695485	0.289385744	0.316061062
3	0.287695485	0.238731314	0.316061062	0.282973059
4	0.28389351	0.28992629	0.25766956	0.284193336
4	0.28992629	0.280563402	0.284193336	0.255953894

Mutual Sensitivity

	1	2
1	0.313915315	0.326741554
2	22.41001471	0.32679036
3	0.287695485	0.316061062
4	0.28992629	0.284193336

Online LOD Simulation:

- Red elements are the Self Capacitance (Capacitance to the ground) and relative Sensitivity;
- Green elements are the Mutual Capacitance and relative Sensitivity;
- Light Blue elements are the Transmitter and Receiver Self, Mutual and coupling elements;
- The Black boxes indicate the elements for the positional matrices $\hat{C}$ and $\hat{C}_M$;
- The Yellow box indicate the basic cell with the presence of the LO.

Matrix $\hat{C}_{tot}$ of Eq. 3.9 without (first Matrix) and with (second Matrix) the LO, Online.

Capacitance [pF] without the LO

	C13.1	C24.1	C57.1	C68.1	C911.1	C1012.1	C1315.1	C1416.1	C1719.1	C1820.1	C2123.1	C2224.1	C2527.1	C2628.1	C2931.1	C3032.1	Ctx	Crx
C13.1	58.685	-50.552	-1.2191	-1.325	-0.27615	-0.39775	-0.087133	-0.11923	-0.017145	-0.021411	-0.0094713	-0.012341	-0.0043579	-0.0049231	-0.0055325	-0.0068672	-4.3058	-0.32074
C24.1	-50.552	60.975	-2.1181	-1.7452	-0.32556	-0.46829	-0.10436	-0.14296	-0.019947	-0.025019	-0.01115	-0.014513	-0.0050639	-0.0057337	-0.0065869	-0.0081696	-5.0342	-0.38807
C57.1	-1.2191	-2.1181	67.01	-55.212	-0.61782	-0.75508	-0.38507	-0.54836	-0.038001	-0.049023	-0.022908	-0.030212	-0.0057237	-0.0066895	-0.0076156	-0.0094579	-5.605	-0.37959
C68.1	-1.325	-1.7452	-55.212	68.649	-0.76324	-0.93295	-0.48222	-0.68691	-0.048027	-0.06177	-0.029135	-0.038416	-0.0074858	-0.0087261	-0.010018	-0.01244	-6.7888	-0.49678
C911.1	-0.27615	-0.32556	-0.61782	-0.76324	59.612	-49.341	-1.3532	-1.5956	-0.30339	-0.4336	-0.10249	-0.13624	-0.017422	-0.021925	-0.01097	-0.013963	-4.0379	-0.26117
C1012.1	-0.39775	-0.46829	-0.75508	-0.93295	-49.341	62.452	-2.2726	-2.0073	-0.35524	-0.50726	-0.12115	-0.16116	-0.019933	-0.02521	-0.012464	-0.015868	-4.7579	-0.30083
C1315.1	-0.087133	-0.10436	-0.38507	-0.48222	-1.3532	-2.2726	74.423	-61.973	-0.68488	-0.83947	-0.42052	-0.57716	-0.039173	-0.050416	-0.025414	-0.032803	-4.7636	-0.33172
C1416.1	-0.11923	-0.14296	-0.54836	-0.68691	-1.5956	-2.0073	-61.973	76.757	-0.8495	-1.0439	-0.51838	-0.71102	-0.048967	-0.062884	-0.031907	-0.041161	-5.9527	-0.42231
C1719.1	-0.017145	-0.019947	-0.038001	-0.048027	-0.30339	-0.35524	-0.68488	-0.8495	60.045	-49.795	-1.3686	-1.5973	-0.28452	-0.40638	-0.099199	-0.12797	-3.7882	-0.26176
C1820.1	-0.021411	-0.025019	-0.049023	-0.06177	-0.4336	-0.50726	-0.83947	-1.0439	-49.795	62.888	-2.2804	-2.0101	-0.33306	-0.4753	-0.1169	-0.151	-4.4426	-0.30264
C2123.1	-0.0094713	-0.01115	-0.022908	-0.029135	-0.10249	-0.12115	-0.42052	-0.51838	-1.3686	-2.2804	68.89	-56.39	-0.64612	-0.78628	-0.40137	-0.54297	-4.9066	-0.33334
C2224.1	-0.012341	-0.014513	-0.030212	-0.038416	-0.13624	-0.16116	-0.57716	-0.71102	-1.5973	-2.0101	-56.39	70.946	-0.78571	-0.9585	-0.48581	-0.65657	-5.965	-0.41676
C2527.1	-0.0043579	-0.0050639	-0.0057237	-0.0074858	-0.017422	-0.019933	-0.039173	-0.048967	-0.28452	-0.33306	-0.64612	-0.78571	58.626	-48.174	-1.519	-1.6872	-4.7382	-0.30962
C2628.1	-0.0049231	-0.0057337	-0.0066895	-0.0087261	-0.021925	-0.02521	-0.050416	-0.062884	-0.40638	-0.4753	-0.78628	-0.9585	-48.174	61.303	-2.4195	-2.0554	-5.4863	-0.35493
C2931.1	-0.0055325	-0.0065869	-0.0076156	-0.010018	-0.01097	-0.012464	-0.025414	-0.031907	-0.099199	-0.1169	-0.40137	-0.48581	-1.519	-2.4195	65.614	-53.509	-6.4432	-0.50921
C3032.1	-0.0068672	-0.0081696	-0.0094579	-0.01244	-0.013963	-0.015868	-0.032803	-0.041161	-0.12797	-0.151	-0.54297	-0.65657	-1.6872	-2.0554	-53.509	67.104	-7.6105	-0.62227
Ctx	-4.3058	-5.0342	-5.605	-6.7888	-4.0379	-4.7579	-4.7636	-5.9527	-3.7882	-4.4426	-4.9066	-5.965	-4.7382	-5.4863	-6.4432	-7.6105	88.515	-3.8885
Crx	-0.32074	-0.38807	-0.37959	-0.49678	-0.26117	-0.30083	-0.33172	-0.42231	-0.26176	-0.30264	-0.33334	-0.41676	-0.30962	-0.35493	-0.50921	-0.62227	-3.8885	9.9002

Capacitance [pF] with the LO

	C13.1	C24.1	C57.1	C68.1	C911.1	C1012.1	C1315.1	C1416.1	C1719.1	C1820.1	C2123.1	C2224.1	C2527.1	C2628.1	C2931.1	C3032.1	Ctx	Crx
C13.1	54.244	-46.15	-1.2133	-1.2989	-0.26072	-0.37574	-0.083782	-0.11085	-0.016702	-0.020653	-0.0092189	-0.011837	-0.0043094	-0.0048035	-0.0053011	-0.0065628	-4.3115	-0.32066
C24.1	-46.15	56.446	-2.0595	-1.7061	-0.30563	-0.4399	-0.099924	-0.13234	-0.019354	-0.024032	-0.010816	-0.013874	-0.0049988	-0.0055837	-0.0063011	-0.007795	-5.0248	-0.38723
C57.1	-1.2133	-2.0595	62.787	-51.08	-0.60104	-0.72653	-0.37149	-0.50896	-0.036132	-0.046238	-0.021773	-0.0283	-0.0055818	-0.0064277	-0.0072505	-0.0089789	-5.6374	-0.38002
C68.1	-1.2989	-1.7061	-51.08	64.201	-0.72442	-0.8769	-0.44752	-0.6125	-0.044328	-0.05655	-0.027047	-0.035115	-0.0072492	-0.0083186	-0.0095821	-0.01186	-6.6999	-0.49434
C911.1	-0.26072	-0.30563	-0.60104	-0.72442	54.724	-35.711	-1.3146	-1.5121	-0.29231	-0.41435	-0.096856	-0.12718	-0.016378	-0.020346	-0.010032	-0.012739	-3.9886	-0.2207
C1012.1	-0.37574	-0.4399	-0.72653	-0.8769	-35.711	57.995	-2.1486	-1.8861	-0.33843	-0.4793	-0.11318	-0.14875	-0.018512	-0.023117	-0.011255	-0.014295	-4.6495	-0.25178
C1315.1	-0.083782	-0.099924	-0.37149	-0.44752	-1.3146	-2.1486	63.625	-51.282	-0.6864	-0.83344	-0.42028	-0.57002	-0.038919	-0.049443	-0.02488	-0.031982	-4.7898	-0.3306
C1416.1	-0.11085	-0.13234	-0.50896	-0.6125	-1.5121	-1.8861	-51.282	65.537	-0.82626	-1.0055	-0.50297	-0.68177	-0.047265	-0.05991	-0.030361	-0.039005	-5.7848	-0.40948
C1719.1	-0.016702	-0.019354	-0.036132	-0.044328	-0.29231	-0.33843	-0.6864	-0.82626	55.393	-45.219	-1.3605	-1.5595	-0.28422	-0.40101	-0.097169	-0.12475	-3.7989	-0.26256
C1820.1	-0.020653	-0.024032	-0.046238	-0.05655	-0.41435	-0.4793	-0.83344	-1.0055	-45.219	58.071	-2.2049	-1.9522	-0.33027	-0.46559	-0.11366	-0.14612	-4.4229	-0.30105
C2123.1	-0.0092189	-0.010816	-0.021773	-0.027047	-0.096856	-0.11318	-0.42028	-0.50297	-1.3605	-2.2049	63.665	-51.278	-0.64556	-0.77518	-0.39896	-0.53724	-4.9187	-0.33478
C2224.1	-0.011837	-0.013874	-0.0283	-0.035115	-0.12718	-0.14875	-0.57002	-0.68177	-1.5595	-1.9522	-51.278	65.571	-0.77591	-0.9339	-0.47735	-0.6422	-5.9103	-0.41361
C2527.1	-0.0043094	-0.0049988	-0.0055818	-0.0072492	-0.016378	-0.018512	-0.038919	-0.047265	-0.28422	-0.33027	-0.64556	-0.77591	54.786	-44.33	-1.518	-1.6783	-4.7685	-0.30947
C2628.1	-0.0048035	-0.0055837	-0.0064277	-0.0083186	-0.020346	-0.023117	-0.049443	-0.05991	-0.40101	-0.46559	-0.77518	-0.9339	-44.33	57.283	-2.3625	-2.0219	-5.461	-0.35061
C2931.1	-0.0053011	-0.0063011	-0.0072505	-0.0095821	-0.010032	-0.011255	-0.02488	-0.030361	-0.097169	-0.11366	-0.39896	-0.47735	-1.518	-2.3625	62.572	-50.563	-6.4402	-0.49473
C3032.1	-0.0065628	-0.007795	-0.0089789	-0.01186	-0.012739	-0.014295	-0.031982	-0.039005	-0.12475	-0.14612	-0.53724	-0.6422	-1.6783	-2.0219	-50.563	64.033	-7.5817	-0.60292
Ctx	-4.3115	-5.0248	-5.6374	-6.6999	-3.9886	-4.6495	-4.7898	-5.7848	-3.7989	-4.4229	-4.9187	-5.9103	-4.7685	-5.461	-6.4402	-7.5817	88.308	-3.9122
Crx	-0.32066	-0.38723	-0.38002	-0.49434	-0.2207	-0.25178	-0.3306	-0.40948	-0.26256	-0.30105	-0.33478	-0.41361	-0.30947	-0.35061	-0.49473	-0.60292	-3.9122	9.881

Matrix Online $\hat{S}_E$% of Eq. 3.12 and Matrix $\hat{S}_{E,Online}$% of Eq. 3.14.

Total Sensitivity

	1	**1**	**2**	**2**
1	8.187080599	9.538461538	6.7259146	8.089271731
1	9.538461538	8.023597775	8.089271731	6.928240993
2	8.932095607	38.16751141	16.97131631	20.84747085
2	38.16751141	7.685145271	20.84747085	17.1201001
3	8.398173054	10.11963997	8.207021126	9.969187566
3	10.11963997	8.295018167	9.969187566	8.197221333
4	7.009089913	8.671328671	4.861599437	5.826394795
4	8.671328671	7.017788873	5.826394795	4.795964581

Mutual Sensitivity

	1	**2**
1	9.538461538	8.089271731
2	38.16751141	20.84747085
3	10.11963997	9.969187566
4	8.671328671	5.826394795

APPENDIX C

Offline MOD Simulation:

- Red elements are the Self Inductance and relative Sensitivity;
- Green elements are the Mutual Inductance and relative Sensitivity;
- The Black boxes indicate the elements for the positional matrices $\hat{L}$ and $\hat{L}_M$;
- The Yellow box indicate the basic cell with the presence of the MO.

Matrix $\hat{Z}_{tot}$ of Eq. 3.17 without the MO, Offline.

Inductance [nH] and Resistance [Ohm] without the MO

	Z13.1	Z24.1	Z57.1	Z68.1	Z911.1	Z1012.1	Z1315.1	Z1416.1	Z1719.1	Z1820.1	Z2123.1	Z2224.1	Z2527.1	Z2628.1	Z2931.1	Z3032.1
Z13.1	0.17745, 1859.1	0.029187, 1624.2	-0.00050946, -6.9571	-0.00024755, -3.1275	0.00018436, -5.3535	0.00020972, -7.5104	-2.3028E-005, 1.3717	-2.6511E-005, 1.6836	1.0425E-005, 0.042157	1.1611E-005, 0.029822	-3.2886E-006, 0.14416	-4.2388E-006, 0.16876	9.0197E-007, -0.016849	9.734E-007, -0.02203	-9.4788E-007, -0.015117	-1.1777E-006, -0.018569
Z24.1	0.029187, 1624.2	0.1932, 2154.6	-0.0010444, -12.281	-0.00037119, -6.2294	0.00017648, -5.9008	0.00019643, -8.2583	-1.5743E-005, 1.5616	-1.7267E-005, 1.9114	1.2326E-005, 0.067916	1.3519E-005, 0.054107	-2.9945E-006, 0.16421	-3.9652E-006, 0.19133	8.6429E-007, -0.024428	8.5733E-007, -0.031947	-1.0745E-006, -0.016421	-1.34E-006, -0.020388
Z57.1	-0.00050946, -6.9571	-0.0010444, -12.281	0.20793, 1960.5	0.031396, 1639.9	3.1579E-005, 0.51916	3.7068E-005, 0.72216	0.00042181, -9.694	0.00051258, -12.797	1.886E-005, -0.90454	2.1381E-005, -1.0525	-8.0317E-006, 0.085068	-1.0738E-005, 0.16549	1.5473E-006, -0.10387	1.6736E-006, -0.13183	-8.1554E-007, 0.084245	-7.6061E-007, 0.10142
Z68.1	-0.00024755, -3.1275	-0.00037119, -6.2294	0.031396, 1639.9	0.2233, 2250.9	3.187E-005, 0.77349	3.706E-005, 1.0469	0.00043892, -10.657	0.0005356, -14.035	2.0279E-005, -1.0337	2.2886E-005, -1.2044	-9.4746E-006, 0.085046	-1.2514E-005, 0.17467	1.624E-006, -0.12467	1.701E-006, -0.1584	-8.1854E-007, 0.10041	-7.1909E-007, 0.12067
Z911.1	0.00018436, -5.3535	0.00017648, -5.9008	3.1579E-005, 0.51916	3.187E-005, 0.77349	0.17975, 2131.4	0.032369, 1918.1	-0.0003932, 6.0185	-0.00016782, 13.107	-0.00010292, -28.867	-0.00013608, -33.575	-3.9982E-005, 4.967	-4.1617E-005, 6.856	-1.6007E-005, -1.6459	-2.3616E-005, -2.0698	1.5589E-005, 1.4445	2.199E-005, 1.7384
Z1012.1	0.00020972, -7.5104	0.00019643, -8.2583	3.7068E-005, 0.72216	3.706E-005, 1.0469	0.032369, 1918.1	0.19648, 2472.1	-0.0009867, 3.2178	-0.00038658, 13.648	-0.00014512, -33.573	-0.00018885, -39.066	-4.0819E-005, 5.7984	-4.1152E-005, 7.9981	-1.9821E-005, -1.937	-2.9149E-005, -2.437	1.9112E-005, 1.6867	2.6765E-005, 2.0292
Z1315.1	-2.3028E-005, 1.3717	-1.5743E-005, 1.5616	0.00042181, -9.694	0.00043892, -10.657	-0.0003932, 6.0185	-0.0009867, 3.2178	0.20613, 2184.9	0.031553, 1874.8	-6.0019E-005, 5.1021	-6.1696E-005, 6.0075	-2.7774E-006, -3.6707	-6.6254E-006, -4.6589	1.2565E-006, 0.55377	3.5277E-006, 0.70458	-3.1777E-006, -0.4687	-4.8566E-006, -0.5608
Z1416.1	-2.6511E-005, 1.6836	-1.7267E-005, 1.9114	0.00051258, -12.797	0.0005356, -14.035	-0.00016782, 13.107	-0.00038658, 13.648	0.031553, 1874.8	0.22275, 2509	-5.5462E-005, 7.1271	-5.3945E-005, 8.3757	-2.1986E-006, -4.9871	-8.0005E-006, -6.3525	3.0595E-006, 0.72467	6.3008E-006, 0.92077	-5.1591E-006, -0.61791	-7.621E-006, -0.74107
Z1719.1	1.0425E-005, 0.042157	1.2326E-005, 0.067916	1.886E-005, -0.90454	2.0279E-005, -1.0337	-0.00010292, -28.867	-0.00014512, -33.573	-6.0019E-005, 5.1021	-5.5462E-005, 7.1271	0.18005, 2145.6	0.032578, 1934.3	-0.00047272, -0.46327	-0.0002494, 5.2245	-8.0833E-005, -3.1305	-0.00010037, -3.7992	2.4572E-005, 1.5471	3.2802E-005, 1.9307
Z1820.1	1.1611E-005, 0.029822	1.3519E-005, 0.054107	2.1381E-005, -1.0525	2.2886E-005, -1.2044	-0.00013608, -33.575	-0.00018885, -39.066	-6.1696E-005, 6.0075	-5.3945E-005, 8.3757	0.032578, 1934.3	0.19656, 2491.3	-0.0010718, -4.3815	-0.00046761, 4.4348	-0.00010115, -3.754	-0.00012641, -4.5661	3.1102E-005, 1.8206	4.1243E-005, 2.2686
Z2123.1	-3.2886E-006, 0.14416	-2.9945E-006, 0.16421	-8.0317E-006, 0.085068	-9.4746E-006, 0.085046	-3.9982E-005, 4.967	-4.0819E-005, 5.7984	-2.7774E-006, -3.6707	-2.1986E-006, -4.9871	-0.00047272, -0.46327	-0.0010718, -4.3815	0.206, 2194.1	0.031641, 1885.8	9.9696E-006, 0.64447	1.536E-005, 0.81108	-3.1892E-005, -1.5329	-4.1082E-005, -1.8574
Z2224.1	-4.2388E-006, 0.16876	-3.9652E-006, 0.19133	-1.0738E-005, 0.16549	-1.2514E-005, 0.17467	-4.1617E-005, 6.856	-4.1152E-005, 7.9981	-6.6254E-006, -4.6589	-8.0005E-006, -6.3525	-0.0002494, 5.2245	-0.00046761, 4.4348	0.031641, 1885.8	0.22287, 2523.4	1.3236E-005, 0.86266	1.9865E-005, 1.081	-4.0379E-005, -1.9498	-5.2378E-005, -2.3756
Z2527.1	9.0197E-007, -0.016849	8.6429E-007, -0.024428	1.5473E-006, -0.10387	1.624E-006, -0.12467	-1.6007E-005, -1.6459	-1.9821E-005, -1.937	1.2565E-006, 0.55377	3.0595E-006, 0.72467	-8.0833E-005, -3.1305	-0.00010115, -3.754	9.9696E-006, 0.64447	1.3236E-005, 0.86266	0.17958, 1776.8	0.032209, 1523.4	-0.0003732, -8.1143	-0.00019588, -5.0835
Z2628.1	9.734E-007, -0.02203	8.5733E-007, -0.031947	1.6736E-006, -0.13183	1.701E-006, -0.1584	-2.3616E-005, -2.0698	-2.9149E-005, -2.437	3.5277E-006, 0.70458	6.3008E-006, 0.92077	-0.00010037, -3.7992	-0.00012641, -4.5661	1.536E-005, 0.81108	1.9865E-005, 1.081	0.032209, 1523.4	0.19619, 2033.8	-0.0009194, -13.471	-0.00041589, -7.7086
Z2931.1	-9.4788E-007, -0.015117	-1.0745E-006, -0.016421	-8.1554E-007, 0.084245	-8.1854E-007, 0.10041	1.5589E-005, 1.4445	1.9112E-005, 1.6867	-3.1777E-006, -0.4687	-5.1591E-006, -0.61791	2.4572E-005, 1.5471	3.1102E-005, 1.8206	-3.1892E-005, -1.5329	-4.0379E-005, -1.9498	-0.0003732, -8.1143	-0.0009194, -13.471	0.20524, 1862.1	0.030463, 1513.9
Z3032.1	-1.1777E-006, -0.018569	-1.34E-006, -0.020388	-7.6061E-007, 0.10142	-7.1909E-007, 0.12067	2.199E-005, 1.7384	2.6765E-005, 2.0292	-4.8566E-006, -0.5608	-7.621E-006, -0.74107	3.2802E-005, 1.9307	4.1243E-005, 2.2686	-4.1082E-005, -1.8574	-5.2378E-005, -2.3756	-0.00019588, -5.0835	-0.00041589, -7.7086	0.030463, 1513.9	0.22148, 2103.8

Matrix $\hat{Z}_{tot}$ of Eq. 3.17 with the MO, Offline.

Inductance [nH] and Resistance [Ohm] with the MO

	Z13.1	Z24.1	Z57.1	Z68.1	Z911.1	Z1012.1	Z1315.1	Z1416.1	Z1719.1	Z1820.1	Z2123.1	Z2224.1	Z2527.1	Z2628.1	Z2931.1	Z3032.1
Z13.1	0.17784, 1859.8	0.029849, 1624.5	-0.0005141, -7.1384	-0.00027825, -3.3415	4.0695E-005, -1.5423	4.1392E-005, -2.6464	-2.9453E-005, 1.3706	-3.5386E-005, 1.6986	2.1929E-005, -0.18802	2.4653E-005, -0.23796	-6.0813E-006, 0.19198	-7.8315E-006, 0.23589	1.3556E-006, -0.038269	1.5564E-006, -0.049217	-1.4402E-006, 0.000581	-1.7328E-006, 0.00027153
Z24.1	0.029849, 1624.5	0.19368, 2156.1	-0.00099477, -12.509	-0.00036671, -6.5064	2.5272E-005, -1.7764	2.0033E-005, -2.9974	-2.1703E-005, 1.5529	-2.5646E-005, 1.9185	2.4543E-005, -0.18506	2.7299E-005, -0.24052	-5.8551E-006, 0.21646	-7.6391E-006, 0.26478	1.191E-006, -0.049493	1.2802E-006, -0.063834	-1.5344E-006, 0.0015701	-1.8605E-006, 0.0011448
Z57.1	-0.0005141, -7.1384	-0.00099477, -12.509	0.20688, 1963.1	0.030629, 1641.6	4.4854E-005, -0.59488	5.362E-005, -0.58608	0.000417, -9.4248	0.0005157, -12.485	1.5586E-005, -0.83804	1.7434E-005, -0.97441	-7.7813E-006, 0.095279	-1.0043E-005, 0.17663	9.7797E-007, -0.096782	9.0905E-007, -0.12212	-2.5342E-007, 0.074156	-3.1937E-007, 0.090005
Z68.1	-0.00027825, -3.3415	-0.00036671, -6.5064	0.030629, 1641.6	0.22241, 2253.9	5.0284E-005, -0.64294	6.0425E-005, -0.61865	0.00044169, -10.347	0.00054914, -13.677	1.8894E-005, -0.95014	2.1141E-005, -1.1065	-9.4323E-006, 0.094886	-1.2138E-005, 0.18478	1.3007E-006, -0.11698	1.241E-006, -0.14786	-4.6606E-007, 0.089134	-5.7317E-007, 0.10788
Z911.1	4.0695E-005, -1.5423	2.5272E-005, -1.7764	4.4854E-005, -0.59488	5.0284E-005, -0.64294	0.10923, 990.37	0.017411, 811	-0.00027013, -5.794	-0.00011211, -3.4115	-7.8224E-005, -2.2785	-9.6154E-005, -2.7288	7.4156E-006, 0.35128	1.0474E-005, 0.50915	-4.7355E-006, -0.33707	-7.32E-006, -0.43046	6.0656E-006, 0.21324	7.1289E-006, 0.25188
Z1012.1	4.1392E-005, -2.6464	2.0033E-005, -2.9974	5.362E-005, -0.58608	6.0425E-005, -0.61865	0.017411, 811	0.12199, 1135.1	0.00079389, -10.408	-0.000286, -5.3779	0.00018807, -3.2676	0.00022632, -3.909	3.0058E-005, 0.5519	4.0551E-005, 0.77857	-9.8092E-006, -0.43828	-1.4044E-005, -0.5595	1.0814E-005, 0.27604	1.2856E-005, 0.32628
Z1315.1	-2.9453E-005, 1.3706	-2.1703E-005, 1.5529	0.000417, -9.4248	0.00044169, -10.347	-0.00027013, -5.794	-0.00079389, -10.408	0.20606, 2187	0.031776, 1877.1	-7.431E-005, 6.0084	-7.7013E-005, 7.0528	-9.1008E-007, -3.7564	-5.2794E-006, -4.805	2.0876E-006, 0.62541	4.9296E-006, 0.79131	-5.1138E-006, 0.52794	-6.0718E-006, 0.63447
Z1416.1	-3.5386E-005, 1.6986	-2.5646E-005, 1.9185	0.0005157, -12.485	0.00054914, -13.677	-0.00011211, -3.4115	-0.000286, -5.3779	0.031776, 1877.1	0.22281, 2511.3	-8.0474E-005, 8.3458	-8.1094E-005, 9.7819	4.4866E-006, -5.1091	-1.0825E-006, -6.5557	4.3941E-006, 0.82034	8.4659E-006, 1.0364	-7.6032E-006, 0.69602	-9.1259E-006, 0.83841
Z1719.1	2.1929E-005, -0.18802	2.4543E-005, -0.18506	1.5586E-005, -0.83804	1.8894E-005, -0.95014	-7.8224E-005, -2.2785	-0.00018807, -3.2676	-7.431E-005, 6.0084	-8.0474E-005, 8.3458	0.17999, 2149.5	0.032642, 1937	-0.00041513, -0.11255	-0.00020546, 5.7022	-7.4983E-005, -3.0446	-9.2505E-005, -3.702	2.4266E-005, 1.6268	3.2708E-005, 2.0319
Z1820.1	2.4653E-005, -0.23796	2.7299E-005, -0.24052	1.7434E-005, -0.97441	2.1141E-005, -1.1065	-9.6154E-005, -2.7288	-0.00022632, -3.909	-7.7013E-005, 7.0528	-8.1094E-005, 9.7819	0.032642, 1937	0.19644, 2494.7	-0.00097521, -3.9588	-0.00041185, 4.9801	-9.3746E-005, -3.6471	-0.00011643, -4.4444	3.1123E-005, 1.9123	4.1488E-005, 2.3849
Z2123.1	-6.0813E-006, 0.19198	-5.8551E-006, 0.21646	-7.7813E-006, 0.095279	-9.4323E-006, 0.094886	7.4156E-006, 0.35128	3.0058E-005, 0.5519	-9.1008E-007, -3.7564	4.4866E-006, -5.1091	-0.00041513, -0.11255	-0.00097521, -3.9588	0.20587, 2194.5	0.031475, 1886.6	8.7357E-006, 0.70785	1.349E-005, 0.88616	-3.1599E-005, -1.5024	-4.1354E-005, -1.8218
Z2224.1	-7.8315E-006, 0.23589	-7.6391E-006, 0.26478	-1.0043E-005, 0.17663	-1.2138E-005, 0.18478	1.0474E-005, 0.50915	4.0551E-005, 0.77857	-5.2794E-006, -4.805	-1.0825E-006, -6.5557	-0.00020546, 5.7022	-0.00041185, 4.9801	0.031475, 1886.6	0.22259, 2524.2	1.6226E-005, 0.93901	2.3252E-005, 1.1714	-4.0675E-005, -1.9083	-5.3331E-005, -2.3268
Z2527.1	1.3556E-006, -0.038269	1.191E-006, -0.049493	9.7797E-007, -0.096782	1.3007E-006, -0.11698	-4.7355E-006, -0.33707	-9.8092E-006, -0.43828	2.0876E-006, 0.62541	4.3941E-006, 0.82034	-7.4983E-005, -3.0446	-9.3746E-005, -3.6471	8.7357E-006, 0.70785	1.6226E-005, 0.93901	0.17993, 1775.7	0.032599, 1521.3	-0.00037152, -8.0648	-0.00020706, -5.038
Z2628.1	1.5564E-006, -0.049217	1.2802E-006, -0.063834	9.0905E-007, -0.12212	1.241E-006, -0.14786	-7.32E-006, -0.43046	-1.4044E-005, -0.5595	4.9296E-006, 0.79131	8.4659E-006, 1.0364	-9.2505E-005, -3.702	-0.00011643, -4.4444	1.349E-005, 0.88616	2.3252E-005, 1.1714	0.032599, 1521.3	0.19645, 2031.3	-0.00095325, -13.379	-0.00044255, -7.6423
Z2931.1	-1.4402E-006, 0.000581	-1.5344E-006, 0.0015701	-2.5342E-007, 0.074156	-4.6606E-007, 0.089134	6.0656E-006, 0.21324	1.0814E-005, 0.27604	-5.1138E-006, -0.52794	-7.6032E-006, -0.69602	2.4266E-005, 1.6268	3.1123E-005, 1.9123	-3.1599E-005, -1.5024	-4.0675E-005, -1.9083	-0.00037152, -8.0648	-0.00095325, -13.379	0.20529, 1860	0.030343, 1511.8
Z3032.1	-1.7328E-006, 0.00027153	-1.8605E-006, 0.0011448	-3.1937E-007, 0.090005	-5.7317E-007, 0.10788	7.1289E-006, 0.25188	1.2856E-005, 0.32628	-6.0718E-006, 0.63447	-9.1259E-006, 0.83841	3.2708E-005, 2.0319	4.1488E-005, 2.3849	-4.1354E-005, -1.8218	-5.3331E-005, -2.3268	-0.00020706, -5.038	-0.00044255, -7.6423	0.030343, 1511.8	0.22106, 2102.1

Matrix Offline $\hat{S}_M$% of Eq. 3.20 and Matrix $\hat{S}_{M,Offline}$% of Eq. 3.21.

Total Sensitivity

	1	1	2	2
1	0.037652628	0.018470632	0.13261923	0.103664858
1	0.018470632	0.069618491	0.103664858	0.133280021
2	-53.53429671	-57.71857567	0.096114239	0.122679753
2	-57.71857567	-54.08357267	0.122679753	0.091669988
3	0.181767338	0.13958538	0.01823071	0.042422314
3	0.13958538	0.136474933	0.042422314	0.031703258
4	-0.06190905	-0.137849547	-0.112775898	-0.138714578
4	-0.137849547	-0.122922608	-0.138714578	-0.08080616

Mutual Sensitivity

	1	2
1	0.018470632	0.103664858
2	-57.71857567	0.122679753
3	0.13958538	0.042422314
4	-0.137849547	-0.138714578

Online MOD Simulation:

- Red elements are the Self Inductance and relative Sensitivity;
- Green elements are the Mutual Inductance and relative Sensitivity;
- The Black boxes indicate the elements for the positional matrices $\hat{L}$ and $\hat{L}_M$;
- The Yellow box indicate the basic cell with the presence of the MO.
- Light Blue elements are the Transmitter and Receiver Self, Mutual and coupling elements;

Matrix $\hat{Z}_{tot}$ of Eq. 3.17 without the MO, Online.

Inductance [nH] and Resistance [Ohm] without the MO

	Z13.1	Z24.1	Z57.1	Z68.1	Z911.1	Z1012.1	Z1315.1	Z1416.1	Z1719.1	Z1820.1	Z2123.1	Z2224.1	Z2527.1	Z2628.1	Z2931.1	Z3032.1	Ztx	Zrx
Z13.1	0.16294, 1920.3	0.015857, 1651	-0.0001065, -8.0953	-4.5204E-05, -5.0055	-1.2795E-05, -0.59303	-1.8381E-05, -0.76456	1.0776E-05, 0.5785	1.3818E-05, 0.70923	-2.855E-08, 0.044356	-4.9E-07, 0.042145	1.1974E-06, 0.069539	1.4893E-06, 0.081739	-8.5427E-07, -0.012373	-1.1545E-06, -0.016109	4.5523E-07, -0.0045368	4.4685E-07, -0.0056787	0.0002031, 4.3732	2.9426E-05, 1.7896
Z24.1	0.015857, 1651	0.17705, 2222.8	-0.0003768, -13.319	-0.0001451, -7.6455	-1.6041E-05, -0.77856	-2.3368E-05, -1.0049	1.343E-05, 0.7063	1.7166E-05, 0.86362	-5.0314E-07, 0.054385	-1.2563E-06, 0.049297	1.6115E-06, 0.083609	1.9986E-06, 0.097484	-1.4051E-06, -0.023237	-1.9029E-06, -0.030668	8.0883E-07, 0.0016837	8.4885E-07, 0.0010081	0.0002690, 5.6.4101	4.0777E-05, 2.3525
Z57.1	-0.0001065, -8.0953	-0.0003768, -13.319	0.18812, 2036.7	0.015393, 1675.1	1.292E-05, 0.37915	1.5964E-05, 0.46809	-2.4183E-05, -1.5556	-3.016E-05, -1.8174	-5.5625E-06, -0.46311	-6.4666E-06, -0.53359	9.746E-07, 0.050094	1.5319E-06, 0.096424	-3.8136E-07, -0.037792	-3.7618E-07, -0.044639	-1.5552E-08, 0.019433	2.0276E-07, 0.026872	-4.1509E-05, -3.4603	6.0349E-07, 0.29946
Z68.1	-4.5204E-05, -5.0055	-0.0001451, -7.6455	0.015393, 1675.1	0.20232, 2338.6	7.2264E-06, 0.48959	9.5609E-06, 0.59636	-2.8179E-05, -1.8301	-3.4878E-05, -2.139	-6.74E-06, -0.53501	-7.8529E-06, -0.61818	1.0007E-06, 0.052545	1.5991E-06, 0.10479	-5.1167E-07, -0.050218	-5.3824E-07, -0.060405	-1.4064E-09, 0.028315	2.6821E-07, 0.03754	-5.6049E-05, -3.6168	-1.108E-06, 0.4435
Z911.1	-1.2795E-05, -0.59303	-1.6041E-05, -0.77856	1.292E-05, 0.37915	7.2264E-06, 0.48959	0.16341, 2181.8	0.016092, 1936.9	1.8057E-05, 4.6037	0.0001592, 11.493	-0.0002819, -28.517	0.0003396, -33.165	7.1549E-05, 5.9544	9.8904E-05, 8.2457	-2.84E-05, -1.9891	-3.6173E-05, -2.4591	1.4252E-05, 1.5546	2.4629E-05, 1.9103	0.0002016, 19.013	1.7155E-05, -0.94949
Z1012.1	-1.8381E-05, -0.76456	-2.3368E-05, -1.0049	1.5964E-05, 0.46809	9.5609E-06, 0.59636	0.016092, 1936.9	0.17722, 2533.2	-0.0002264, 1.5815	0.0001005, 11.613	-0.0003390, -33.145	0.0004084, -38.561	8.6538E-05, 6.927	0.00011941, 9.5868	-3.4535E-05, -2.3248	-4.4027E-05, -2.876	1.7544E-05, 1.8138	2.9786E-05, 2.2273	0.0002797, 23.564	3.1961E-05, -0.60392
Z1315.1	1.0776E-05, 0.5785	1.343E-05, 0.7063	-2.4183E-05, -1.5556	-2.8179E-05, -1.8301	1.8057E-05, 4.6037	-0.0002264, 1.5815	0.18817, 2236.8	0.01577, 1890.1	6.5823E-05, 6.4721	8.1209E-05, 7.5653	-6.3289E-05, -3.4784	-8.2198E-05, -4.5343	1.1669E-05, 0.69609	1.4885E-05, 0.86671	-6.0723E-06, -0.5427	-9.8338E-06, -0.66453	-3.7097E-06, -0.051005	-1.7527E-05, -1.4218
Z1416.1	1.3818E-05, 0.70923	1.7166E-05, 0.86362	-3.016E-05, -1.8174	-3.4878E-05, -2.139	0.0001592, 11.493	0.0001005, 11.613	0.01577, 1890.1	0.20248, 2574.4	9.4456E-05, 8.9264	0.0001158, 10.425	-7.9249E-05, -4.7545	-0.0001036, -6.2078	1.5856E-05, 0.91942	2.0179E-05, 1.1431	-8.4467E-06, -0.71586	-1.3531E-05, -0.87852	-3.2246E-06, 0.5757	-2.2679E-05, -1.6362
Z1719.1	-2.855E-08, 0.044356	-5.0314E-07, 0.054385	-5.5625E-06, -0.46311	-6.74E-06, -0.53501	0.0002819, -28.517	0.0003390, -33.145	6.5823E-05, 6.4721	9.4456E-05, 8.9264	0.16354, 2192.2	0.016189, 1947.3	-2.6505E-05, -0.56039	8.5438E-05, 5.1964	-3.8407E-05, -2.9214	-5.3006E-05, -3.5744	1.5648E-05, 1.5412	2.6808E-05, 1.9302	0.0002083, 20.027	1.436E-05, -1.4748
Z1820.1	-4.9E-07, 0.042145	-1.2563E-06, 0.049297	-6.4666E-06, -0.53359	-7.8529E-06, -0.61818	0.0003396, -33.165	0.0004084, -38.561	8.1209E-05, 7.5653	0.0001158, 10.425	0.016189, 1947.3	0.1771, 2545.6	-0.0002748, -4.3859	1.5307E-05, 4.3339	-4.848E-05, -3.4744	-6.6728E-05, -4.2587	1.9478E-05, 1.8099	3.2717E-05, 2.2636	0.0002743, 24.713	2.9095E-05, -1.1784
Z2123.1	1.1974E-06, 0.069539	1.6115E-06, 0.083609	9.746E-07, 0.050094	1.0007E-06, 0.052545	7.1549E-05, 5.9544	8.6538E-05, 6.927	-6.3289E-05, -3.4784	-7.9249E-05, -4.7545	-2.6505E-05, -0.56039	-0.0002748, -4.3859	0.18812, 2241.8	0.015692, 1896.5	1.3657E-05, 0.70209	1.7863E-05, 0.87442	-2.2281E-05, -1.3765	-3.0313E-05, -1.6729	-1.8191E-05, -1.7546	-1.1953E-05, -0.53243
Z2224.1	1.4893E-06, 0.081739	1.9986E-06, 0.097484	1.5319E-06, 0.096424	1.5991E-06, 0.10479	9.8904E-05, 8.2457	0.00011941, 9.5868	-8.2198E-05, -4.5343	-0.0001036, -6.2078	8.5438E-05, 5.1964	1.5307E-05, 4.3339	0.015692, 1896.5	0.20225, 2581.9	1.9695E-05, 0.93872	2.5524E-05, 1.1659	-2.8045E-05, -1.7595	-3.8191E-05, -2.149	-2.4309E-05, -1.4522	-1.2857E-05, -0.56996
Z2527.1	-8.5427E-07, -0.012373	-1.4051E-06, -0.023237	-3.8136E-07, -0.037792	-5.1167E-07, -0.050218	-2.84E-05, -1.9891	-3.4535E-05, -2.3248	1.1669E-05, 0.69609	1.5856E-05, 0.91942	-3.8407E-05, -2.9214	-4.848E-05, -3.4744	1.3657E-05, 0.70209	1.9695E-05, 0.93872	0.16105, 1821.4	0.013701, 1534.5	-0.0001297, -8.2721	-6.4419E-05, -5.2214	0.0002096, 3.11.408	3.072E-05, 2.0579
Z2628.1	-1.1545E-06, -0.016109	-1.9029E-06, -0.030668	-3.7618E-07, -0.044639	-5.3824E-07, -0.060405	-3.6173E-05, -2.4591	-4.4027E-05, -2.876	1.4885E-05, 0.86671	2.0179E-05, 1.1431	-5.3006E-05, -3.5744	-6.6728E-05, -4.2587	1.7863E-05, 0.87442	2.5524E-05, 1.1659	0.013701, 1534.5	0.17444, 2084.3	0.0003982, -13.526	0.0001637, -7.9053	0.0003302, 3.15.219	4.4296E-05, 2.7389
Z2931.1	4.5523E-07, -0.0045368	8.0883E-07, 0.0016837	-1.5552E-08, 0.019433	-1.4064E-09, 0.028315	1.4252E-05, 1.5546	1.7544E-05, 1.8138	-6.0723E-06, -0.5427	-8.4467E-06, -0.71586	1.5648E-05, 1.5412	1.9478E-05, 1.8099	-2.2281E-05, -1.3765	-2.8045E-05, -1.7595	-0.0001297, -8.2721	-0.0003982, -13.526	0.18633, 1912.7	0.013335, 1526.7	-5.5068E-05, -2.9305	-4.5066E-06, -0.24126
Z3032.1	4.4685E-07, -0.0056787	8.4885E-07, 0.0010081	2.0276E-07, 0.026872	2.6821E-07, 0.03754	2.4629E-05, 1.9103	2.9786E-05, 2.2273	-9.8338E-06, -0.66453	-1.3531E-05, -0.87852	2.6808E-05, 1.9302	3.2717E-05, 2.2636	-3.0313E-05, -1.6729	-3.8191E-05, -2.149	-6.4419E-05, -5.2214	-0.0001637, -7.9053	0.013335, 1526.7	0.19949, 2164.8	-4.9391E-05, -2.337	-4.2816E-06, -0.20823
Ztx	0.0002031, 9.4.3732	0.0002690, 5.6.4101	-4.1509E-05, -3.4603	-5.6049E-05, -3.6168	0.0002016, 19.013	0.0002797, 23.564	-3.7097E-06, -0.051005	-3.2246E-06, 0.5757	0.0002083, 20.027	0.0002743, 24.713	-1.8191E-05, -1.7546	-2.4309E-05, -1.4522	0.0002096, 3.11.408	0.0003302, 3.15.219	-5.5068E-05, -2.9305	-4.9391E-05, -2.337	0.0201, 413.93	5.7046E-05, 68.296
Zrx	2.9426E-05, 1.7896	4.0777E-05, 2.3525	6.0349E-07, 0.29946	-1.108E-06, 0.4435	1.7155E-05, -0.94949	3.1961E-05, -0.60392	-1.7527E-05, -1.4218	-2.2679E-05, -1.6362	1.436E-05, -1.4748	2.9095E-05, -1.1784	-1.1953E-05, -0.53243	-1.2857E-05, -0.56996	3.072E-05, 2.0579	4.4296E-05, 2.7389	-4.5066E-06, -0.24126	-4.2816E-06, -0.20823	5.7046E-05, 68.296	0.020354, 411.03

Matrix $\hat{Z}_{tot}$ of Eq. 3.17 with the MO, Online.

Inductance [nH] and Resistance [Ohm] with the MO

	Z13.1	Z24.1	Z57.1	Z68.1	Z911.1	Z1012.1	Z1315.1	Z1416.1	Z1719.1	Z1820.1	Z2123.1	Z2224.1	Z2527.1	Z2628.1	Z2931.1	Z3032.1	Ztx	Zrx
Z13.1	0.1627, 1919.3	0.015615, 1650	-0.0001188, -8.0919	-4.7345E-05, -5.0126	-1.1955E-05, -0.40536	-1.7851E-05, -0.528	1.057E-05, 0.58222	1.3395E-05, 0.71503	1.8647E-07, 0.025136	-1.2486E-07, 0.019734	1.1342E-06, 0.073866	1.4373E-06, 0.087867	-5.8798E-07, -0.014822	-8.0669E-07, -0.019118	2.5147E-07, -0.0029094	2.4586E-07, -0.0037373	0.0001402, 5.4.6427	2.6707E-05, 1.7848
Z24.1	0.015615, 1650	0.17715, 2221.5	-0.0003991, -2.13.315	-0.0001492, -7.6533	-1.5602E-05, -0.55747	-2.3203E-05, -0.72449	1.375E-05, 0.71144	1.7296E-05, 0.87136	8.5837E-07, 0.03253	4.9306E-07, 0.023811	1.3541E-06, 0.088685	1.6369E-06, 0.10468	-8.3571E-07, -0.026196	-1.1556E-06, -0.034294	3.5964E-07, 0.0035861	3.7273E-07, 0.0032791	0.0002091, 8, 6.6949	3.7241E-05, 2.3467
Z57.1	-0.0001188, -8.0919	-0.0003991, -13.315	0.18822, 2036.8	0.015648, 1671.5	7.1455E-06, 0.28102	1.0593E-05, 0.36782	-1.6278E-05, -1.5836	-2.0685E-05, -1.8507	4.8972E-07, -0.48817	5.0688E-07, -0.56305	9.8412E-08, 0.052575	3.579E-07, 0.10018	4.7994E-07, -0.040888	7.241E-07, -0.048739	-9.3063E-07, 0.023101	-8.7484E-07, 0.031253	-2.9353E-05, -3.5104	1.8021E-06, 0.29511
Z68.1	-4.7345E-05, -5.0126	-0.0001492, -7.6533	0.015648, 1671.5	0.20225, 2336.8	7.9479E-06, 0.3066	1.2167E-05, 0.40206	-2.2852E-05, -1.858	-2.8485E-05, -2.1723	-2.7237E-06, -0.55747	-3.2985E-06, -0.64461	4.4523E-07, 0.054382	9.3305E-07, 0.10762	-1.4959E-08, -0.05301	1.0342E-07, -0.064136	-6.2842E-07, 0.031852	-4.673E-07, 0.041775	-4.3747E-05, -3.6709	9.9094E-07, 0.43862
Z911.1	-1.1955E-05, -0.40536	-1.5602E-05, -0.55747	7.1455E-06, 0.28102	7.9479E-06, 0.3066	0.099365, 1017.9	0.0073067, 818.3	-7.7902E-05, -5.6322	-1.1039E-06, -3.1231	-8.4203E-05, -2.219	0.0001014, -2.6336	1.4715E-05, 0.39521	2.0438E-05, 0.55567	-9.286E-06, -0.28965	-1.1779E-05, -0.37028	5.3719E-06, 0.21186	7.313E-06, 0.25002	0.0001797, 12.488	2.6043E-05, 2.534
Z1012.1	-1.7851E-05, -0.528	-2.3203E-05, -0.72449	1.0593E-05, 0.36782	1.2167E-05, 0.40206	0.0073067, 818.3	0.1099, 1168.2	-0.0003249, -10.163	-5.5782E-05, -5.167	-0.0001833, -3.1649	-0.00002186, -3.7561	3.7648E-05, 0.58961	5.1196E-05, 0.81658	-1.5756E-05, -0.37846	-1.9871E-05, -0.48358	9.8021E-06, 0.27594	1.2998E-05, 0.32593	0.0002619, 7, 16.106	3.7869E-05, 3.37
Z1315.1	1.057E-05, 0.58222	1.375E-05, 0.71144	-1.6278E-05, -1.5836	-2.2852E-05, -1.858	-7.7902E-05, -5.6322	-0.0003249, -10.163	0.18835, 2239.2	0.015695, 1890.4	6.7041E-05, 6.776	8.4572E-05, 7.9175	-6.2244E-05, -3.5486	-8.2436E-05, -4.6309	1.2172E-05, 0.70953	1.5358E-05, 0.88356	-5.6799E-06, -0.55977	-9.366E-06, -0.68661	-7.4804E-07, -0.12898	-1.7698E-05, -1.3877
Z1416.1	1.3395E-05, 0.71503	1.7296E-05, 0.87136	-2.0685E-05, -1.8507	-2.8485E-05, -2.1723	-1.1039E-06, -3.1231	-5.5782E-05, -5.167	0.015695, 1890.4	0.20242, 2577.1	8.9315E-05, 9.3764	0.0001126, 10.947	-7.6065E-05, -4.8543	-0.0001020, -6.3446	1.6775E-05, 0.93884	2.1148E-05, 1.1674	-7.981E-06, -0.74009	-1.2988E-05, -0.9098	2.8011E-06, 0.46294	-2.195E-05, -1.5842
Z1719.1	1.8647E-07, 0.025136	8.5837E-07, 0.03253	4.8972E-07, -0.48817	-2.7237E-06, -0.55747	-8.4203E-05, -2.219	-0.0001833, -3.1649	6.7041E-05, 6.776	8.9315E-05, 9.3764	0.1634, 2188.1	0.016508, 1943.1	-4.7358E-05, -0.38292	8.073E-05, 5.4194	-4.0396E-05, -2.9219	-5.6808E-05, -3.5751	1.5447E-05, 1.5816	2.5779E-05, 1.9825	0.0002244, 6, 19.983	2.6797E-05, -1.6684
Z1820.1	-1.2486E-07, 0.019734	4.9306E-07, 0.023811	5.0688E-07, -0.56305	-3.2985E-06, -0.64461	-0.0001014, -2.6336	-0.0002186, -3.7561	8.4572E-05, 7.9175	0.0001126, 10.947	0.016508, 1943.1	0.17768, 2549.4	-0.0003043, -4.2454	1.422E-05, 4.59	-5.2219E-05, -3.475	-7.288E-05, -4.2593	1.9712E-05, 1.8566	3.2109E-05, 2.324	0.0003100, 3, 24.65	4.3475E-05, -1.4031
Z2123.1	1.1342E-06, 0.073866	1.3541E-06, 0.088685	9.8412E-08, 0.052575	4.4523E-07, 0.054382	1.4715E-05, 0.39521	3.7648E-05, 0.58961	-6.2244E-05, -3.5486	-7.6065E-05, -4.8543	-4.7358E-05, -0.38292	-0.0003043, -4.2454	0.1884, 2240.2	0.015742, 1894.8	1.3048E-05, 0.71186	1.7091E-05, 0.88644	-2.263E-05, -1.3802	-3.1227E-05, -1.6773	-1.6049E-05, -1.8051	-1.2374E-05, -0.50694
Z2224.1	1.4373E-06, 0.087867	1.6369E-06, 0.10468	3.579E-07, 0.10018	9.3305E-07, 0.10762	2.0438E-05, 0.55567	5.1196E-05, 0.81658	-8.2436E-05, -4.6309	-0.0001020, -6.3446	8.073E-05, 5.4194	1.422E-05, 4.59	0.015742, 1894.8	0.20243, 2580.6	1.7461E-05, 0.9522	2.2684E-05, 1.1826	-2.6595E-05, -1.7675	-3.7143E-05, -2.1588	-1.9654E-05, -1.5248	-1.3406E-05, -0.53415
Z2527.1	-5.8798E-07, -0.014822	-8.3571E-07, -0.026196	4.7994E-07, -0.040888	-1.4959E-08, -0.05301	-9.286E-06, -0.28965	-1.5756E-05, -0.37846	1.2172E-05, 0.70953	1.6775E-05, 0.93884	-4.0396E-05, -2.9219	-5.2219E-05, -3.475	1.3048E-05, 0.71186	1.7461E-05, 0.9522	0.16082, 1821.8	0.013609, 1536	-0.0001216, -8.3228	-6.0306E-05, -5.2445	0.0001800, 7, 11.574	2.7746E-05, 2.0803
Z2628.1	-8.0669E-07, -0.019118	-1.1556E-06, -0.034294	7.241E-07, -0.048739	1.0342E-07, -0.064136	-1.1779E-05, -0.37028	-1.9871E-05, -0.48358	1.5358E-05, 0.88356	2.1148E-05, 1.1674	-5.6808E-05, -3.5751	-7.288E-05, -4.2593	1.7091E-05, 0.88644	2.2684E-05, 1.1826	0.013609, 1536	0.17418, 2085.9	-0.0003907, 8, -13.614	-0.0001608, 4, -7.9363	0.0002664, 3, 15.415	3.934E-05, 2.7645
Z2931.1	2.5147E-07, -0.0029094	3.5964E-07, 0.0035861	-9.3063E-07, 0.023101	-6.2842E-07, 0.031852	5.3719E-06, 0.21186	9.8021E-06, 0.27594	-5.6799E-06, -0.55977	-7.981E-06, -0.74009	1.5447E-05, 1.5816	1.9712E-05, 1.8566	-2.263E-05, -1.3802	-2.6595E-05, -1.7675	-0.0001216, -8.3228	-0.0003907, 8, -13.614	0.18615, 1913.9	0.013192, 1527.6	-3.5114E-05, -2.9592	-3.2298E-06, -0.23608
Z3032.1	2.4586E-07, -0.0037373	3.7273E-07, 0.0032791	-8.7484E-07, 0.031253	-4.673E-07, 0.041775	7.313E-06, 0.25002	1.2998E-05, 0.32593	-9.366E-06, 0.68661	-1.2988E-05, 0.9098	2.5779E-05, 1.9825	3.2109E-05, 2.324	-3.1227E-05, -1.6773	-3.7143E-05, -2.1588	-6.0306E-05, -5.2445	0.0001608, 4, -7.9363	0.013192, 1527.6	0.19949, 2167.6	-3.9321E-05, -2.3605	-4.4688E-06, -0.20162
Ztx	0.0001402, 5.4.6427	0.0002091, 8, 6.6949	-2.9353E-05, -3.5104	-4.3747E-05, -3.6709	0.0001797, 5, 12.488	0.0002619, 7, 16.106	-7.4804E-07, -0.12898	2.8011E-06, 0.46294	0.0002244, 6, 19.983	0.0003100, 3, 24.65	-1.6049E-05, -1.8051	-1.9654E-05, -1.5248	0.0001800, 7, 11.574	0.0002664, 3, 15.415	-3.5114E-05, -2.9592	-3.9321E-05, -2.3605	0.020063, 413.53	5.4077E-05, 68.378
Zrx	2.6707E-05, 1.7848	3.7241E-05, 2.3467	1.8021E-06, 0.29511	9.9094E-07, 0.43862	2.6043E-05, 2.534	3.7869E-05, 3.37	-1.7698E-05, -1.3877	-2.195E-05, -1.5842	2.6797E-05, -1.6684	4.3475E-05, -1.4031	-1.2374E-05, -0.50694	-1.3406E-05, -0.53415	2.7746E-05, 2.0803	3.934E-05, 2.7645	-3.2298E-06, -0.23608	-4.4688E-06, -0.20162	5.4077E-05, 68.378	0.02033, 410.39

Matrix Online $\hat{S}_M$% of Eq. 3.20 and Matrix $\hat{S}_{M,online}$% of Eq. 3.22.

Total Sensitivity

	1	1	2	2
1	-0.052075197	-0.060569352	0.004909903	-0.214912543
1	-0.060569352	-0.058484794	-0.214912543	-0.076969127
2	-53.34586122	-57.75207806	0.107296137	0.015872176
2	-57.75207806	-53.88441497	0.015872176	0.104878807
3	-0.187026731	-0.215683254	-0.07137122	-0.089638808
3	-0.215683254	-0.204274041	-0.089638808	-0.050350517
4	0.021961129	0.097751711	0.062738537	0.058950678
4	0.097751711	0.076764381	0.058950678	0.129342203

Mutual Sensitivity

	1	2
1	-0.060569352	-0.214912543
2	-57.75207806	0.015872176
3	-0.215683254	-0.089638808
4	0.097751711	0.058950678